PITT | IRISE

CENTER FOR IMPACTFUL RESILIENT INFRASTRUCTURE SCIENCE & ENGINEERING



Developing Lightweight and High-Performance Metamaterial Concrete

FINAL REPORT

IRISE-25-P23-01-01
DECEMBER 2024

1. Report No. IRISE-25-P23-01-01	2. Government Accession No.	3. Recipient's Catalog No.	
4. Title and Subtitle Developing Lightweight and High-Performance Metamaterial Concrete		**5. Report Date** 12/31/24 **6. Performing Organization Code**	
7. Author(s) Amir Alavi, Wenyun Lu, Jianzhe Luo, Wenxuan Meng		**8. Performing Organization Report No.** IRISE-25-P23-01-01	
9. Performing Organization Name and Address Department of Civil and Environmental Engineering University of Pittsburgh Benedum Hall 3700 O'Hara Street | Pittsburgh, PA 15261		**10. Work Unit No. (TRAIS)** **11. Contract or Grant No.** **PITTIRISE2018**	
12. Sponsoring Agency Name and Address IRISE - Department of Civil and Environmental Engineering University of Pittsburgh Benedum Hall 3700 O'Hara Street | Pittsburgh, PA 15261		**13. Type of Report and Period Covered** January 1, 2023 – December 31, 2024 **14. Sponsoring Agency Code**	

15. Supplementary Notes

Amir H Alavi, PhD
Assistant Professor
Department of Civil & Environmental Engineering, University of Pittsburgh
209 Benedum Hall Pittsburgh, PA 15261-2294 USA. Telephone: (412) 648-4385 | Fax: (412) 624-0135

16. Abstract

Civil infrastructure faces the pressing challenge of reducing its environmental impact while maintaining safety and longevity. Concrete, a fundamental material, is responsible for approximately 8% of global CO_2 emissions due to its carbon-intensive production. Traditional solutions, such as modifying cement mixtures or reinjecting CO_2, encounter cost and scalability issues. A promising alternative is the use of a metamaterial concrete design approach, which leverages engineered microstructures to enhance performance with less material. This research explores the development of a novel mechanical metamaterial lightweight concrete (MM-LWC) systems. The study focuses on two innovative strategies: embedding polymeric metamaterial structures as reinforcement and designing fully cementitious metamaterial structures. These approaches aim to achieve a balance of low density and high compressive strength without altering the concrete mix. The unit cells forming the structure of metamaterial concrete can take various sizes and shapes. Identifying configurations for target performance requires exploring a design space with astronomically large potential configurations. To address this, we deploy an evolutionary generative artificial intelligence (GAI) paradigm to efficiently explore the design space for intricate metamaterial structures. Through experimental validation and the creation of high-performance concrete specimens, the research evaluates the mechanical properties of lightweight metamaterial concrete materials. One of the most outstanding observations was that the explored metamaterial concrete structures offer a high strength-to-density ratio. Some of the proposed designs can provide 92.2 MPa ultimate strength at 1726 kg/m³ density, only 2.6% less strength than a solid concrete cube with 94.69 MPa at 2208 kg/m³ density, translating to 22% less weight. This design boasts a strength-to-density ratio of 0.06 MPa·m³/kg, significantly outperforming solid concrete and various construction metals, including mild steel (~0.027 MPa·m³/kg) and structural steel (~0.025-0.035 MPa·m³/kg). The results indicate that the proposed lightweight metamaterial concrete concept has the potential to transform the concrete technology by reducing weight and material use while maintaining or improving structural performance. This research offers a sustainable, high-performance solution for civil infrastructure, addressing both environmental and functional challenges.

17. Key Words	18. Distribution Statement		
Mechanical Metamaterial, Lightweight Concrete, Evolutionary Generative AI, 3D Printing	No restrictions. Report available at: https://www.engineering.pitt.edu/IRISE/Research-Projects/Completed/		
19. Security Classif. (of this report) Unclassified	**20. Security Classif. (of this page)** Unclassified	**21. No. of Pages** 84	**22. Price**

IRISE

The Impactful Resilient Infrastructure Science & Engineering consortium was established in the Department of Civil and Environmental Engineering in the Swanson School of Engineering at the University of Pittsburgh to address the challenges associated with aging transportation infrastructure. IRISE is addressing these challenges with a comprehensive approach that includes knowledge gathering, decision making, design of materials and assets and interventions. It features a collaborative effort among the public agencies that own and operate the infrastructure, the private companies that design and build it and the academic community to develop creative solutions that can be implemented to meet the needs of its members. To learn more, visit: https://www.engineering.pitt.edu/irise/.



Acknowledgements

The authors gratefully acknowledge the financial support of all contributing members of IRISE. In addition, we are indebted to the advice and assistance provided by Kenneth Urbanec of the Allegheny County, Ezequiel Lujan of the Federal Highway Administration, Tyler Culhane of the Pennsylvania Department of Transportation, Ryan Rago and Viswanath Venkatesh of the Pennsylvania Turnpike Commission.

Disclaimer

The views and conclusions contained in this document are those of the authors and should not be interpreted as representing official policies, either expressed or implied, of the Pennsylvania Department of Transportation, the Pennsylvania Turnpike Commission, Allegheny County, Golden Triangle Construction, Michael Baker International, the Constructors Association of Western Pennsylvania or CDR Maguire.

Table of Contents

1. Introduction 5
1.1 Background 5
1.2 Problem statement 7
1.3 Research plan 9
2. State-of-art of the lightweight concrete and metamaterial research 12
2.1 Literature review of LWC 12
2.2 Literature review of MMs 18
2.2.1 Metamaterial types 19
2.2.2 Fabrication methods 29
3. Design and discover MM-LWC structures 32
3.1 The proposed GAI approach 32
3.1.1 Traditional deep-learning-based GAI 32
3.1.2 The proposed evolutionary GAI 34
3.1.3 Comparison of the traditional and evolutionary GAI approaches 36
3.2 Exploring MM structure with desirable properties 38
3.3 Objective functions for the revolutionary GAI 40
3.4 Parameter setting for the evolutionary GAI algorithm 41
4. Concrete mix design 44
4.1 Material selection 44
5. Design and fabrication polymeric and cementitious MM unit cells 45
5.1 MM unit cell structures 45
5.1.1 Bulk modulus unit cell structures 45
5.1.2 NPR's unit cell structures 46
5.2 3D printing of polymeric MM unit cells 48
5.3 Unit cell fabrication 51
5.3.1 Bulk modulus unit cells 51
5.4 Mechanical testing of the unit cells 53

5.4.1 Bulk modulus and Poisson's ratio tests 53
5.4.2 Compression tests 55
5.5 FE simulations 58
5.6 Experiment vs. simulation results 61
6. Design and fabrication of MM-LWC structures 63
6.1 Composite MM-LWC structure with embedded 3D polymeric MM reinforcement 63
6.1.1 Design 63
6.1.2 Fabrication of the composite MM-LWC structure 64
6. Fully cementitious MM-LWC structure 65
6.3 Compression tests 66
7. MM-LWC beam with embedded 3D polymeric reinforcement 67
7.1 Composite MM-LWC beam fabrication 67
7.2 Three-point bending testing of the composite MM-LWC beams 69
8. Large-scale implementation of the MM-LWC structures 70
9. Implementation guideline 71
10. Conclusion and future works 73
10.1 Conclusion 73
10.2 Future works 74
References 75

1. Introduction

1.1 Background

Lightweight concrete (LWC) has become a crucial material in modern construction, especially for applications requiring a balance between structural performance and reduced weight. Its inherent properties, including low density, reduced shrinkage, accelerated construction rates, design flexibility, and cost efficiency, have driven its adoption in diverse structural applications such as multistory buildings, long-span bridges, offshore platforms, and other large-scale structures [1]. The ACI Committee 213 Guide for Structural Lightweight Aggregate Concrete provides a detailed classification system for LWC based on its unit weight, ranging from 300 to 1920 kg/m³, and its 28-day compressive strength. This classification divides LWC into three primary categories [2, 3]. The first category, low-density concretes, has a unit weight between 300 and 800 kg/m³ and compressive strengths ranging from 0.7 to 2.0 MPa. These concretes are primarily used for non-structural purposes, such as thermal and acoustic insulation, due to their exceptionally low density and minimal load-bearing capacity. The second category, moderate-strength concretes, is characterized by a unit weight of 800 to 1350 kg/m³ and compressive strengths of 7 to 14 MPa. These concretes offer a balance of reduced weight and moderate structural performance, making them suitable for precast elements, secondary structural components, and applications requiring some degree of load resistance. The third and most robust category, structural concretes, has a unit weight ranging from 1350 to 1920 kg/m³ and compressive strengths between 17 and 63 MPa. Structural LWC is specifically engineered for load-bearing applications, providing a significant reduction in dead load while maintaining the strength necessary for use in high-rise buildings, bridges, and other demanding infrastructure. This detailed classification system underscores the versatility of LWC, demonstrating its adaptability to diverse construction requirements. From non-structural applications that prioritize insulation to robust structural uses demanding high strength, LWC offers tailored solutions based on the desired balance of weight and performance.

The production of LWC typically involves the use of lightweight aggregates (LWA) such as expanded clay, pumice, and perlite, which replace traditional aggregates in the concrete mix. These LWAs reduce the overall density of the material, delivering the weight-saving benefits of LWC [4]. However, the reduced density often leads to a substantial decrease in compressive strength, limiting its applicability in more demanding structural scenarios. The challenge lies in developing LWC that combines both low density and high compressive strength, a critical requirement for its broader adoption in structural engineering. This ongoing research and development focus is driving innovations aimed at overcoming the inherent trade-offs of LWC, paving the way for next-generation materials that further expand its capabilities and applications.

Over the past three decades, substantial research efforts have been dedicated to the development of high-performance concrete (HPC) and ultra-high-performance concrete (UHPC), two advanced concrete types that offer exceptional mechanical properties and durability. HPC is characterized by a minimum compressive strength of 55 MPa, while UHPC achieves even greater performance, with compressive strengths of at least 120 MPa [5, 6]. These advancements have expanded the

potential applications of concrete in demanding structural environments, from high-rise buildings and long-span bridges to infrastructure requiring exceptional durability and resistance to harsh conditions.

Recent innovations have extended these advancements to lightweight, high-strength mixtures, such as high-performance lightweight concrete (HPC-LWC), which aim to combine the benefits of HPC and LWC. These mixtures have shown promise in achieving enhanced performance while maintaining a relatively low density, making them an attractive option for applications where reducing deadload is critical [7]. Despite these advancements, HPC-LWC faces notable limitations that constrain its widespread adoption. One of the primary challenges is the significantly higher cement paste content required in these mixtures compared to traditional concrete. This high paste content leads to reduced aggregate proportions, which negatively impacts cost-efficiency and sustainability. Moreover, the increased density of HPC-LWC, while lower than traditional HPC, still partially offsets the weight-saving benefits of LWC. In addition to technical challenges, the environmental impact of these mixtures is a growing concern, as the production of cement is energy-intensive and a major contributor to carbon dioxide emissions. Furthermore, the higher initial costs associated with these advanced mixtures, stemming from the use of specialized materials and production methods, limit their economic feasibility for many projects [8]. These combined factors—higher density, environmental impact, and elevated costs—pose significant barriers to the broader application of HPC-LWC and reduce its long-term sustainability. Addressing these challenges remains a critical area of research, with a focus on optimizing mixture designs and exploring innovative materials to enhance the balance between performance, sustainability, and cost-effectiveness.

Interestingly, while reducing the amount of cement in concrete through its rational architectural design may seem like the most straightforward solution, this approach has not been pursued due to concerns about achieving comparable or superior mechanical properties with less material. Only limited and scattered studies have explored the development of concrete structures with hollow sections (Figure 1). Most of these studies design concrete structures with simplistic cellular or lattice architectures, often resulting in reduced compressive and flexural strengths [9, 10]. For example, Aghdasi et al. [10] investigated concrete elements with octet-truss cells. Despite its promise, their study revealed that solid concrete cubes achieved a significantly higher compressive strength of 128.3 MPa compared to the octet-truss cubic specimens, which exhibited a compressive strength of only 16.6 MPa [10]. This underscores a clear unmet need for a systematic and comprehensive metamaterial-based approach to concrete, focused on exploring rational designs that not only achieve lightweight and cement-efficient structures but also maintain acceptable mechanical performance.

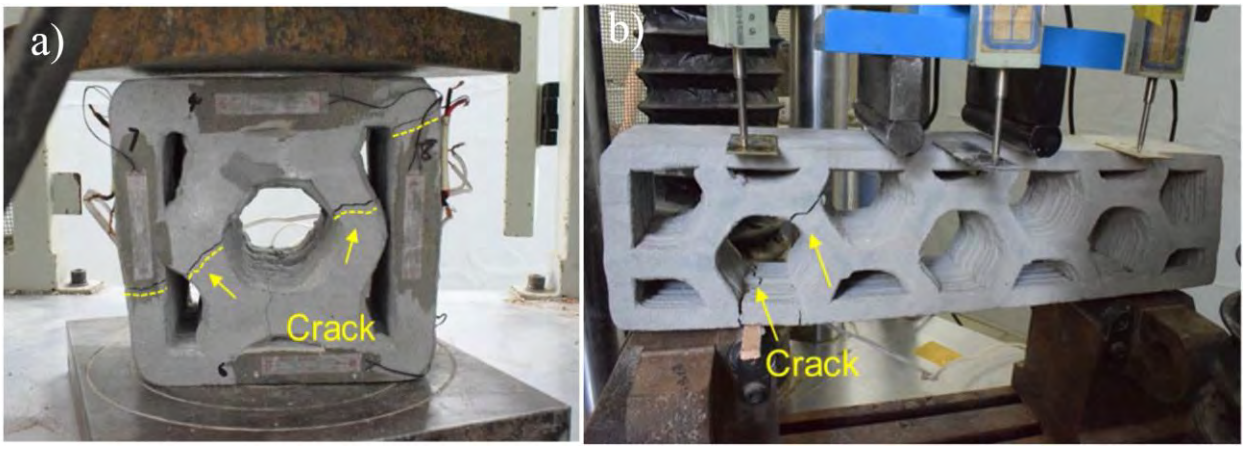


Figure 1. Failure patterns of unreinforced hollow honeycomb concrete structures during a) uniaxial compression and b) 3-point flexural tests [9].

Traditional reinforcement methods, such as labor-intensive steel rebar cages and the incorporation of discrete steel or polymer fibers, have long been utilized to enhance the ductility of LWC. While these techniques can improve certain mechanical properties, they are often accompanied by significant challenges that limit their overall effectiveness. One of the primary issues with fiber-based reinforcements is the uneven distribution of fibers within the concrete matrix, which leads to material heterogeneity and localized weak points. This inconsistency can compromise the predictability of the material's behavior under various loading conditions. Furthermore, traditional reinforcement methods often fail to provide adequate crack control, which reduces the tensile strength and fracture toughness of the final concrete structure [11, 12]. These limitations are particularly problematic in applications where precise mechanical performance and long-term durability are critical. In light of these challenges, emerging three-dimensional (3D) reinforcement techniques have garnered significant attention as a promising alternative to traditional approaches. Unlike conventional reinforcements, 3D systems involve integrating lattice-like or interconnected structures within the concrete matrix, offering enhanced ductility and superior crack control. Preliminary studies, such as those investigating octet lattice structures, have demonstrated that these innovative reinforcements can significantly improve the mechanical performance of concrete materials, particularly by increasing their ability to resist deformation and distribute stresses more evenly [13]. These findings suggest that 3D reinforcement could address many of the shortcomings associated with traditional methods.

1.2 Problem statement

Current studies dealing with designing LWC structures are limited in scope, focusing primarily on exploratory investigations rather than comprehensive, large-scale applications. The primary challenge in advancing LWC lies in achieving an optimal balance between low density and acceptable mechanical performance. The inclusion of LWA, while effective at significantly

reducing density, leads to a disproportionate loss of strength. This inherent trade-off severely limits the structural applications of LWC, particularly in load-bearing components for demanding scenarios such as multistory buildings, long-span bridges, and other large-scale infrastructure. Efforts to address these limitations, such as HPC-LWC mixtures, have succeeded in achieving high strengths but have introduced new challenges. These mixtures typically require increased cement paste content, leading to higher densities, greater environmental impact from cement production, and elevated initial costs. These factors collectively hinder the broad adoption of HPC-LWC, especially in cost-sensitive and sustainability-focused projects.

Innovative structural designs, such as hollow honeycomb configurations (Figure 1), have emerged as a promising alternative to traditional approaches. These designs enable moderate compressive strengths while significantly reducing weight, making them suitable for lightweight structural applications. However, the inherent lack of adequate reinforcement in these configurations results in limited ductility and susceptibility to cracking under flexural loading. Furthermore, attempts to increase the compressive strength of LWC often exacerbate its brittleness, highlighting the critical need for effective reinforcement strategies that enhance ductility, fracture toughness, and overall resilience. Traditional reinforcement methods, including labor-intensive steel rebar cages and the addition of discrete fibers (steel or polymer-based), have been employed to address these shortcomings. While these techniques provide some improvements in ductility and crack control, they are not without significant drawbacks. These include uneven distribution of fibers, resulting in material heterogeneity, insufficient crack control, and reduced predictability under structural loading. These limitations are particularly pronounced in applications requiring uniform mechanical behavior and high reliability, further restricting the use of LWC in critical structural engineering contexts. Recent advances in 3D reinforcement offer a promising avenue for addressing challenges in enhancing the mechanical performance of concrete materials. Despite some advancements in this field, it remains in its infancy and lacks a systematic framework for optimizing 3D reinforcement integration, particularly for LWC systems incorporating polymeric materials. Such materials present advantages in reducing weight and increasing flexibility, aligning with the broader goals of advanced concrete design.

A metamaterial design approach offers a compelling pathway to accelerate the development of innovative concrete systems by enabling precise tailoring of mechanical properties. For example, our recent work has demonstrated the feasibility of designing super-compressible metamaterial concrete systems using polymeric architected materials with self-recovering mechanisms [14], as illustrated in Figure 2. This success has inspired the vision for the proposed research, which aims to leverage similar metamaterial strategies to create LWC structures with tunable mechanical performance.

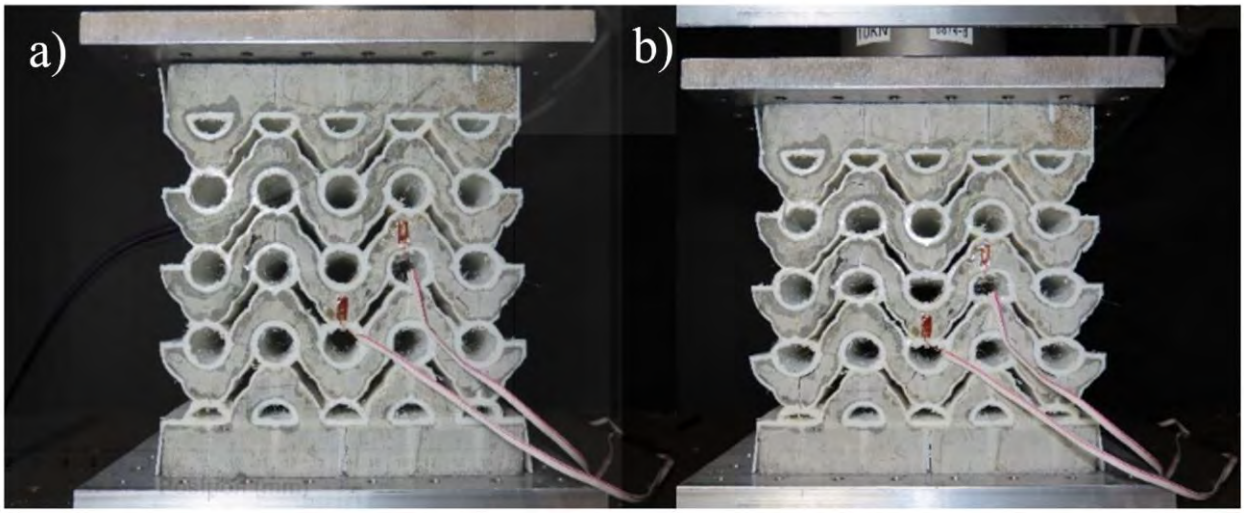


Figure 2. Super-compressible metamaterial concrete systems fabricated at the University of Pittsburgh with a) 3×3 unit cells b) 5×5 unit cells. The proposed concrete systems are tuned to achieve up to 15% compressibility under cycling loading [14].

Additionally, the use of polymeric 3D reinforcement in LWC systems has not been fully explored. Polymers offer unique benefits, including reduced weight, improved durability, and enhanced design flexibility. The application in 3D-reinforced LWC remains limited, leaving a critical gap in the development of lightweight, HPC systems capable of meeting the diverse needs of modern construction. The mechanical performance of LWC depends heavily on the specific requirements of its structural application, including the type of loading conditions and environmental factors it will encounter. As such, there is a growing need for materials with tunable properties, allowing for precise adjustments to compressive strength and ductility to suit particular use cases. This study aims to address these gaps by proposing a novel framework for the design of polymeric 3D-reinforced LWC systems. By systematically optimizing these materials, the research seeks to achieve a synergy of low density, high strength, and enhanced ductility, thereby overcoming the limitations of traditional LWC systems. This approach has the potential to significantly expand the applicability of LWC in structural engineering, offering sustainable, lightweight, and high-performance solutions for the challenges of modern construction.

1.3 Research plan

To tackle the issues listed above, the proposed research aims to address the critical challenges associated with LWC by developing a mechanical metamaterial (MM) technology that integrates rational architectural design. This approach seeks to create lightweight, high-performance structural elements for applications such as pavement systems, bridge decks, and prefabricated bridge components. By leveraging the principles of MMs, which derive their mechanical properties from the geometry of their microstructures rather than their chemical composition, the

research focuses on achieving a balance between low density, high compressive strength, and enhanced ductility. Two innovative design strategies are explored: (1) rational design to create cementitious MM-LWC structures, and (2) embedding polymeric MM lattices within the concrete matrix as 3D reinforcement elements. These designs can potentially allow full control over the mechanical response and density of LWC through precise manipulation of lattice properties, rather than altering the concrete mixture itself. We hypothesize that incorporating a metamaterial approach into the concrete design can create "structure-specific" designs with a significant reduction in density and cement usage, while maintaining the structural integrity of equivalent solid concrete volumes. The research plan can separate into two major parts:

1) Literature review

The first phase of this research involves a comprehensive literature review to examine the current state of LWC and MM research. The review focuses on recent advancements in LWC fabrication techniques, mix designs, and reinforcement strategies, with the goal of identifying their strengths and limitations. Particular attention is paid to the challenges of achieving a balance between low density, high compressive strength, and enhanced ductility in LWC. This includes an evaluation of the performance trade-offs inherent in current methods, such as the brittleness of high-strength LWC and the limitations of traditional reinforcement techniques like steel rebar cages and discrete fibers. Simultaneously, the study explores MM structures with exceptional mechanical properties, such as high stiffness-to-weight ratios and fracture toughness. These structures, defined by their rational architectural designs rather than their material composition, hold significant promise for improving the mechanical performance of LWC systems.

2) Experiment with hypothesis verification

The proposed experimental phases for designing and fabricating cementitious MM-LWC structures and LWC systems with embedded 3D polymeric MM reinforcements are designed to validate the research hypothesis. This first phase focuses on the creation of metamaterial LWC cubic specimens with high specific strength (strength-to-density ratio). Figure 3 shows the vision for the proposed metamaterial LWC systems with tunable mechanical performance. The unit cells forming the structure of MM-LWC can take various sizes and shapes. Identifying configurations for target performance requires exploring a design space with astronomically large potential configurations. To address this, we deploy an evolutionary generative artificial intelligence (GAI) paradigm to efficiently explore the design space for intricate metamaterial structures. We consider fine-grained concrete mixes to fabricate the MM structures. Specimens undergo uniaxial compression tests to assess their compressive strength (Figure 4). Control specimens in the form of solid cubic specimens are fabricated to serve as benchmarks. Finite element (FE) simulations are performed to enable prediction and optimization of performance in specimens.

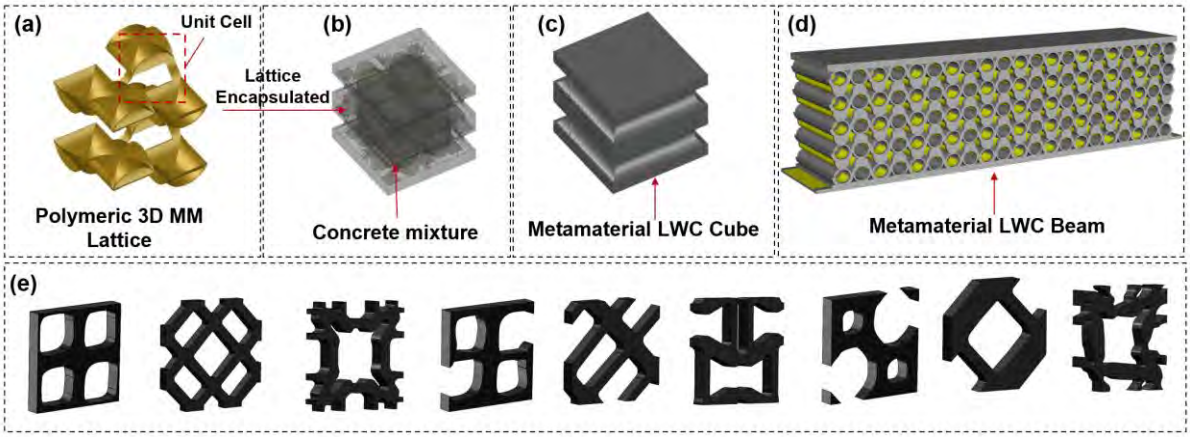


Figure 3. Vision for the proposed metamaterial LWC systems with tunable mechanical performance. a) Schematic representation of a polymeric MM lattice that can be encapsulated inside the concrete mix. b) X-ray showing the lattice encapsulated inside the concrete mix. c) A composite metamaterial LWC cube with embedded MM lattice. d) An auxetic metamaterial LWC beam with rational design of its unit cells. In this design approach, the concrete mix and the reinforcing lattice follow similar periodic patterns to form the auxetic structure. e) Examples of potential unit cell designs for 3D MMs, as reported in our recent study [15]. There are many potential MM structures that can be arranged in numerous ways over various length scales, and therefore the number of possible configurations rapidly approaches astronomical values.

The second experimental phase focuses on designing MM beams and verifying their performance through a series of three-point bending tests (Figure 4). The auxetic MM lattices serve as both a mold and a reinforcement for the matrix, creating a composite system where the lattice geometry dictates mechanical properties.

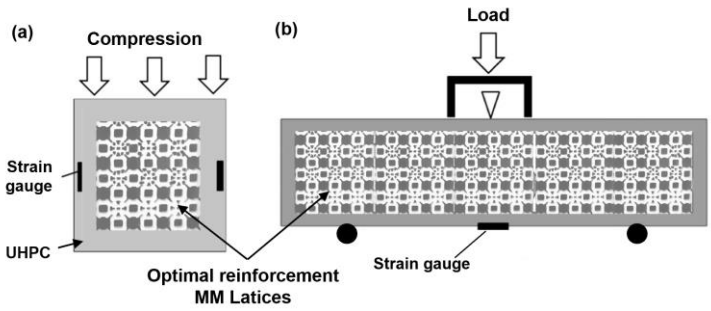


Figure 4. Schematic of compressive and flexural bending tests.

The experiments in both phases aim to verify the hypothesis that a metamaterial approach to concrete design can overcome the limitations of conventional LWC by providing tunable mechanical properties. By systematically comparing the mechanical properties of MM-LWC specimens with soil benchmark specimens, this research highlights the potential of the metamaterial paradigm for designing lightweight, high-strength, and cement-efficient structures.

2. State-of-art of the lightweight concrete and metamaterial research

2.1 Literature review of LWC

LWC is not a recent innovation but has historical roots extending back to ancient times. It served as a precursor to modern concrete technology, with one of the most prominent examples being the Pantheon in Rome, constructed around 128 A.D. The Pantheon stands as a testament to the advanced engineering of the era, demonstrating the intentional use of natural lightweight particles in concrete involves the methodical inclusion of natural LWA in opus caementitium [16]. Despite the widespread use of LWC during Roman times, its prevalence diminished after the Roman Empire, largely owing to the scarcity and inconsistency of volcanic aggregates essential for its production. The resurgence of LWC began in the late 19th and early 20th centuries, spurred by the advent of industrial production techniques for LWAs, a development that marked a pivotal moment in construction material technology [17]. Initially, this innovation was primarily directed toward military applications, such as the U.S. Navy's use of expanded aggregates for shipbuilding during World War I [18]. Notably, the USS Selma and 13 other LWC vessels were constructed during this period, showing the material's reliability. This success was further underscored during World War II, when 104 supply ships were built using LWC, establishing their reputation as a dependable material for large-scale engineering applications [19].

The establishment of the first commercial plant for expanded aggregates in Kansas in 1920 signaled the formal introduction of LWC into structural engineering [20]. This breakthrough enabled the construction of lightweight bridges and high-rise buildings, including iconic structures such as the Prudential Plaza Building and Marina City Towers in Chicago. By the mid-20th century, LWC had become a preferred material in structural engineering due to its ability to reduce dead loads, enhance design flexibility, and improve cost efficiency. However, its application remained primarily structural, with limited adoption in architectural designs. The global energy crisis of 1973 brought about a renewed focus on energy efficiency, leading to the implementation of energy-saving regulations in several countries, including Germany [21]. This shift in priorities highlighted the potential of LWC for meeting stricter thermal insulation requirements, driving further innovations in its technology and applications.

By the 1990s, LWC experienced a resurgence in popularity, fueled by advancements aimed at reducing its density while maintaining or enhancing its mechanical properties, such as strength and durability [22]. Among these advancements, infra-lightweight concrete (ILC) emerged as a transformative solution. ILC offered the dual benefits of fulfilling structural requirements and providing excellent thermal insulation, enabling the construction of monolithic wall designs without the need for additional insulation layers [23]. While regulatory challenges and the absence of standardized guidelines have somewhat limited its widespread application, ILC demonstrates significant potential as a commercially viable material that aligns with contemporary energy efficiency and environmental sustainability demands. Its ability to adapt to modern construction requirements underscores LWC's enduring relevance and its capacity to address the evolving needs of the built environment.

LWC has established itself as a versatile and increasingly important material in modern construction due to its ability to meet diverse structural and thermal performance requirements. However, varying definitions and classifications often lead to inconsistencies in terminology and specifications. Deviations in strength, density, and types of LWC are particularly notable, necessitating precision when referring to LWC. According to ACI 213R-14, "Guide for Structural Lightweight-Aggregate Concrete," structural LWC (SLC) is defined by a minimum cylinder strength of 17 MPa and an equilibrium density range between 1120 and 1920 kg/m³. Specified density concrete (SDC), on the other hand, requires no minimum strength but features an equilibrium density between 800 and 2240 kg/m³. High-strength LWC is classified as SLC with a compressive strength of 40 MPa at 28 days [3].

In Europe, LWC is governed under EN 206 and its applications are regulated by EN 1992. The minimum strength class for structural lightweight concrete (LC) begins at LC8/9, corresponding to characteristic cylinder and cube strengths of 8 MPa and 9 MPa, respectively. The design standard mandates a minimum strength class of LC12/13. For high-strength LC, such as LC70/77 or LC80/88, technical approvals are required in Germany due to limited practical experience. LC exhibits an oven-dry density between 800 and 2000 kg/m³, categorized into density classes with increments of 200 kg/m³. Importantly, strength and density classes cannot be freely combined, as specific strength classes require corresponding density classes for accurate definitions [24, 25]. Unlike other LWC types, LC features a dense cement matrix, making its surface visually indistinguishable from normal-weight concrete (NC), except on cut or damaged surfaces where LWA become apparent.

A distinct variation, lightweight aggregate concrete with an open structure (LAC), is defined in EN 1520 and features dry densities ranging from 400 to 2000 kg/m³. Strength classes for LAC range from LAC2 to LAC25, based on the characteristic strength of 100-mm cores drilled from structural elements. LAC is widely used in structural applications, such as loadbearing walls and roof elements, as well as in non-structural components like noise barriers. Its open structure is achieved by limiting cement paste content to bind aggregates only at contact points, resulting in defined voids. These voids, comprising about 10% of the total volume, differentiate LAC from standard LC, making it more porous and less dense [26]. Another recent innovation in LWC is infra-lightweight concrete (ILC), initially developed for marine applications like sandwich ship hulls and later adapted for construction. ILC exhibits a dry density below 800 kg/m³ and compressive strengths up to LC8/9. It features a fair-faced surface, allowing for monolithic external walls without additional insulation. Structurally, it resembles LAC with a porous matrix but requires extrapolated design rules due to its lower densities. Current efforts, such as those at Universität der Bundeswehr München, aim to standardize ILC under European Technical Approval (ETA) guidelines [27, 28].

The diverse classifications and properties of LWC demonstrate its adaptability to a range of construction needs. With densities ranging from 300 to 2000 kg/m³, compressive strengths between 1 MPa and over 60 MPa, and thermal conductivity values from 0.2 to 1.0 W/mK, LWC offers

significant advantages over normal-weight concrete, which typically features densities of 2100–2500 kg/m³, strengths of 15 MPa and higher, and thermal conductivities of 1.6–1.9 W/mK [29, 30]. These attributes make LWC indispensable in reducing dead loads, improving energy efficiency, and achieving sustainable construction goals across applications ranging from high-rise buildings and bridges to precast panels and marine structures.

LWA are integral components in the production of LWC, providing significant advantages such as reduced density, improved thermal insulation, and enhanced fire resistance compared to traditional aggregates. LWAs can be classified based on their origin as natural or manufactured. Natural LWAs include pumice, scoria, volcanic ash, and tuff, which are naturally porous and widely available in specific regions. Manufactured LWAs, such as expanded clay, shale, slate, perlite, and vermiculite, are created through processes like heating, expanding, pelletizing, or sintering. These processes cause the materials to develop cellular structures, resulting in reduced densities that typically range from 300 to 1200 kg/m³. Synthetic LWAs, including sintered fly ash and other industrial by-products, are also used for specialized applications, such as structural and insulating concrete. Standards like EN 13055 and ASTM provide guidelines for classifying and using LWAs in various LWC applications, ensuring their compatibility with construction requirements [3, 30].

EN 13055, the European standard, governs LWAs for use in LWC, specifying their origin and properties. It defines LWAs as being derived from natural materials, manufactured from by-products of industrial processes, recycled materials, or directly processed natural sources. Unlike EN 13055, ASTM standards provide explicit lists of covered LWAs, distinguishing them by their preparation processes. These include expanding, pelletizing, or sintering materials such as clay, slate, shale, fly ash, blast-furnace slag, and natural aggregates like pumice and scoria. Additionally, ASTM C331M identifies aggregates derived from coal or coke combustion as suitable for lightweight masonry concrete [3,32].

The ASTM standards also specify bulk density limits to distinguish lightweight from normal-weight aggregates. For structural applications, ASTM C330M sets upper limits for the loose bulk density of LWAs: 1120 kg/m³ for fine aggregates, 880 kg/m³ for coarse aggregates, and 1040 kg/m³ for a combination of fine and coarse aggregates. These properties allow the production of structural LWC with compressive strengths determined on cylindrical specimens, ensuring suitability for high-performance applications. EN 13055 aligns with these guidelines, setting loose bulk density limits at ≤1200 kg/m³ and particle density limits at ≤2000 kg/m³, encompassing very LWAs such as expanded perlite and exfoliated vermiculite. These ultra-light aggregates are primarily used in mortars, plasters, or concrete with a focus on thermal insulation rather than structural performance [29, 31].

While international standards cover a wide range of LWAs, there are notable exclusions. For instance, cold-bound LWAs, organic materials like wood chips, rubber crumbs, plastic beads, and expanded polystyrene (EPS) are not included in standardized specifications. These materials often require project-specific or technical approvals before being applied in practice[32]. Additionally,

recycling waste products such as rice husk ash, dredged silt, or polyethylene terephthalate (PET) waste are being investigated as potential LWAs, showing the industry's growing interest in sustainable alternatives [33]. However, the use of these materials is often limited to research and experimental applications rather than widespread industry adoption. A key property of coarse LWAs for LWC is their crushing resistance, as specified in EN 13055 [3]. This test, originally part of a Soviet standard, measures the resistance of LWAs under a compaction strain of 20%, primarily for production conformity control. It is important to note that the test's original purpose is quality assurance during production and not for predicting the end-use performance of LWAs in concrete. As highlighted in EN 13055, there is no direct correlation between the crushing resistance of an aggregate and the mechanical properties of the resulting LWC. Misusing this test for applications beyond its intended scope may lead to incorrect interpretations and flawed conclusions [34].

The broad range of LWAs covered by EN 13055 and ASTM standards ensures their applicability in both structural and non-structural LWC. Structural LWC applications include bridge decks, high-rise buildings, and precast panels, while non-structural uses include noise barriers, thermal insulation, and fire-resistant construction. The reduced weight and enhanced thermal properties of LWAs make them indispensable for modern sustainable construction. However, non-standard LWAs, such as organic or recycled materials, continue to evolve as experimental solutions, offering opportunities for innovation in LWC design. By adhering to international standards and leveraging the unique properties of LWAs, engineers can optimize the performance of LWC for diverse construction needs, from reducing structural loads to improving energy efficiency. The continued exploration of non-traditional LWAs and advancements in recycling technologies further highlight the potential for sustainable and innovative developments in this field.

The mix design of LWC fundamentally differs from normal-weight concrete (NWC) due to the predominant influence of LWAs, which account for a substantial portion of its properties such as strength, density, and durability [35]. LC mix proportioning requires careful consideration of boundary conditions like casting methods, equipment, and target performance criteria. For achieving a specific compressive strength, it is critical to select a coarse LWA with sufficient strength, as the strength of the LWA sets an upper limit for the achievable LC strength. Beyond this threshold, referred to as the "strength limit," the matrix properties (such as binder content and water-to-binder ratio) become secondary but still significantly influence the durability of LC. Standards like DIN 1045-2 emphasize the importance of choosing proper binder and water ratios for durability [36, 37]. A unique aspect of LC mix design is the need to account for the high water absorption of LWA. Coarse LWA typically absorbs significant amounts of water, with the "w60 value" indicating the water absorbed within 60 minutes [38]. Fine LWA, which can absorb 25–40% of its weight in water, poses an even greater challenge. If this water absorption is not adequately accounted for during mix design, uncontrolled water uptake from the matrix can lead to microcrack formation during the plastic stage, compromising the strength and durability of LWC. Proper pre-soaking of LWAs or adjusting the mix design to include additional water to offset absorption is essential. Current best practices recommend incorporating 70% of the absorption measured

according to DIN V 18004 in the design, which will also be reflected in the upcoming revision of EN 1097-6 [37].

For accurate mix design, LWC proportions must be expressed in volumetric terms (dm^3/m^3) rather than weight-based measures. This ensures proper representation of the material's air void content, which significantly impacts density and performance. ASTM C173 offers a standard method for measuring air voids, but it requires validation through yield and density measurements to differentiate between voids in the paste and those entrapped in the LWA. These factors are critical for ensuring conformity in practice [29, 31]. The production and availability of suitable LWAs significantly influence the cost and properties of LC. Naturally occurring LWAs, such as scoria, pumice, and diatomite, and artificial aggregates, including expanded clay, shale, slate, and industrial by-products like fly ash and recycled glass, are commonly used. Despite these options, production trends in LWAs have stagnated over recent decades, with ratios of sand and gravel (S&G) to LWA production increasing significantly [39]. Between 1975 and 2015, the S&G/LWA ratio grew from 15–21 to 30–36, indicating a declining share of LWC in the market, likely attributed to the increasing preference for NC in recent years [40]. While LC offers clear advantages in reducing density and improving thermal insulation, its mix design requires precise control over material properties, water absorption, and air content. Adherence to standards and innovative use of natural and recycled LWAs can enhance its competitiveness in the concrete market, despite current challenges in production and application.

The LWC market in the United States reflects a mix of opportunities and challenges, marked by its specialized applications and limited but promising adoption. LWC's notable advantages include reduced structural dead loads, enhanced thermal insulation, and significant sustainability benefits, such as lower carbon emissions and the incorporation of recycled materials. These attributes make it an appealing option for high-performance and eco-conscious construction. However, LWC occupies only 5–7% of the U.S. concrete market, with its growth hindered by higher upfront costs—25–30% more than NWC [41]. This cost disparity often overshadows the potential indirect savings LWC offers, such as reduced material and labor needs, enhanced durability, and better fire resistance. LWC is primarily used in high-value applications, such as bridge decks, long-span bridges, and high-rise buildings, where its weight reduction properties significantly influence project feasibility and cost efficiency. Prominent projects, such as the Pulaski Skyway rehabilitation, highlight its role in enabling lightweight retrofits and structural improvements. Geographically, its adoption is concentrated in urban regions with large-scale infrastructure demands, particularly in the Northeast, whereas rural areas and less industrialized regions have seen minimal uptake. Key challenges extend beyond cost to include technical concerns, such as pumpability, strength limitations, and variability in long-term performance. A lack of awareness and familiarity among designers and contractors further constrains adoption, while limited availability of LWAs and regional disparities in production exacerbate supply chain issues. Resistance to change within the construction industry, favoring traditional NWC, also slows LWC's broader implementation. Despite these barriers, LWC aligns well with modern priorities in

sustainable construction, offering energy efficiency and reduced environmental impact [42]. Expanding its market presence will require focused efforts to educate stakeholders, enhance the reliability and supply of LWA, and address misconceptions through rigorous research and development. Integrating LWC into building codes, certifications, and green initiatives, alongside targeted marketing campaigns, can further accelerate its adoption, unlocking its full potential across diverse construction applications.

The LWC market is experiencing notable growth on a global scale, with its value estimated at approximately USD 30.81 billion in 2023 and projected to reach USD 48.87 billion by 2032, reflecting a compound annual growth rate (CAGR) of 5.26% during the forecast period [43]. This expansion is driven by the increasing demand for innovative construction materials that offer weight reduction, thermal insulation, and sustainability. In the United States, the adoption of LWC has been particularly significant in infrastructure projects, including bridges and high-rise buildings, where its ability to lower dead loads and enhance structural performance provides considerable advantages. Although specific market size data for the U.S. is limited, the nation's focus on sustainable construction practices and ongoing investments in infrastructure development suggest a strong and positive growth trajectory for LWC applications in both traditional and emerging construction markets [44].

The LWC market offers diverse applications in both structural and non-structural sectors, leveraging its benefits of reduced weight, improved thermal insulation, and environmental advantages. In the United States, LWC is extensively utilized in infrastructure projects such as bridge decks, high-rise buildings, offshore platforms, and architectural designs [43]. Its ability to minimize dead loads makes it particularly effective for retrofits and long-span structures, exemplified by its application in projects like the Pulaski Skyway rehabilitation. These characteristics underscore its value in achieving cost-effective and structurally efficient solutions for demanding projects. In residential and commercial construction, LWC is a preferred material for exterior walls due to its ability to combine load-bearing functionality with thermal insulation, contributing to energy-efficient designs. Its aesthetic potential, particularly with fair-faced finishes, further enhances its appeal in architectural applications. Innovations like infra-lightweight concrete (ILC) have expanded the market, allowing ultra-lightweight solutions with densities under 800 kg/m^3, which meet both structural and insulation needs [28, 35].

However, the LWC market faces notable challenges. High material costs and the limited availability of LWAs significantly impact its adoption. Technical difficulties, such as managing LWA's high water absorption and ensuring pumpability, require skilled expertise and advanced mix designs. Despite these barriers, the market is poised for growth due to increasing interest in sustainable construction and evolving production techniques. Addressing logistical constraints, improving aggregate availability, and raising awareness of LWC's multifaceted benefits are critical steps. Future initiatives are likely to focus on integrating LWC into mainstream construction practices, driven by its alignment with green building standards and innovative applications.

2.2 Literature review of MMs

The mechanical properties of materials are fundamental to the field of material science, underpinning a wide range of applications in engineering and technology. These properties have been rigorously studied due to their pivotal role in determining how materials perform under various conditions. Historically, the enhancement of mechanical properties has been achieved predominantly by altering the material's composition to optimize attributes such as strength, elasticity, and toughness [45]. In natural materials, there is often a well-defined relationship between physical and mechanical properties, commonly explained by the power-law. For instance, denser materials tend to exhibit higher strength, illustrating the direct correlation between these properties. This intrinsic relationship provides a predictable framework for understanding and developing material performance [46]. However, while this correlation is prevalent, it also imposes limitations on the ability to independently control mechanical and physical properties, spurring innovation in the design of engineered materials.

However, certain natural materials possess remarkable properties that are unattainable with conventional natural or synthetic materials. Cellular materials, such as bones, sponges, and honeycombs, have evolved over millions of years to achieve highly optimized architectures. These structures exemplify the intricate balance between material composition and geometry, resulting in properties that outperform many artificial materials in specific applications. For instance, the porous structure of bone exhibits a carefully engineered density gradient and network of complexly formed ligaments. This architecture enables bones to achieve exceptional structural efficiency, far surpassing that of most human-made cellular materials [47]. The synergy of optimized architecture and material composition allows natural cellular materials to combine lightweight properties with high strength and durability, making them ideal for applications requiring a balance of load-bearing capacity and material efficiency. This has inspired the development of bioinspired and architected materials, seeking to replicate or even improve upon these naturally evolved designs.

Metamaterials, on the other hand, are artificially engineered structures specifically designed to display properties that do not occur in natural materials. Although the concept of leveraging architecture to enhance material properties has existed for decades, the introduction of advanced fabrication technologies, such as 3D printing and other additive manufacturing techniques, has transformed the field. These advancements allow for the creation of highly intricate designs at micro- and nano-scales, enabling unprecedented control over the material's mechanical and physical properties across a variety of materials and scales. Initially, metamaterials found applications in fields like electromagnetism and optics, where they were used to manipulate electromagnetic waves in ways previously thought impossible, such as creating negative refractive indices [48]. More recently, the concept of "mechanical metamaterials" has emerged, offering a new frontier in material science. Unlike traditional materials, MMs derive their unique properties from their engineered internal architectures rather than their composition. This emerging field has gained significant traction as it explores novel ways to achieve properties like negative Poisson’s

ratio (NPR), tunable stiffness, and high energy absorption, revolutionizing applications in fields ranging from aerospace and robotics to biomedical engineering.

Historically, the exploration of MM was limited to a few specific categories. However, advancements in micro- and nano-scale design have enabled the development of a wide variety of MMs with extraordinary and often unprecedented properties. By precisely tailoring the topology and internal architecture of these materials, researchers have unlocked the ability to achieve distinctive mechanical and physical behaviors, including tunable stiffness, NPR, negative compressibility, zero shear modulus, and even programmable responses. These breakthroughs significantly expand the material design space, offering unprecedented flexibility in achieving specific performance criteria. As a result, MMs are now being applied in diverse fields such as aerospace, where lightweight and strong materials are critical; medical devices, where tailored mechanical properties can enhance biocompatibility and functionality; and energy absorption systems, where advanced damping and impact resistance are required. These innovations not only solve longstanding challenges in traditional material science but also open doors to entirely new applications, redefining the possibilities in material engineering [47].

The convergence of advanced manufacturing technologies and theoretical advancements in material architecture has marked the dawn of a transformative era in material science. MMs, with their architecturally engineered properties, are redefining the principles of structural efficiency and multifunctionality. These materials offer highly customizable solutions to address complex challenges across a wide range of industries, including aerospace, robotics, biomedical engineering, and energy systems. As research continues to advance, the focus is shifting towards exploring nonlinear mechanical behaviors, adaptive responses, and dynamic functionalities in these materials. This includes the development of programmable metamaterials capable of altering their properties on demand, self-healing systems that can recover from damage, and materials that respond intelligently to environmental stimuli such as temperature, pressure, or electromagnetic fields. Such innovations not only enhance performance in existing applications but also enable entirely new functionalities, such as shape-shifting structures, energy harvesting systems, and highly efficient vibration and impact mitigation solutions. The ongoing integration of computational modeling, additive manufacturing, and experimental validation is expected to further accelerate progress in the field. These synergies will likely unlock even more advanced capabilities, paving the way for metamaterials to become indispensable in future technologies. Ultimately, MMs are poised to revolutionize the way materials are designed, fabricated, and utilized, offering unprecedented opportunities to tackle some of the most pressing challenges in science and engineering.

2.2.1 Metamaterial types

2.2.1.1 Electromagnetic metamaterials

Electromagnetic (EM) metamaterials are an innovative class of materials designed to achieve electromagnetic properties that surpass those found in natural materials. By manipulating the

microscopic parameters of permittivity (ε) and permeability (μ), these materials can be classified into distinct categories based on their electromagnetic response [49]. EM metamaterials are particularly notable for their ability to achieve properties such as negative permittivity, high or negative magnetic permeability, and even negative refractive index. These characteristics are directly influenced by the structural elements, geometrical configurations, dimensions, and operational frequencies of the materials [50]. These extraordinary properties enable precise control over electromagnetic wave behavior, including bending light in unconventional ways, focusing beyond the diffraction limit, and creating electromagnetic cloaks that render objects effectively invisible. Such capabilities open a wide range of applications, including ultra-high-resolution imaging with perfect lenses, advanced stealth technologies for radar evasion, efficient antennas, and energy harvesting systems. The transformative potential of EM metamaterials lies in their versatility to manipulate multiple wave parameters, such as amplitude, phase, polarization, and frequency, making them essential in modern telecommunications, medical imaging, and beyond.

EM metamaterials are categorized into classical and quantum regimes [51]. In the classical domain, effective medium theory serves as the foundation for designing materials capable of controlling wave characteristics. However, traditional classical metamaterials often suffer from fixed functionalities and lack adaptability. To address this, the concept of information metamaterials has emerged, integrating digital coding and programmable architectures. These advanced designs enable real-time reconfiguration of electromagnetic properties, allowing for adaptive responses to changing environmental or operational conditions. The incorporation of artificial intelligence into these systems has further evolved them into intelligent metamaterials, capable of making autonomous adjustments. This leap from static to dynamic systems has revolutionized applications in fields like adaptive optics, smart sensor networks, and next-generation telecommunications.

In the quantum regime, topological metamaterials and quantum metamaterials have emerged as groundbreaking innovations. Topological metamaterials leverage the principles of topological states to robustly guide electromagnetic waves, even in the presence of defects or environmental disorder [52, 53]. This resilience makes them ideal for precision applications, such as fault-tolerant waveguides and secure communication networks. Meanwhile, quantum metamaterials are designed to manipulate quantum states, enabling control over phenomena such as superposition, entanglement, and quantum coherence. These capabilities are critical for advancing quantum information processing, secure quantum communication, and highly sensitive quantum sensing systems.

By bridging classical and quantum paradigms, EM metamaterials expand their potential far beyond traditional applications. In imaging, they enable sub-wavelength resolution, surpassing diffraction limits for applications like high-resolution medical diagnostics. In defense, they enhance electromagnetic cloaking technologies, improving stealth capabilities. Furthermore, their precision and adaptability position them as transformative tools in advanced sensor design, energy-efficient systems, and quantum computing. The ongoing integration of dynamic programmability, artificial intelligence, and quantum mechanics into metamaterials is redefining their scope and impact. From

enabling real-time environmental adaptability to controlling quantum states for cutting-edge technologies, EM metamaterials represent a cornerstone for future innovations in science and engineering. As research continues to push the boundaries of these materials, they hold the promise of revolutionizing industries ranging from healthcare to telecommunications, aerospace, and beyond.

2.2.1.2 Photonic or optical metamaterials

Photonic or optical metamaterials are a class of artificially engineered materials designed to manipulate and control light waves at optical frequencies, achieving functionalities beyond those of natural materials. These metamaterials operate by tailoring their nanoscale structures to interact with electromagnetic waves at visible, infrared, and ultraviolet wavelengths, enabling extraordinary optical properties such as a negative refractive index, zero refractive index, super-resolution imaging, and invisibility cloaking. Unlike conventional materials, photonic metamaterials can bend light in unconventional ways (e.g., negative refraction), focus light beyond the diffraction limit, and guide electromagnetic waves around objects to create cloaking effects. These properties are made possible by the periodic architecture of these materials, with common designs including split-ring resonators, fishnet structures, and plasmonic nanostructures [49].

A notable feature of photonic metamaterials is their ability to achieve zero or negative values for the refractive index, which leads to unconventional reflection and transmission of light. For instance, Figure 5. illustrates the fundamental difference in light beam reflection between ordinary materials with a positive refractive index and artificially enhanced materials like photonic metamaterials, which exhibit a negative refractive index [54]. These unique optical properties enable transformative applications, ranging from super lenses for high-resolution imaging in medical diagnostics and biological research to compact photonic circuits for advanced optical communication systems. Photonic metamaterials are also integral to stealth technologies, enabling radar and infrared invisibility, as well as solar energy harvesting, where they enhance light absorption and efficiency.

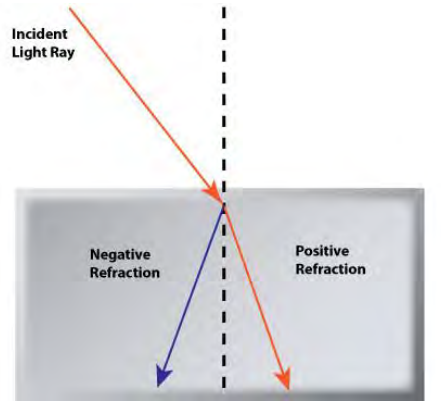


Figure 5. Positive index (ordinary material) and negative index materials [54].

Despite their groundbreaking potential, photonic metamaterials face challenges in large-scale fabrication due to the complexity of their nanoscale designs, high energy losses (particularly in metallic components), and the difficulty of achieving broadband and dynamically tunable functionality. Addressing these limitations requires advances in nanofabrication techniques, material innovation, and integration with adaptive technologies [55]. Progress in these areas promises to unlock the full potential of photonic metamaterials, paving the way for innovations in imaging, energy harvesting, quantum computing, and telecommunications. Their ability to redefine the interaction between light and matter positions photonic metamaterials as a cornerstone for future breakthroughs in science and engineering.

2.2.1.3 Mechanical metamaterials

Mechanical metamaterials are an advanced class of artificially engineered materials designed to achieve exceptional mechanical properties through their internal architectures rather than their material compositions. These materials are characterized by micro- or nanoscale structures that enable unique behaviors such as an NPR (auxetic behavior), tunable stiffness, negative compressibility, and zero or programmable shear modulus. Unlike traditional materials, whose mechanical performance is dictated by their chemical composition, MMs derive their properties from tailored geometries and structural designs [47]. Common architectures include lattice frameworks, cellular structures, and origami-inspired designs, allowing for extraordinary properties such as superior energy absorption, vibration isolation, and lightweight stiffness.

The applications of MMs are vast and transformative. In aerospace, they provide lightweight, high-strength materials for structural components. In biomedical engineering, they enable the creation of implants and scaffolds that replicate the mechanical properties of natural tissues, promoting better integration and functionality. In robotics, they contribute to the development of soft and flexible mechanisms capable of complex movements. Despite their potential, challenges remain, particularly in scaling up fabrication techniques and ensuring reliability under various loading conditions. However, advances in additive manufacturing and computational design are addressing these issues, making MMs a cornerstone of future innovations in materials science. These materials exemplify how architectural engineering can unlock new mechanical properties, positioning them as critical tools in solving complex engineering challenges.

- Extremal mechanical metamaterials
  Extremal mechanical metamaterials are a unique class of engineered materials designed to exhibit extraordinary mechanical properties by being extremely stiff in certain deformation modes while remaining highly flexible in others. This behavior is governed by the eigenvalues of their elasticity tensors, where a very large eigenvalue corresponds to stiffness and a very small eigenvalue indicates compliance in the associated deformation direction. The number of near-zero eigenvalues determines the classification of these metamaterials: unimode, bimode, trimode, quadramode, and pentamode. Unimode

extremal materials have one very small eigenvalue, while pentamode materials have five, making them highly flexible in five of the six principal directions [48]. Among these categories, pentamode metamaterials have received significant attention due to their unique ability to decouple bulk and shear modulus. Pentamode metamaterials (Figure 6.) possess a very high bulk modulus compared to their shear modulus, resulting in near-constant volume during deformation. This characteristic allows their Poisson's ratio to approach 0.5, the theoretical maximum [55]. These designs, realized through advanced fabrication techniques such as 3D printing, provide near-ideal properties for applications in wave manipulation, including acoustic cloaking and elastic wave steering, as well as in lightweight, load-bearing structures.

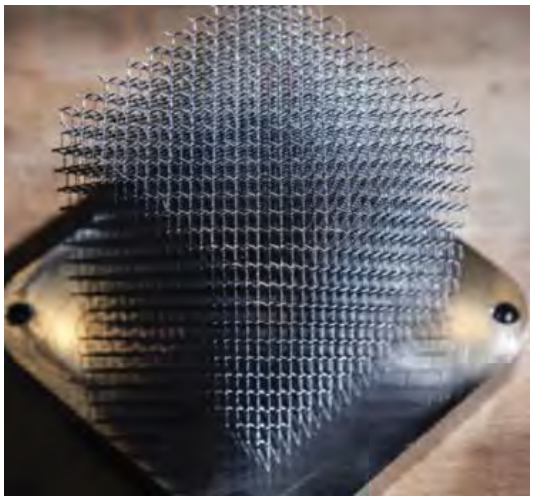


Figure 6. Penta-mode metamaterial [46].

Conversely, unimode metamaterials (Figure 7.), such as auxetic materials, exhibit the opposite mechanical behavior. These materials have a high shear modulus and an extremely low bulk modulus, resulting in a Poisson's ratio of -1, the lowest theoretical value [47]. This behavior means that unimode metamaterials deform by scaling uniformly without altering their overall shape. Auxetic materials have applications in impact resistance, energy absorption, and enhanced flexibility, making them suitable for use in protective gear, biomedical implants, and dynamic load-bearing systems.

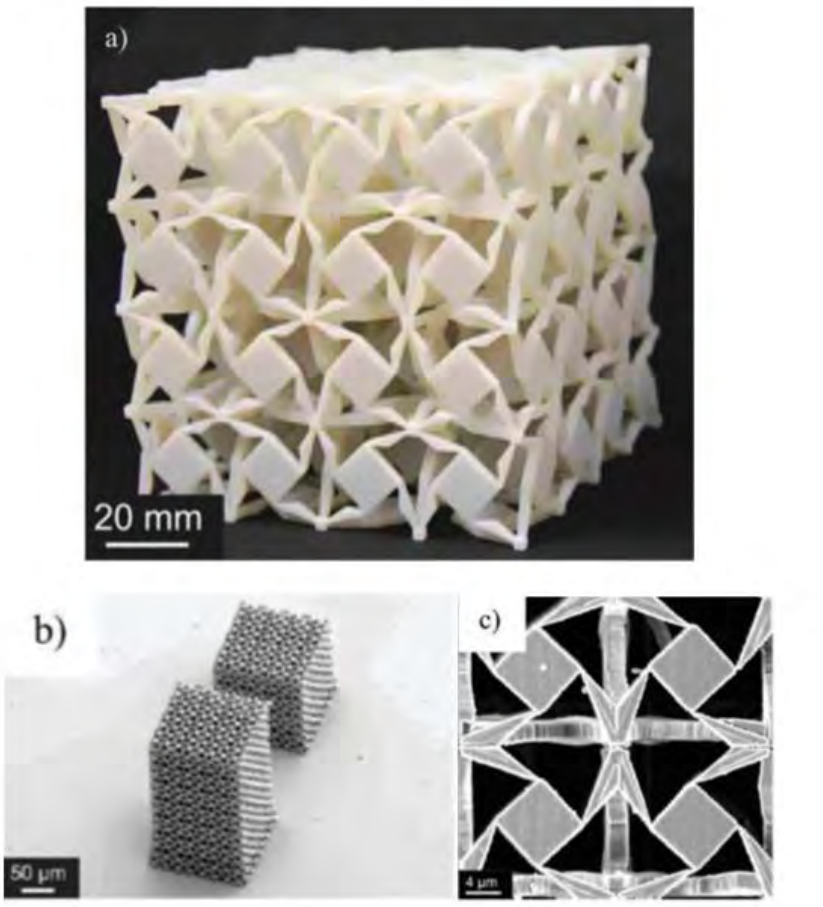


Figure 7. a)A three dimensional auxetic metamaterial (unimode metamaterial) at macroscopic scale, b) and c) at microscopic scale [47].

The comparison between pentamode and unimode metamaterials highlights their complementary roles in engineering applications. Pentamode metamaterials, often referred to as "meta-fluids," are ideal for scenarios requiring compliance in multiple directions, while unimode materials excel in isotropic deformation resistance. Together, they represent the extremes of mechanical behavior and expand the design possibilities for materials with highly specialized functionalities [46, 56]. Despite their remarkable properties, the development of extremal MMs faces challenges, including the precision required in fabrication, scalability for industrial applications, and maintaining structural integrity under complex loading conditions. Advances in additive manufacturing, computational modeling, and material science are gradually overcoming these hurdles. The ability to independently tune bulk and shear moduli in extremal metamaterials offers transformative opportunities across various fields, including aerospace, biomedical engineering, robotics, and acoustic technologies. By leveraging their unique mechanical properties, extremal MMs are paving the way for innovative solutions to complex engineering challenges, driving forward the frontier of material science.

- Negative mechanical metamaterials

  Negative mechanical metamaterials are a remarkable category of artificially engineered materials designed to exhibit unconventional mechanical properties that challenge the traditional principles of continuum mechanics. These properties include negative Poisson's ratio (auxetic behavior), negative compressibility, and negative stiffness. Such behaviors are typically not found in natural materials and arise from the carefully tailored architecture of these metamaterials rather than their composition. These unique mechanical properties enable applications that are unattainable with conventional materials, making negative MMs an area of significant research and technological interest.

  One notable property of negative MM is negative compressibility, which occurs when a material expands under hydrostatic pressure rather than contracting as conventional materials do. This counterintuitive behavior results in negative volume compressibility, meaning the material increases in size when external pressure is applied. This property can be achieved by using cellular structures, such as hexagonal honeycombs, or through combinations of materials with contrasting mechanical properties. The behavior of a system with negative compressibility compared to a conventional material, demonstrating how negative metamaterials expand under pressure while conventional systems shrink (Figure 8.) [57, 58]. Materials with negative compressibility are often engineered using composite systems. For example, Gatt and Grima (2008) demonstrated a design where multiple materials are combined to create a structure capable of exhibiting negative compressibility [57]. Such designs leverage the differences in mechanical properties between the constituent materials to produce this counterintuitive behavior. Although materials with negative compressibility are theoretically unstable, practical stability can be achieved by imposing appropriate constraints, enabling their use in real-world applications.

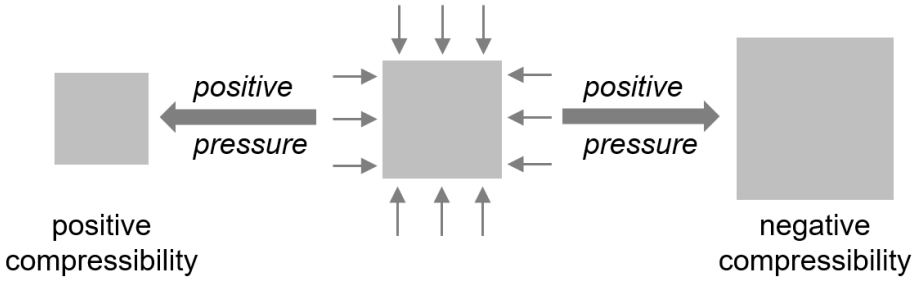


Figure 8. Unlike conventional systems (left), which contract under increasing pressure, systems exhibiting negative compressibility (right) expand in response to an increase in external pressure [57].

Another extraordinary property of negative MM is negative stiffness, where the direction of deformation opposes the applied force. For conventional materials with positive stiffness, deformation occurs in the direction of the applied force, and internal forces resist the deformation to maintain the original geometry. However, in materials with negative

stiffness, the internal forces act in the same direction as the applied load, amplifying the deformation [59]. As a result, negative stiffness materials exhibit much greater deformation under similar loading conditions compared to their positive stiffness counterparts. While negative stiffness materials are inherently unstable when used alone, combining them with positive stiffness materials can produce composites with extraordinary mechanical properties. For example, these composites can achieve high stiffness and high damping ratios simultaneously—an otherwise unattainable combination for conventional materials. In engineering, higher stiffness is typically associated with lower damping, and materials with high damping are often less stiff. By integrating negative stiffness materials into composite designs, it becomes possible to create systems that are both stiff and capable of absorbing significant amounts of energy, making them ideal for applications such as vibration isolation.

The equivalent stiffness of such composite systems can be calculated using the following formula:

$$Equivalent\ K = \frac{1}{\frac{1}{k_-} + \frac{1}{k_+}} \tag{1}$$

Here, k- and k+ represent the stiffness of the negative and positive stiffness materials, respectively. As the absolute values of k- and k+ approach each other, the equivalent stiffness approaches infinity. This result indicates that the composite material can achieve extremely high stiffness. However, such configurations require stabilization through external constraints to ensure practical usability [47].

Negative MMs offer numerous applications across various fields, thanks to their unique mechanical behaviors. Materials with negative compressibility can be used in adaptive structures, energy absorption systems, and responsive materials that change shape or size under pressure. Negative stiffness materials, when combined into composites, provide excellent vibration isolation and energy dissipation capabilities, making them suitable for high-performance damping systems in aerospace, automotive, and seismic engineering. Despite their potential, several challenges remain. The inherent instability of negative stiffness and negative compressibility materials must be mitigated through design strategies and constraints. Additionally, fabricating these materials at scale with the required precision is a significant obstacle, particularly for complex architectures. Ensuring consistent performance under dynamic and real-world loading conditions is another critical area of focus.

Negative MMs represent a transformative innovation in material science, defying conventional mechanical behaviors to achieve unprecedented properties such as negative compressibility and negative stiffness. By leveraging carefully engineered architectures and composite designs, these materials enable applications in energy absorption, vibration isolation, and adaptive systems. Ongoing advancements in additive manufacturing,

computational modeling, and design optimization continue to push the boundaries of what is achievable with these extraordinary materials, positioning them as a cornerstone of future engineering and technological breakthroughs. With continued research and development, negative MMs are poised to address complex engineering challenges and redefine the possibilities of material science.

- Ultra-property MMs

  Ultra-property MMs are an exceptional class of materials designed to achieve mechanical properties that are simultaneously extreme and previously unattainable in traditional materials. By utilizing architected micro- and nano-scale structures, these metamaterials overcome the inherent trade-offs between properties like stiffness, toughness, strength, and density. Traditional materials often face conflicts, such as the inverse relationship between strength and toughness, making it nearly impossible to combine these characteristics within a single material. However, ultra-property MMs provide a groundbreaking solution, enabling properties like ultra-high stiffness-to-weight ratios, ultra-strength, ultra-toughness, and ultra-lightweight structures to coexist [46].

  For example, ultra-light metamaterials can achieve remarkable recoverability after deformation while maintaining ultra-low density. This feature is particularly valuable for applications requiring minimal weight without sacrificing mechanical performance, such as in aerospace and automotive industries. These metamaterials are engineered with specialized architectures like hierarchical lattices, origami-inspired folds, and auxetic (NPR) structures [47]. These designs provide precise control over localized mechanical behavior, enabling them to address specific engineering challenges effectively. Hierarchical lattices enhance energy dissipation and improve durability under catastrophic loading, while auxetic structures expand laterally under tension, offering exceptional flexibility and impact resistance. Figure 9. illustrates an example of an ultra-light metamaterial exhibiting exceptional recoverability [47].



Figure 9. Ultra-light metamaterial showing exceptional characteristics of ultra-low density and remarkable recoverability [47].

Applications of ultra-property MMs are vast and transformative. In aerospace, these materials reduce structural weight while maintaining high strength, improving fuel efficiency and performance. In protective gear and crash-resistant structures, their energy absorption capabilities provide superior impact mitigation. In robotics, tunable properties like programmable stiffness and morphing capabilities allow for the creation of adaptive actuators and flexible mechanisms. Furthermore, in biomedical engineering, their biomimetic properties facilitate the design of implants, scaffolds, and prosthetics that mimic natural tissue behavior, enhancing integration with biological systems and promoting healing [46, 47].

Despite their promise, challenges remain in scaling up the fabrication of ultra-property MMs for widespread use. Complex architectures often require nanoscale precision, which can be costly and time-intensive. Additionally, ensuring consistent performance under multi-directional and dynamic loading conditions is an ongoing research focus. Advances in additive manufacturing, multi-material 3D printing, and computational design are gradually addressing these obstacles, allowing for more complex, scalable, and cost-effective production of these metamaterials. Ultra-property MMs are reshaping the boundaries of materials science by offering solutions that combine extreme mechanical properties in unprecedented ways. Their innovative architectures and multifunctional capabilities open up new opportunities across industries, from aerospace and robotics to biomedical devices and protective systems. As fabrication technologies and computational tools continue to advance, ultra-property MMs are set to revolutionize material design,

offering transformative solutions for some of the most demanding engineering challenges of the modern era.

2.2.2 Fabrication methods

The development of MMs has been greatly facilitated by advancements in 3D printing technologies, which enable precise control over micro- and nanoscale architectures. Among the various methods available, ink extrusion and photopolymerization are two of the most commonly used techniques for fabricating MMs, known for their versatility and ability to create intricate designs. MMs can be synthesized using a range of fabrication techniques; however, one of the most effective and widely adopted approaches is Additive Manufacturing (AM). Also known as 3D printing, additive manufacturing encompasses various processes that build structures by adding raw material layer by layer, allowing for exceptional precision and complex geometries. Additive manufacturing techniques are broadly categorized into three main classes: ink extrusion, photopolymerization, and powder fusion methods. These approaches provide unique advantages for tailoring MMs to meet specific functional and structural requirements, making them indispensable in this field.

- Ink extrusion
  Ink extrusion 3D printing is a widely used technique for fabricating MMs, involving the layer-by-layer deposition of raw material through a nozzle onto a substrate or bed. This method is particularly effective for creating complex, porous, or lattice-like structures and supports a broad range of materials, including polymers, ceramics, and composites. One of the most common variants of this technique is Fused Deposition Modeling (FDM), where a thermoplastic filament, such as Polylactic Acid (PLA), Polycarbonate (PC), or Acrylonitrile Butadiene Styrene (ABS), is heated to its melting point and extruded through a heated nozzle [60]. The extruded material is deposited onto the substrate, where it rapidly cools and solidifies, forming the base for subsequent layers. FDM is known for its scalability, cost-effectiveness, and compatibility with large-scale metamaterial fabrication, though its resolution is limited to mesoscale structures (Figure 10). Another prominent method under ink extrusion is Direct Ink Writing (DIW), which uses viscoelastic or viscoplastic inks, typically polymer solutions or melts, extruded through a micro nozzle onto a bed using external forces [47]. These forces can be applied through hydraulic pressure, pressurized gas, screws, or other mechanical means. DIW enables precise control over material deposition, allowing for intricate designs and multi-material structures with tailored properties. While ink extrusion methods are versatile and scalable, they are more suited for mesoscale features rather than nanoscale precision. Their ability to fabricate functionally graded materials and integrate multiple material types makes them indispensable for metamaterial fabrication in applications requiring customized mechanical properties [47].

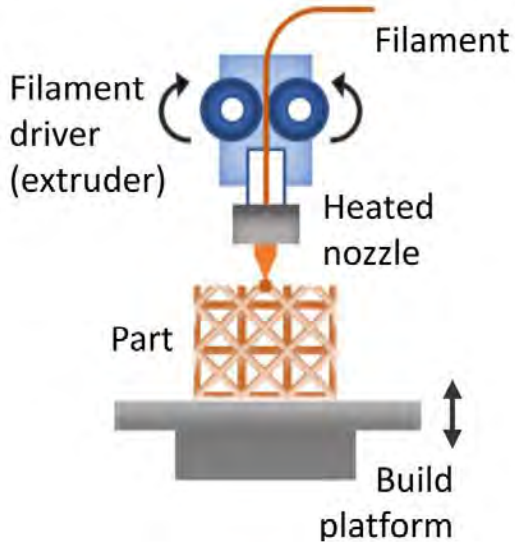


Figure 10. Schematic illustration of the FDM process [47].

- Photopolymerization

  Photopolymerization 3D printing is a light-based technique widely used for fabricating MMs, particularly at the micro- and nanoscale. This method employs a focused light source, such as a laser or UV light, to cure liquid photopolymer resin layer by layer, transforming it into solid structures. Compared to ink extrusion methods, which are constrained by nozzle dimensions and result in limitations on feature resolution and overall size, photopolymerization techniques are not restricted by these dimensional factors. This allows for the creation of finer and more intricate features, making photopolymerization ideal for applications requiring high precision and complex geometries [47].

  Stereolithography (SLA), one of the earliest and most established photopolymerization methods, uses a high-powered UV laser to cure and harden a photocurable resin, producing high-quality solid parts layer by layer. Another widely adopted technique is Digital Light Processing (DLP), which uses a digital micromirror device to project patterns of UV light, enabling the simultaneous curing of entire layers, improving speed and accuracy [59]. Both SLA and DLP are extensively used for fabricating MMs with intricate lattice structures, such as biomedical scaffolds, optical metamaterials, and highly detailed components for engineering applications. Recent advancements in photopolymerization have further enhanced its capabilities. Techniques like Two-Photon Lithography (TPL), Projection Micro Stereolithography (PμSL), and Continuous Liquid Interface Production (CLIP) allow for the fabrication of even more complex structures with finer details and improved quality [60]. These methods expand the range of applications by enabling the production of highly intricate designs that were previously unattainable. However, photopolymerization remains somewhat limited in terms of material diversity, as it is primarily restricted to photopolymers. Ongoing research and development are addressing this limitation by expanding the material palette to include composites and functional materials [48].

Photopolymerization 3D printing is a powerful tool for manufacturing high-resolution and complex MMs. Its ability to overcome dimensional constraints and produce intricate structures positions it as a key technology in fields like biomedical engineering, optics, and advanced material design. With continued innovation, photopolymerization techniques are expected to push the boundaries of precision manufacturing even further.



Figure 11. The SLA printing machine [60].

- Power fusion

  Power fusion is the process of combining lighter atomic nuclei to form a heavier nucleus, releasing immense amounts of energy in the process. This reaction, which powers stars like the Sun, is seen as a clean, sustainable, and nearly limitless energy source for humanity. The most promising fusion reaction involves hydrogen isotopes—deuterium and tritium—which fuse under extreme temperatures and pressures to form helium and high-energy neutrons, releasing 17.6 MeV per reaction [61]. Achieving this requires temperatures exceeding 100 million degrees Celsius to overcome the Coulomb barrier, using methods such as magnetic confinement (tokamaks or stellarators) or inertial confinement (laser compression). Power fusion offers abundant fuel sources, high energy density, minimal waste, and inherent safety, but challenges include achieving net-positive energy output, extreme plasma conditions, material durability, and economic scalability. Projects like ITER in France and advancements in inertial confinement are driving progress, positioning fusion as a cornerstone of future energy systems.

  Conversely, powder fusion is a laser-based manufacturing technique primarily used in additive manufacturing (3D printing) to fuse powder particles into solid structures. In this process, a laser melts or sinters powder particles layer by layer, often using a binding agent, to create highly detailed components. A common example is Selective Laser Sintering (SLS), where polymeric powders are distributed in a powder bed, fused layer by layer, and shaped with precision [62]. Figure 12. Schematic representation of the Selective Laser Sintering (SLS) process [61]. Factors such as powder size, shape, and distribution critically

influence the resolution and quality of the printed object. Smaller powders yield thinner fused layers and higher resolutions. Variants like Direct Metal Laser Sintering (DMLS) use metallic powders, enabling the creation of metal components with high strength and complexity. Other related methods include Selective Laser Melting (SLM), Electron Beam Melting (EBM), and Direct Energy Deposition (DED), which cater to different material systems and industrial needs [47].

While power fusion targets global energy solutions, powder fusion revolutionizes manufacturing by enabling the precise and efficient production of complex geometries, especially in industries like aerospace, automotive, and healthcare. Both technologies showcase the innovative potential of harnessing fusion processes for transformative applications.

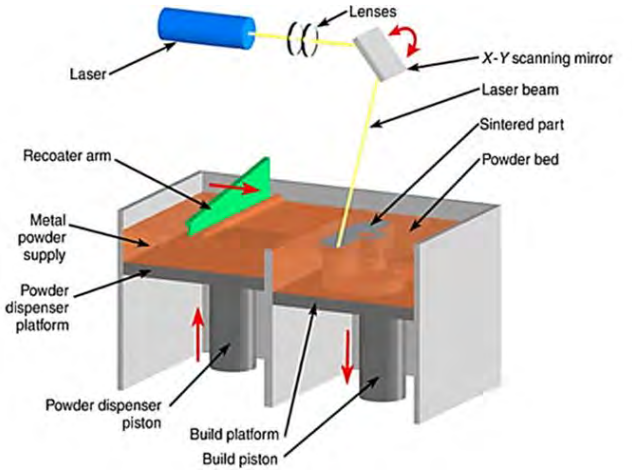


Figure 12. The SLS process [61].

3. Design and discover MM-LWC structures

The challenge of exploring MMs lies in the vast design space, where unit cells can take millions of possible shapes and sizes. This complexity makes it nearly impossible to manually identify optimal designs for specific functions. To navigate this enormous space efficiently, computational tools are essential. We propose a novel form of GAI based on evolutionary computation to systematically explore and generate innovative metamaterial architectures. This AI-driven approach accelerates discovery, enabling the identification of high-performance designs that would be difficult to find through traditional methods, ultimately unlocking new possibilities in MMs for diverse applications.

3.1 The proposed GAI approach

3.1.1 Traditional deep-learning-based GAI

The release of ChatGPT on November 30, 2022, marked a transformative milestone, igniting unprecedented interest and adoption of deep-learning-based GAI among the public. This

breakthrough traces its origins to the 1956 Dartmouth College summer project led by John McCarthy, which laid the groundwork for AI [63]. The project's goal was to develop machines capable of performing tasks requiring human-like intelligence, including natural language processing (NLP), computer vision, and robotics. Over the years, AI has evolved from classical machine learning algorithms, such as regression, decision trees, and support vector machines (SVMs), to advanced deep learning frameworks like Convolutional Neural Networks (CNNs), Recurrent Neural Networks (RNNs), and Long Short-Term Memory (LSTM) [64].

A significant catalyst for this evolution was the 2010 ImageNet Large Scale Visual Recognition Challenge, which spurred advances in deep learning, particularly in computer vision [65]. CNNs emerged as a pivotal technology, with innovations like AlexNet, ResNet, and EfficientNet revolutionizing image classification and inspiring techniques such as transfer learning, attention mechanisms, and self-supervised learning. These developments paved the way for GAI breakthroughs, beginning with the introduction of Generative Adversarial Networks (GANs) by Goodfellow et al. in 2014 [66]. GANs marked a shift from descriptive deep learning models, which analyze and predict data patterns, to generative models that learn underlying data distributions to create novel and realistic samples. Deep learning-based GAI, using neural networks such as GANs and Variational Autoencoders (VAEs), has proven highly effective at generating realistic outputs across various domains, including images, text, audio, and video [67]. These models capture the structural patterns and variability of training data, enabling applications such as synthetic data generation, artistic content creation, and realistic simulations. Training generative models involves iterative processes like loss minimization across multiple epochs to refine their parameters. Unlike evolutionary algorithms, which evolve based on external fitness criteria, generative AI models optimize internally, enhancing accuracy and fidelity. However, their reliance on large, high-quality datasets poses challenges, as training on biased or limited data can replicate these biases, restricting creativity and diversity.

GAI’s transformative impact is evident in industries where high-quality data is abundant. In content creation, it powers tools for generating human-like text, crafting digital art, and developing immersive virtual environments for gaming and media [68]. In simulations, generative models produce synthetic data to train machine learning systems, improving their robustness and reducing reliance on real-world datasets. These applications have made generative AI indispensable in fields such as healthcare, entertainment, and manufacturing. The evolution of generative AI continues to be driven by innovations in neural network architectures and learning methodologies. The introduction of GANs revolutionized generative modeling by enabling the creation of highly realistic synthetic data. These advancements have expanded generative AI’s capabilities, enabling the development of models that learn and generate creative solutions by leveraging probability distributions. Looking ahead, future advancements in transfer learning, unsupervised learning, and reinforcement learning aim to enhance the adaptability and flexibility of generative models, reducing their dependency on extensive datasets.

Integrating hybrid architectures and novel optimization techniques could further enable generative AI to explore beyond data-driven constraints, fostering innovation in design and problem-solving. As generative AI matures, its potential to transform workflows, reduce costs, and create groundbreaking applications across industries continues to grow. Continued research and development are crucial to unlocking its full capabilities, positioning generative AI as a cornerstone of advanced artificial intelligence, driving progress across countless disciplines, and shaping the future of innovation.

3.1.2 The proposed evolutionary GAI

The next generation of material structures demands innovation in the form of adaptive, multifunctional, and tunable properties that are unattainable with natural materials alone. This limitation has driven substantial efforts to create synthetic materials whose unique properties are determined not by their intrinsic chemical composition but by their carefully designed internal architectures. However, a significant challenge lies in identifying metamaterial structures with desired performance characteristics, especially given the vast design space and the need to optimize across multiple criteria. Despite considerable advancements in material design, there remains a notable gap in research leveraging the principles of natural evolution to automate the exploration and discovery of novel metamaterial systems. Addressing this gap, we have recently introduced evolutionary GAI, a novel approach to material science and metamaterial design [68].

The evolutionary GAI method marks a paradigm shift by enabling automated exploration and evolution of novel metastructures inspired by biological evolution. Unlike traditional approaches, such as topology optimization or supervised machine learning, this method eliminates the reliance on pre-existing datasets and strict parameter initialization. Instead, it employs iterative processes based on evolutionary principles, such as reproduction, variation, and selection, to discover optimal designs. By simulating these natural processes, evolutionary GAI facilitates the direct morphological evolution of representative unit cells (RUCs) to achieve targeted properties like maximum bulk modulus, shear modulus, or minimized Poisson's ratios. This methodology fundamentally transforms the design and optimization of metamaterials by mimicking biological evolution.

Figure 13. illustrate the framework of the evolutionary GAI [15]. The process begins with Population Initialization (Stage I), where a diverse set of RUCs is generated. These RUCs are created either randomly or derived from simple geometric configurations such as circles, hexagons, or other basic shapes. User-defined parameters, such as volume fraction (VF), penalization range, and minimum radius, are assigned to each RUC, alongside specific optimization objectives like maximizing bulk modulus or shear modulus or minimizing Poisson’s ratio. This stage ensures a broad and rich design space that forms a robust foundation for the evolutionary process. Next, in Topology Optimization (Stage II), the initial RUC designs undergo refinement using a density-based topology optimization algorithm. This stage identifies high-performing configurations,

referred to as "parent" RUCs, which exhibit the desired mechanical properties. These parent designs serve as the foundation for further evolution. Once the parents are established, the process moves to Reproduction (Stage III), where genetic operations, including selection, crossover, and mutation, are applied to generate new "child" RUCs. The selection process uses a roulette wheel mechanism to favor high-performing designs while maintaining diversity by occasionally selecting less optimal configurations. Crossover combines features from two parent RUCs to create novel configurations, while mutation introduces random changes, encouraging exploration of the design space and preventing premature convergence to suboptimal solutions. In Evaluation and Selection (Stage IV), the offspring RUCs undergo further topology optimization and are evaluated for fitness based on objective functions, such as maximizing bulk modulus. The most fit designs are retained for the next generation, while less optimal ones are either modified or discarded. This iterative cycle of reproduction, evaluation, and selection continues over successive generations until the optimization criteria are met or a predefined number of iterations is reached. Through this systematic process, evolutionary GAI explores a vast design space, uncovering novel configurations with optimized mechanical properties.

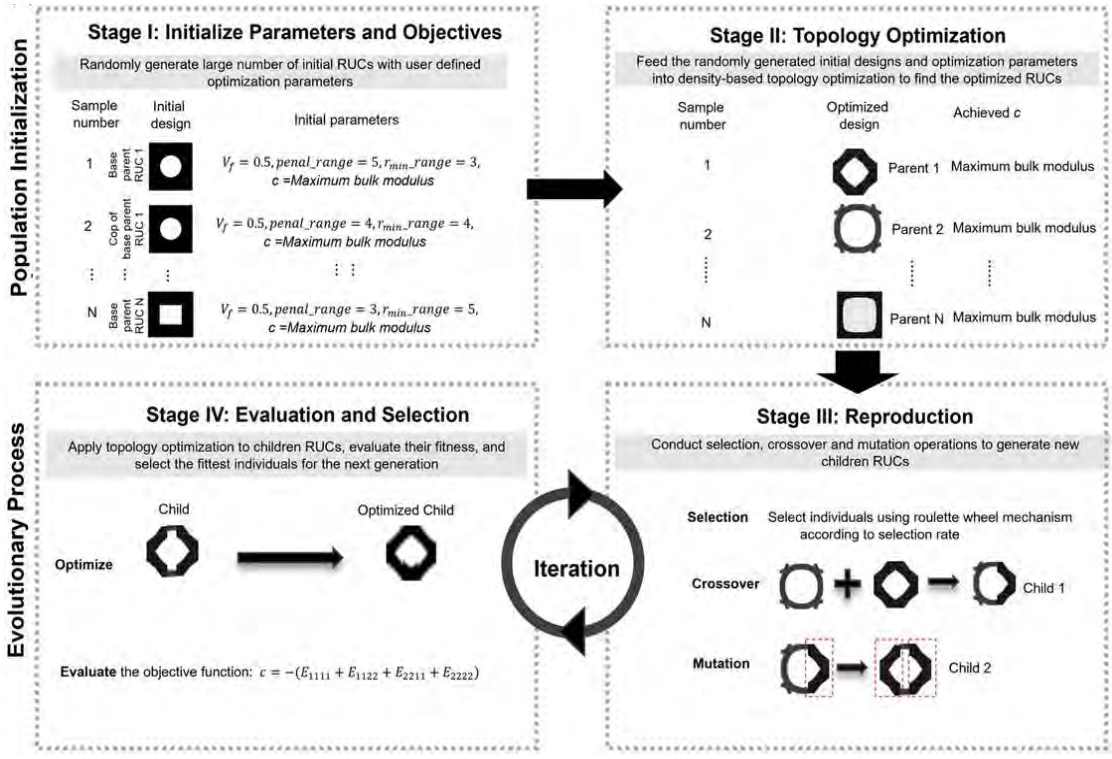


Figure 13. The proposed evolutionary GAI framework [15].

One of the defining strengths of the evolutionary GAI method is its ability to simulate natural selection while incorporating randomness. This combination allows for the discovery of unique metastructures with properties that surpass those achieved through traditional computational methods. By generating thousands of metastructures through iterative processes, the method offers unparalleled versatility in optimizing multidimensional design objectives. Its ability to uncover

configurations that defy conventional intuition makes it a groundbreaking tool in material science. Applications of this method extend from lightweight, high-performance structural components to advanced energy-absorbing systems, showing its transformative potential in engineering and design.

What sets evolutionary GAI apart is its adaptability. Its high adaptability enables it to handle open-ended problems without the need for extensive training datasets, as it generates solutions from fundamental principles rather than pre-calibrated data. This flexibility is especially useful in domains where existing data is sparse or unavailable. Another advantage lies in the iterative improvement process. Designs evolve gradually as the system repeatedly evaluates their fitness against defined criteria, applies genetic modifications, and selects the best-performing options for further refinement. This continuous cycle ensures that designs improve progressively, resulting in solutions that meet or exceed performance expectations. Furthermore, the data requirements for this approach are minimal, as it autonomously explores the design space without the constraints of predefined datasets. Instead of relying on historical data to inform design, evolutionary GAI is guided by fitness functions that define the desired outcomes, such as maximizing strength, stiffness, or energy absorption. Over successive generations, the system evolves structures that meet these criteria, resulting in optimized solutions tailored to specific goals.

The application of this technology to metamaterials is particularly noteworthy. Metamaterials are defined by their unique structural configurations, which dictate their exceptional mechanical or physical properties. Evolutionary GAI excels in this field, as it can iteratively evolve these structures to optimize performance based on defined objectives. The approach generates highly varied and unique designs, unbound by dataset biases, fostering innovation and creativity in solution development. By autonomously navigating vast design spaces, the system enables the discovery of novel configurations that were previously inconceivable.

3.1.3 Comparison of the traditional and evolutionary GAI approaches

GAI goes beyond the familiar landscape of deep learning-based GAI models. The proposed evolutionary GAI does not conform to the standard GAI methods, but it naturally fulfills the required functionalities. By generating unique solutions across a vast design space, it fulfills the core principle of GAI: producing creative, data-driven outputs tailored to specific goals, making it a robust and innovative generative system. Table 1 highlights that both evolutionary GAI and traditional deep learning-based GAI approaches are capable of generating novel outputs. They represent two distinct approaches to generative systems, each with unique capabilities and limitations. Evolutionary GAI employs algorithms inspired by natural selection, iteratively evolving designs over multiple generations through processes like mutation, crossover, and fitness evaluation. This approach starts from scratch, generating a wide variety of designs by exploring the solution space autonomously without relying on large datasets. It is highly adaptable to open-ended problems, as it generates solutions based on fundamental principles rather than existing data

patterns. Gradual refinement of designs is achieved through iterative fitness evaluation, enabling this method to evolve structures optimized for specific performance goals. Its minimal data requirement makes it particularly effective for applications like material design, where structural traits can evolve to meet mechanical or physical performance criteria. Furthermore, this approach often produces highly unique and diverse outputs that are not restricted by biases inherent in training datasets. In contrast, traditional deep learning-based GAI utilizes neural networks to learn patterns from large, domain-specific datasets and generate new samples that mimic the underlying data distribution. Unlike evolutionary methods, these models optimize through internal loss minimization rather than external fitness criteria, refining their outputs across iterative training epochs. While this ensures high fidelity and realistic outputs, it makes the approach highly dependent on high-quality, curated datasets. Poor or biased datasets can limit the diversity of generated solutions, making it less ideal for exploratory tasks like physical design without significant retraining on specialized datasets. Applications for deep learning-based GAI excel in domains with abundant data, such as creating synthetic data, generating artistic content, and simulating realistic environments. However, its reliance on data availability and its tendency to replicate biases present in training datasets can restrict its capacity to generate novel or highly unique outputs.

Table 1. Comparison between evolutionary GAI and traditional deep learning-based GAI.

Feature	Evolutionary Generative AI	Deep Learning-based Generative AI
Generative Process	Uses evolutionary algorithms inspired by natural selection, iteratively evolving designs over multiple generations.	Uses neural networks, often GANs or VAEs, to learn patterns from data and generate new samples.
Design Generation Basis	Starts from scratch, generating millions of designs by applying genetic operators like mutation and crossover.	Learns data patterns, generating samples that mimic learned distributions.
Adaptability	High adaptability for open-ended problems without needing a large training dataset, as it generates from principles.	Often requires large, domain-specific datasets to train effectively, which limits adaptability without retraining.
Iterative Improvement	Gradually evolves optimal designs through fitness evaluation, mutation, and selection processes.	Relies on training epochs for gradual refinement but doesn't evolve through external fitness criteria.
Data Requirement	Minimal pre-existing data needed; explores design space autonomously.	High-quality data is crucial; relies on data availability and quality for generating accurate results.
Generative Approach	Guided by fitness functions defining optimal outcomes; evolves structures that meet these criteria over generations.	Learns patterns based on loss minimization and optimizes sample generation accordingly.
Application for Metamaterials	Effective for material design, where structural traits can evolve based on mechanical or physical performance goals.	Less ideal for physical design exploration unless trained with vast, specific datasets on similar structures.
Output Uniqueness	Produces highly varied, unique designs that are not restricted by dataset biases, enhancing creativity in solutions.	More likely to replicate biases present in training data, potentially limiting the range of unique solutions.

Both approaches have their strengths and are suited to different applications. Evolutionary GAI thrives in scenarios that demand innovation and adaptability, where solutions need to be derived from principles without extensive data. On the other hand, deep learning-based GAI is highly effective for tasks requiring precise pattern replication and optimization, particularly in data-rich fields like image generation, natural language processing, and simulation. The future of GAI may lie in hybrid approaches that combine the adaptability and exploratory capabilities of evolutionary algorithms with the precision and scalability of deep learning, unlocking new possibilities for generative systems across diverse domains.

3.2 Exploring MM structure with desirable properties

The primary objective of this project is to design and develop innovative materials and systems that significantly enhance both compressive and flexural strength, thereby improving the overall mechanical performance for advanced structural applications. By optimizing these critical mechanical properties, the project aims to achieve high-performance cementitious materials tailored for demanding engineering applications. MMs, with their architected structures, offer unique ways to manipulate material properties like bulk modulus and compression strength, Poisson's ratio and flexure strength. Unlike conventional materials, where these properties are largely determined by atomic bonding and composition, metamaterials derive their mechanical behavior from their macro and micro structure. For example, the bulk modulus—representing a material's resistance to uniform volumetric compression—can be significantly influenced by the geometry, topology, and connectivity of the unit cells in a metamaterial. This tunability enables the design of materials with atypical combinations of stiffness and strength. For instance, structures such as lattice-based metamaterials or penta-mode metamaterials can decouple bulk modulus from shear modulus, creating materials that are highly resistant to volumetric changes yet soft under shear stresses. Such designs often enhance or maintain the compression strength by directing stress distribution efficiently through the structural framework, even at low densities.

Bulk modulus, a fundamental material property that measures a material's resistance to uniform compression. It quantifies the relationship between applied pressure and the resulting change in volume. A high bulk modulus indicates a material is less compressible and more resistant to deformation under pressure, while a low bulk modulus suggests higher compressibility. The bulk modulus (K) is defined as [69]:

$$K = -\frac{\Delta P}{\frac{\Delta V}{V}} \tag{2}$$

where, ΔP is the change in pressure, ΔV is the change in volume, and V is the original volume. This property is critical for understanding and optimizing materials in applications requiring compressive strength and deformation control.

A higher bulk modulus is a measure of a material's ability to resist volumetric deformation under uniform pressure, signifying its stiffness against compressive forces. MMs in practical terms indicates that a material with a high bulk modulus requires substantially more pressure to produce the same volume change compared to materials with a lower bulk modulus [69,70]. This makes the bulk modulus a fundamental property in understanding and predicting how materials behave under compressive stresses. The relationship between bulk modulus and compressive strength lies in their complementary roles in assessing a material's performance under compression. While the bulk modulus quantifies the resistance to changes in volume under pressure (elastic behavior), the compressive strength defines the maximum compressive stress a material can endure before failing (inelastic behavior). Together, these parameters provide a comprehensive picture of the material's mechanical resilience. A high bulk modulus indicates that the material can maintain its volume with minimal deformation under stress, while high compressive strength ensures that the material can withstand large compressive loads without failure.

Poisson's ratio is a key material property that characterizes the relationship between longitudinal strain and transverse strain in a material under uniaxial stress. When a material is stretched or compressed along one axis, it simultaneously contracts or expands in the perpendicular directions. Poisson's ratio provides a quantitative measure of this deformation behavior and is mathematically defined as [71]:

$$\nu = -\frac{d\varepsilon_{transverse}}{d\varepsilon_{longitudinal}} \tag{3}$$

Here, transverse strain refers to the relative change in dimensions perpendicular to the applied force, while longitudinal strain represents the relative change along the direction of the force. Poisson's ratio is a dimensionless quantity and plays a crucial role in understanding the elastic behavior of materials.

A negative Poisson's ratio [72], characteristic of auxetic materials, describes a unique mechanical behavior where a material expands laterally when stretched and contracts laterally when compressed, contrary to most conventional materials. This uncommon behavior arises from specific microstructural designs rather than material composition, with mechanisms such as reentrant structures, rotating units, and chiral geometries enabling auxetic responses by allowing internal geometry to deform in ways that promote simultaneous expansion or contraction in all directions. Auxetic materials exhibit remarkable properties, including enhanced energy absorption, improved fracture toughness, increased shear resistance, and superior vibration damping, making them ideal for applications such as protective gear, biomedical implants, lightweight aerospace components, and filtration systems. However, challenges like manufacturing complexity, scalability, and balancing other material properties limit widespread use. Recent advancements, particularly in 3D printing and hybrid material development, are expanding the potential of auxetic materials, paving the way for diverse industrial application. Core structures with auxetic behavior, distinguished by an NPR, offer remarkable mechanical advantages over conventional lattice

designs. These structures achieve enhanced bending strength and demonstrate greater resistance to deformation under flexural loads. Additionally, they effectively minimize out-of-plane shear stresses, improving stability and performance under complex loading conditions. Such attributes make auxetic cores particularly valuable in applications requiring lightweight yet resilient materials, such as aerospace, marine, and biomedical engineering. Their unique deformation characteristics, driven by their NPR, enable optimization of energy absorption, impact resistance, and structural integrity [73].

3.3 Objective functions for the revolutionary GAI

In the realm of linear elasticity, the mechanical properties of periodically patterned metamaterials can be represented by a single RUC, denoted as *Y*. The equivalent constitutive behaviors of these metamaterials are evaluated using homogenization theory combined with periodic boundary conditions (PBCs). The homogenized stiffness tensor, E_{ijkl}^{H}, of the RUC is mathematically defined as [74]:

$$E_{ijkl}^{H} = \frac{1}{|Y|}\int E_{pqrs}\varepsilon_{pq}^{A(kl)}\,\varepsilon_{rs}^{A(ij)}dY \tag{4}$$

$$\varepsilon_{pq}^{A(kl)} = \varepsilon_{pq}^{o(kl)} - \varepsilon_{pq}^{*(kl)} \tag{5}$$

where, $|Y|$ represents the area (or volume in 3D cases) of the RUC. E_{pqrs} denotes the constitutive parameters, $\varepsilon_{pq}^{o(kl)}$ corresponds to independent unit strain fields, and $\varepsilon_{pq}^{*(kl)}$ is the periodic solution derived from the variation problem.

In finite element analysis, the RUC is discretized into *N* finite elements, allowing to be approximated as:

$$E_{ijkl}^{H} = \frac{1}{|Y|}\sum_{e=1}^{N}(u_e^{A(ij)})^T\,k_e u_e^{A(kl)} \tag{6}$$

here, $u_e^{A(ij)}$ represents the element displacement solutions corresponding to the unit strain fields $\varepsilon_{pq}^{o(kl)}$ and k_e denotes the element stiffness matrix.

To optimize the design, the Solid Isotropic Material Penalization (SIMP) [75] method is employed. Each element's density ρ_e acts as the design variable, with the element Young's modulus $E_e(\rho_e)$ defined as:

$$E_e(\rho_e) = E_{min} + \rho_e^p (E_0 - E_{min}) \tag{7}$$

where, E_0 represents Young's modulus of the solid material, E_{min} represents Young's modulus of the Ersatz material (used to approximate void regions) [76], and p represents penalization factor to enforce density distribution. The optimization problem can be formulated as follows:

$$\begin{aligned} &min_\rho : c\left(E_{ijkl}^H(\rho)\right) \\ &\quad s.t. : KU^{A(kl)} = F^{kl}, k, l = 1, \dots, d \\ &\qquad : \sum_{e=1}^{N} \frac{v_e \rho_e}{|Y|} \leq \vartheta \\ &\qquad : 0 \leq \rho_e \leq 1, e = 1, \dots, N \end{aligned} \tag{8}$$

here, K represents global stiffness matrix, $U^{A(kl)}$ represents global displacement vector for the (kl) test case, F^{kl} represents external force vector for the (kl) test case, v_e represents volume of each element, and ϑ represents upper bound on VF.

In 3D cases: objective functions for maximization of bulk modulus is defined as:

$$\begin{aligned} c = -(&E_{1111} + E_{1122} + E_{1133} + E_{2211} + E_{2222} + E_{2233} + E_{3311} + E_{3322} \\ &+ E_{3333}) \end{aligned} \tag{9}$$

In 2D cases: objective function for the NPR is defined as:

$$c = E_{1122} - \beta^l (E_{1111} + E_{2222}) \tag{10}$$

here, $\beta \in (0, 1)$ is a user-defined parameter, with a value of 0.8 used in this study.

The sensitivity of the objective function is computed using the adjoint method [77], expressed as:

$$\frac{\partial E_{ijkl}^H}{\partial \rho_e} = \frac{1}{|Y|} p \rho_e^{p-1} (E_0 - E_{min}) (u_e^{A(ij)})^T k_0 u_e^{A(kl)} \tag{11}$$

here, k_0 is the element stiffness matrix for a unit Young's modulus.

3.4 Parameter setting for the evolutionary GAI algorithm

The evolutionary GAI algorithm is driven by a crafted set of user-defined input parameters that guide both the initialization of the initial population and the dynamic iterative process of evolution. These parameters are pivotal for ensuring effective exploration and refinement of the design space, ultimately enabling the discovery of optimized metamaterial structures. The parameters are categorized into two essential groups: Topology optimization and evolutionary parameters, each of which plays a critical role in shaping the outcomes of the process (Table 2).

The topology optimization parameters are focused on generating a diverse and well-structured initial population of RUCs. These parameters define the foundation of the design space by determining the structural properties and constraints of the initial designs. The RUC_size, specified as user-defined integers (e.g., 100 or 200), controls the scale and dimensions of the unit cells that will undergo optimization. This ensures that the designs are appropriately sized to meet the targeted objectives while allowing scalability for various applications. The volfr_range, which represents the range of VFs, specifies the proportion of material within each RUC. With user-defined ranges (e.g., [0.2, 0.8]), this parameter enables precise control over material density, allowing the generation of lightweight or dense designs based on application needs. The penal_range, defining the penalty factor for topology optimization, typically operates within a range such as [3, 8]. This parameter influences the stiffness properties of the designs by penalizing intermediate material densities, ensuring clear differentiation between solid and void regions. Additionally, the rmin_range, representing the radius of the filter used in topology optimization, ensures smooth transitions and prevents numerical instabilities during the optimization process. With user-defined values (e.g., [3, 10]), this parameter is critical for achieving robust and manufacturable designs.

The evolutionary parameters, on the other hand, govern the iterative refinement process and ensure the effective evolution of the initial population. These parameters dictate how designs are reproduced, selected, and improved over successive generations. The numpop parameter specifies the size of the initial population, typically defined as user-specified integers (e.g., 200). A larger population size allows for a broader exploration of the design space, increasing the likelihood of discovering high-performing configurations. The select_rate, ranging between 0 and 1, determines the proportion of individuals selected for reproduction based on their fitness. This parameter ensures that the best-performing designs are prioritized for further evolution while maintaining diversity by occasionally selecting less optimal designs. The crossover_rate, also within the range of 0 to 1, controls the proportion of offspring generated by combining genetic information from two parent designs. This operation fosters innovation by introducing novel combinations of design traits. Similarly, the mutate_rate, defined within the same range, introduces random modifications in offspring designs, encouraging exploration of uncharted areas of the design space and preventing premature convergence to local optima. Finally, the generation parameter specifies the total number of evolutionary generations (e.g., 10), defining the duration of the iterative process. With each generation, the method progressively refines the population, enhancing the quality and performance of the designs.

Together, these input parameters form the backbone of the evolutionary GAI method, ensuring a seamless integration of exploration and exploitation in the design process. The topology optimization parameters set the stage for the initial diversity and structural integrity of the designs, while the evolutionary parameters drive the dynamic refinement and optimization of the population. By carefully tuning these parameters, the method is able to balance the generation of diverse configurations with the convergence toward high-performance solutions. This dual

capability enables the discovery of novel metamaterial structures with optimized properties, such as maximum bulk modulus, shear modulus, and tailored Poisson's ratios. The significance of these parameters extends beyond their individual contributions. Their combined effect creates a highly adaptable and efficient framework that autonomously navigates vast design spaces, overcoming the limitations of traditional approaches like topology optimization and machine learning. By minimizing reliance on pre-existing datasets and rigid initialization requirements, the evolutionary GAI method harnesses the power of evolutionary algorithms to unlock unprecedented design possibilities. This adaptability allows the method to address complex, open-ended problems across a wide range of engineering applications, from lightweight aerospace structures to advanced energy-absorbing systems.

In conclusion, the input parameters of the evolutionary GAI method are fundamental to its success in metamaterial design. They enable the method to generate, evolve, and optimize designs through a robust combination of initial diversity and iterative refinement. By leveraging these parameters, the method achieves unparalleled versatility and innovation, making it a groundbreaking tool in the field of material science and engineering.

Table 2. Parameter setting for the evolutionary GAI algorithm.

	Parameter	**Definition**	**Range**
Topology optimization parameters for population initialization	RUC_size	The size of RUC for optimization	User defined Integers (e.g., 100,200…)
	volfr_range	The range of volume fraction	User defined, range between (0,1). (e.g. [0.2,0.8])
	penal_range	The penalty factor for topology optimization	User defined (e.g. [3,8])
	rmin_range	Radius of filter in topology optimization	User defined (e.g. [3,10])
	Obj	Optimization objective	Maximizing bulk/shear modulus, minimizing Poisson's ratio
Evolutionary parameters	numpop	Number of initial populations	User defined integers (e.g., 200)
	select_rate	Selection rate of evolution	User defined (0,1)
	crossover_rate	Crossover rate of evolution	User defined (0,1)
	mutate_rate	Mutation rate of evolution	User defined (0,1)
	generation_#	Number of generations	User defined integers (e.g., 10)

4. Concrete mix design

4.1 Material selection

The use fine-grained cementitious mixes is particularly advantageous for fabricating MM cubic and beam samples due to their intricate geometries. Fine-grained mixes enable superior moldability and precision in capturing complex architectures compared to conventional concrete, which contains coarser aggregates that may compromise the fidelity of small-scale features. Importantly, while the choice of base material affects fabrication, it does not impact the validity of performance comparisons, as MM samples are always benchmarked against solid cubes and beams of the same bulk material. The effective mechanical properties of RUCs (e.g. bulk modulus, density, energy absorption, and Poisson's ratio) are primarily governed by their topology and architecture rather than the intrinsic properties of the constituent material. This inherent material independence in generative AI-driven design ensures that the optimized metamaterial structures function in a normalized and geometry-driven manner. Consequently, once an RUC is structurally refined, it can be assigned different base materials to achieve tailored performance characteristics. For instance, an MM RUC fabricated from a high-performance cementitious mix with a density of approximately 2400 kg/m³ and a compressive strength of 100 MPa can be strategically designed to weigh 50% less than a solid counterpart, resulting in an effective density of around 1200 kg/m³ while retaining a compressive strength of 90 MPa. This principle extends to multiscale MM assemblies incorporating these RUCs, enabling scalable and tunable performance across a range of materials, including polymers, metals, and cementitious composites. The ability to decouple effective mechanical behavior from the intrinsic properties of the base material underscores the versatility of MM structures, reinforcing the validity of using fine-grained mixes for precision manufacturing while preserving the integrity of comparative performance assessments. Ultimately, the optimized MM topology dictates structural behavior, allowing for enhanced material efficiency and mechanical resilience, irrespective of the type of fine-grained cementitious materials employed. However, we use a high-performance concrete as the base material as it is also widely recognized as an innovative material celebrated for its outstanding strength and resilience [78-93]. Table 3 shows the properties of the mixture as provided by the manufacturer. This specially formulated premix combines advanced cements, innovative additives, and carefully selected aggregates [94].

Table 3. Mechanical properties of the used concrete mixture.

Density	2200 - 2500	kg/m3
Flow	0.18 to 0.254	m
Compressive strength	1st day	~69 MPa
	7th day	~110 MPa
	28th day	~151 MPa
Flexural Strength	28th day	~18 MPa

To begin the mixing process, we added all dry ingredients to the mixer and started mixing. We added 90% of the water and mixed until the material was fully wetted, which typically takes about 2 minutes. The mixing was continued for an additional 3 minutes to achieve uniform consistency. The remaining water was then mixed for a final 5 minutes, resulting in a total mixing time of approximately 10 minutes. The self-consolidating version of the used mix possesses specific free-flowing properties, necessitating watertight forms to prevent leakage during casting. The mixture should be applied within 30 minutes of mixing to maintain consistency and workability. To ensure proper curing, it is essential to cover cast surfaces immediately, preventing moisture loss from the surface.

5. Design and fabrication polymeric and cementitious MM unit cells

The hypothesis here is that increasing the bulk modulus while controlling the VF rates will lead to an increase in the compressive strength of the MM structures, resulting in a higher strength-to-density ratio. We also hypothesize that there is a relationship between the flexural strength and MM structures with an NPR. These hypotheses are tested by creating polymeric and then cementitious MM cubic and beam specimens.

5.1 MM unit cell structures

5.1.1 Bulk modulus unit cell structures

More than ten thousand 3D bulk modulus RUC designs were generated using the evolutionary GAI method introduced in Section 3.1.2, based on a performance objective function and diverse input parameters. The algorithm reports some of the best designs after each generation. Figure 14a shows some of the 3D unit cells reported by the algorithm during the evolutionary process. Some of the explored designs may exhibit promising performance, but they cannot be feasibly fabricated using cementitious materials. Thus, four representative designs were selected from the extensive array of generated designs (Figure 14b) based on their high bulk modulus, VF, and fabricability. VF reflects the proportion of solid material to the total sample volume. A solid block (VF = 1) was also fabricated to serve as a control group, providing a comparison of mechanical properties with the other designs. This approach ensured a reliable reference point for evaluating the performance and effectiveness of the various designs. These chosen designs span a range of structural and material configurations, enabling a comparative analysis to better understand the impact of VF and bulk moduli on the compression strength and manufacturability of the metamaterials in realistic applications.

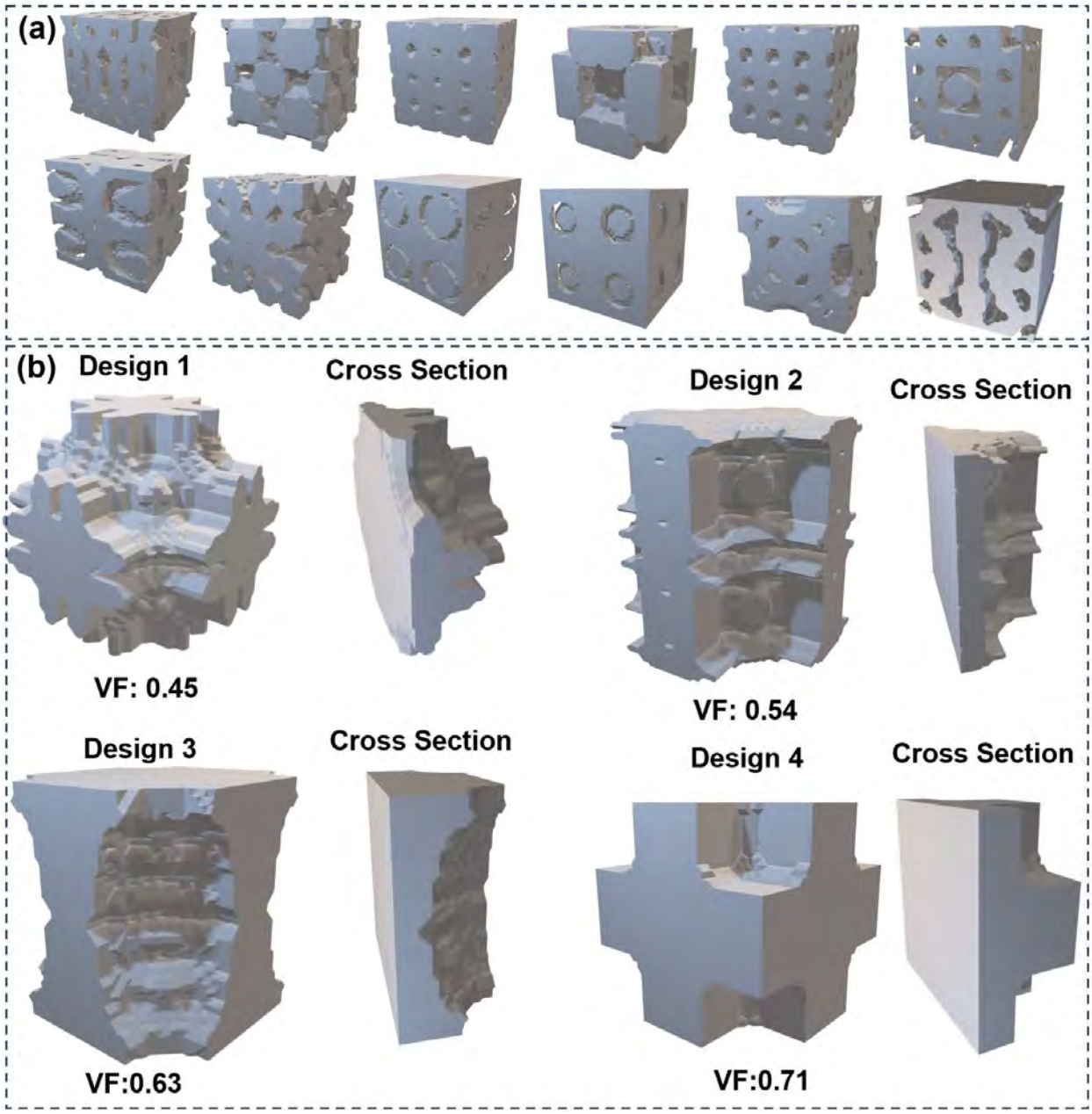


Figure 14. (a) Examples of 3D unit cells created through the evolutionary GAI process. (b) Selected 3D unit cells with maximized bulk modulus.

5.1.2 NPR's unit cell structures

Two-dimensional NPR structures have gained widespread popularity in recent years due to their straightforward analysis. However, while 2D metamaterials offer significant versatility, they are often unable to meet all performance requirements. Three-dimensional metamaterials have emerged as a focus of research, offering superior mechanical and functional properties [95, 96], which include 3D chiral honeycombs [97, 98], re-entrant lattices [99], and tubular NPR [21]

configurations have been developed to address specific mechanical performance needs. Fu et al. [98] introduced a novel chiral 3D honeycomb structure derived from the 2D design. The 3D re-entrant honeycomb structure demonstrated auxetic behavior across multiple directions, providing enhanced stability under uniaxial impact loading. A groundbreaking 3D NPR concave lattice structure pointed out by Li et al. [100], inspired by earlier 2D NPR designs. Their concept was validated through physical experiments, leading to the development of an enhanced version incorporating support pillars. By adjusting these pillars that were able to modify the NPR performance, though the compressive and bending resistance improvements observed in the 3D concave lattice were modest. Building on this, Wang et al. [101] introduced a novel 3D NPR energy-absorbing structure, derived from a two-dimensional nonconvex hexagonal cell. Through theoretical analysis using beam theory, the equivalent Young's modulus and Poisson's ratio were deduced, and these findings were validated through finite element simulations and compression tests, demonstrating strong consistency among the results. Li et al. [102] proposed a novel 3D unit cell structure featuring butterfly-like perforations, achieving both NPR and tunable stiffness. Numerical simulations and experimental testing were conducted to evaluate the Poisson's ratio and stress-strain behavior, with excellent agreement observed between the two approaches

Despite significant advancements in the development of 3D re-entrant structures, theoretical studies in this area remain relatively limited. Moreover, the fabrication of negative Poisson's Ratio structures has predominantly relied on plastics and composite materials due to manufacturing constraints. Research focusing on 3D NPR structures constructed from metals remains scarce, highlighting a substantial gap in the field. Broadening the scope of research to include metal-based 3D NPR designs could pave the way for the creation of robust, high-performance metamaterials with enhanced durability. Such innovations would significantly expand the applicability of NPR structures across various engineering and industrial domains. In this section, several 3D NPR unit cell designs were developed using the proposed evolutionary GAI approach. Figure 15a illustrates one of 2D NPR structures explored by the evolutionary GAI approach, by assembling two vertically interesting 2D structures (Figure 15b), a unitary 3D unit cell structure is created. Building upon this unitary cell, a fully 3D beam lattice structure is developed, as shown in Figure 4 c.

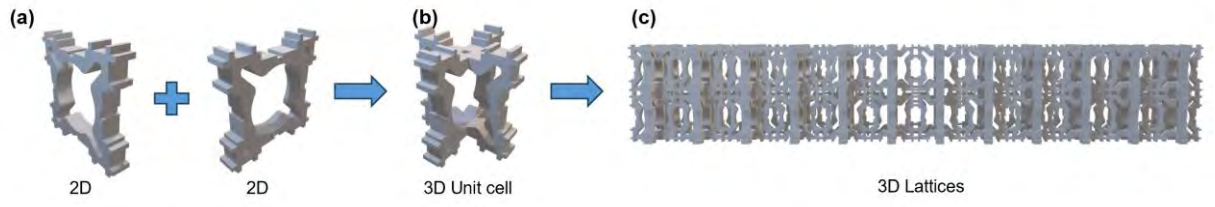


Figure 15. Converting a 2D unit cell into 3D. a) 2D NPR structure. b) 3D unit cell. c) 3D lattice.

More than three thousand NPR RUC designs were generated using the evolutionary GAI method. Figure 16a shows some of the 2D unit cells reported by the algorithm during the evolutionary process. To investigate and validate the relationship between NPR and flexural strength, while

ensuring embeddability with the fabricability requirements of the MM-LWC beam system, five representative designs were selected from generated designs. Figure 16b illustrates the transformation of the selected 2D models into 3D unit cells with varying NPRs.

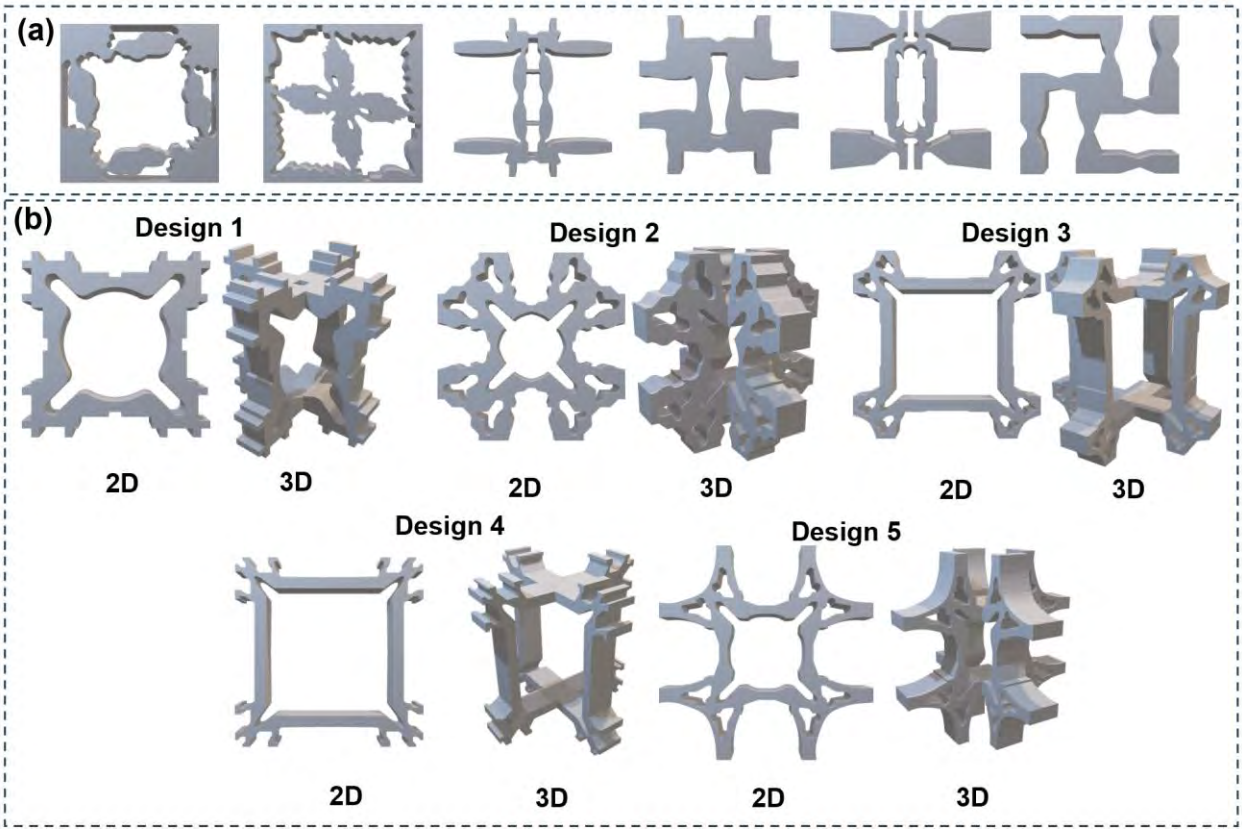


Figure 16. (a) Examples of NPR unit cells created through the evolutionary GAI process. (b) Selected NPR unit cells.

5.2 3D printing of polymeric MM unit cells

3D printing materials have revolutionized manufacturing and design by offering a broad spectrum of options to suit various applications, ranging from prototyping and product development to functional end-use parts. These materials fall into several categories, each with unique properties and uses. Plastics, such as PLA, ABS, PETG, Nylon, TPU, and Polycarbonate, dominate the field due to their versatility, affordability, and compatibility with most FDM printers [103]. PLA, a biodegradable and easy-to-use filament, is popular for general-purpose and aesthetic models, while ABS provides greater heat resistance and toughness, making it ideal for functional prototypes and automotive parts [104]. PETG, a blend of durability and flexibility, is widely used for parts requiring impact resistance [105], and Nylon offers exceptional strength and wear resistance, making it suitable for mechanical components [106]. TPU and other flexible filaments are favored for applications requiring elasticity, such as seals and custom grips. Beyond traditional plastics, composite materials infused with carbon fiber, wood, or metal particles add specialized properties

like increased stiffness or unique textures. In advanced sectors, metals like stainless steel, aluminum, and titanium enable 3D printing of robust, high-precision components, especially in aerospace, medical, and automotive industries [107]. Choosing the right material is crucial as it directly impacts the mechanical properties, durability, and functionality of the printed object. Material selection depends on factors such as thermal stability, strength, flexibility, surface finish, and cost, ensuring that 3D printing remains adaptable to the evolving demands of industries and innovation.

Ultimaker PLA is one of the most widely used materials in 3D printing and was chosen as the main printing material in this project (Figure 17a), due to its numerous advantages that cater to beginners and professionals alike. As a biodegradable thermoplastic derived from renewable resources such as cornstarch or sugarcane, PLA is an environmentally friendly alternative to petroleum-based plastics, making it a sustainable choice for projects with ecological considerations. One of the primary reasons to choose PLA is its ease of use as it extrudes smoothly at relatively low temperatures (150-160°C), making it compatible with most desktop 3D printers without requiring a heated bed [108]. This low extrusion temperature also reduces the risk of warping or cracking, which is especially beneficial when printing larger models or intricate designs. PLA is known for its excellent layer adhesion, enabling high-quality surface finishes and precise details, making it ideal for aesthetic prototypes, educational tools, and creative projects [109].

Furthermore, PLA is available in a wide variety of colors and composite blends, including black, white, red, green, orange and blue, providing designers with creative flexibility. Its non-toxic nature and minimal odor during printing make it a safe material for use in homes, classrooms, and offices, where ventilation might be limited [110, 111]. While PLA lacks the high heat resistance and mechanical durability of alternatives like ABS or Nylon, it compensates with its stability and reliability for applications where those properties are not critical [106]. For example, decorative objects, visual prototypes, and low-stress components are well-suited for PLA. Its eco-friendliness, affordability, and accessibility further enhance its appeal, making it a go-to material for beginners entering the 3D printing world as well as professionals seeking reliable, high-quality results for non-industrial applications. With its blend of user-friendliness, visual appeal, and sustainable properties, PLA remains one of the most practical and versatile choices in 3D printing materials.

When printing hollow and complex objects, the use of support materials becomes essential to ensure successful fabrication, particularly for designs with overhangs, bridges, or intricate internal geometries. These support materials provide temporary stability during the printing process and are designed to be removed after the object is completed, enabling the production of structures that would otherwise be unprintable due to gravity or lack of foundational support. Among the commonly used support materials, Polyvinyl Alcohol (PVA) stands out for its unique properties, making it an ideal choice as a supporting material for this project (Figure 17. b). PVA's water-soluble nature allows for easy and residue-free removal, which is particularly advantageous when working with complex designs featuring overhangs, intricate geometries, or internal cavities [112]. Its compatibility with widely used materials such as PLA ensures seamless integration during the

printing process, maintaining the quality and precision of the final output. Additionally, PVA's biodegradable and environmentally friendly properties align with sustainable manufacturing practices, making it a practical and responsible choice for high-precision applications [113]. By utilizing PVA as the support material, this project benefits from its efficiency, user-friendliness, and ability to facilitate the creation of highly detailed and structurally complex components.

Printing with Ultimaker PLA and PVA is a straightforward process that leverages the dual-extrusion capability of Ultimaker S3 3D printers to create complex geometries with water-soluble supports. Begin by loading PLA and PVA filaments into separate print cores, ensuring the appropriate print settings for each material. Ultimaker PLA typically prints at a nozzle temperature of 200–210°C with a build plate temperature of 60°C, while PVA requires slightly lower temperatures, usually around 190–200°C. In Ultimaker Cura, select the material profiles for PLA and PVA to ensure optimized settings, including print speed, cooling, and layer adhesion. For best results, this project uses a layer height of 0.15 mm and set the support interface to PVA to create a smooth barrier between the printed model and the support structure. PVA dissolves easily in water after printing, so no manual effort is needed to remove supports, minimizing the risk of damage to delicate parts. Allow the print to cool before removing it from the build plate, then immerse it in warm water to dissolve the PVA completely. Proper storage of PVA in a dry environment is essential to prevent moisture absorption and maintain print quality. By following these steps, you can achieve high-quality, intricate prints with clean finishes and precise details, making Ultimaker PLA and PVA a powerful combination for advanced 3D printing in this project.

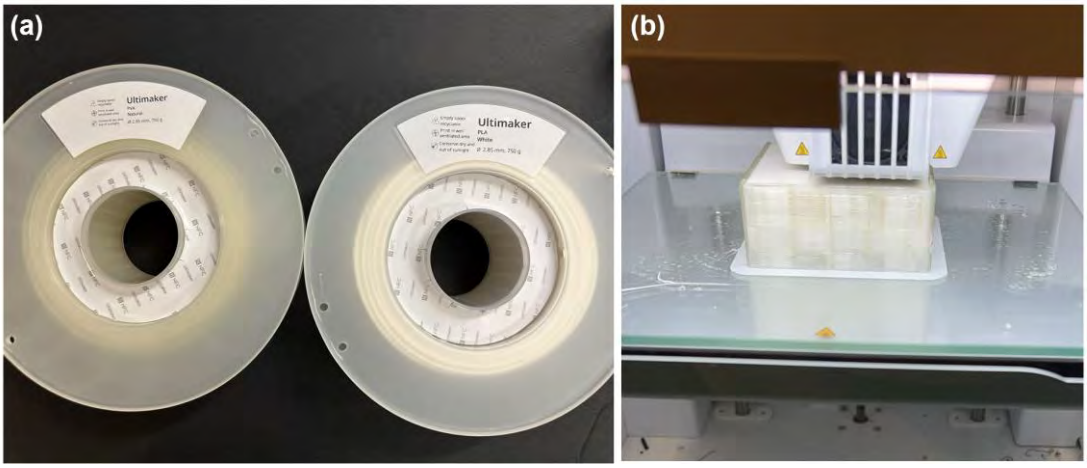


Figure 17. a) PLA and PVA filaments used in this research. b) The printing process.

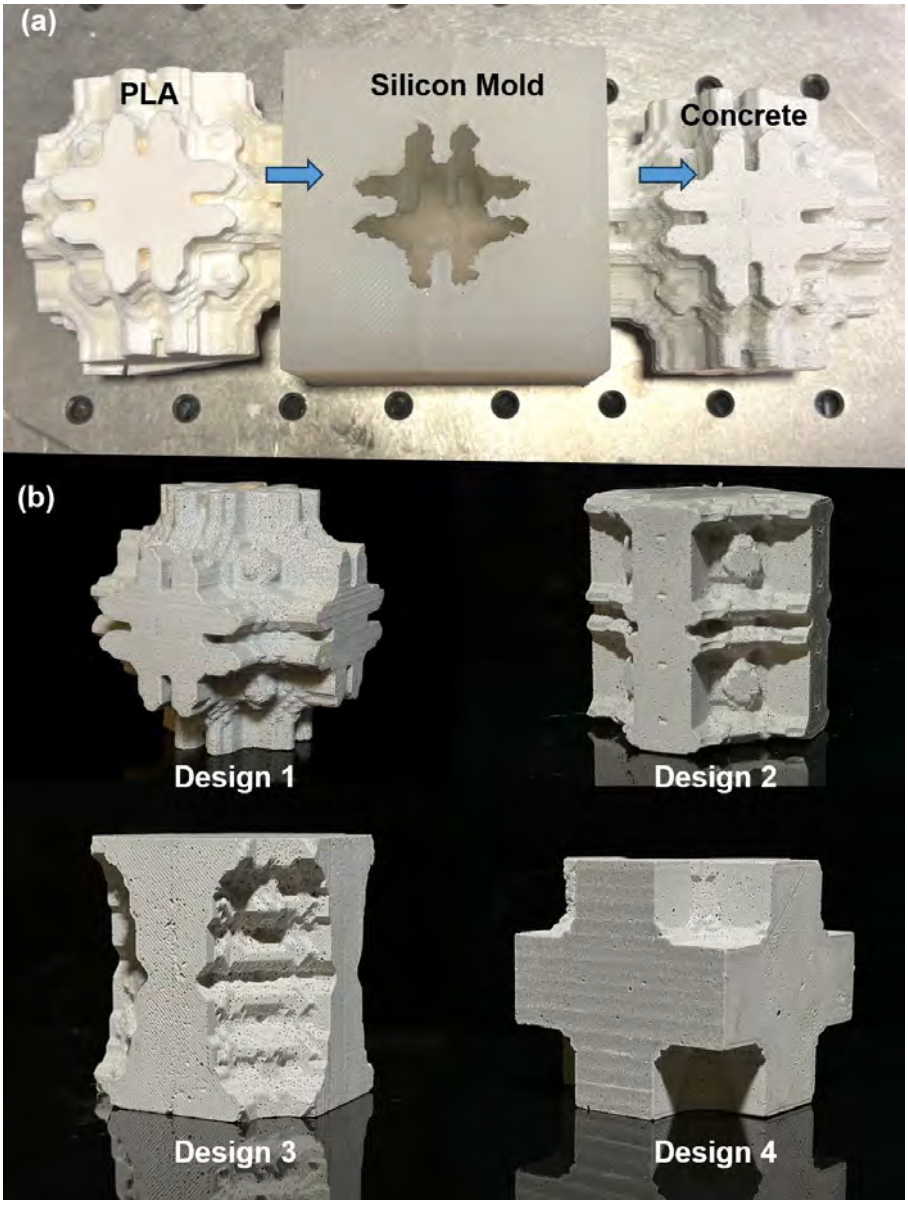


Figure 19. a) MM concrete sample fabrication process. b) Bulk modulus Bulk modulus unit cementitious cell designs.

5.3 Unit cell fabrication

5.3.1 Bulk modulus unit cells

5.3.1.1 Bulk modulus polymeric unit cells

The potential models were developed by SolidWorks and exported as STL files to ensure compatibility with the Ultimaker 3D printing process. These STL files were then imported into Ultimaker Cura, the recommended slicing software for Ultimaker printers, where critical print settings were configured to optimize both print quality and structural integrity. Key settings for the

60×60×60 mm models included a 100% infill density for PLA, a 0.15mm normal printing layer height, and a print speed of 70 mm/s. PVA, used as the support material, was set with a 30% infill density to balance stability during printing and facilitate easy removal during post-processing. Figure 18a shows the printing overview with a detailed layer-by-layer construction plan, and estimated printing times were calculated for four potential designs.

After printing, the samples were immersed in water for over 12 hours to fully dissolve the PVA supports, ensuring the intricate geometries and precision of the PLA structures were maintained. This soaking process eliminated the need for mechanical removal of supports, which could otherwise risk damaging the final product. Once the PVA supports were completely dissolved, the PLA samples were left with smooth surfaces and intricate details, achieving the intended design with precision and integrity. The effectiveness of this post-processing step was critical to the quality of the final product, preserving finer details while maintaining the structural integrity of the samples. The completed PLA models are displayed in Figure 18 b.

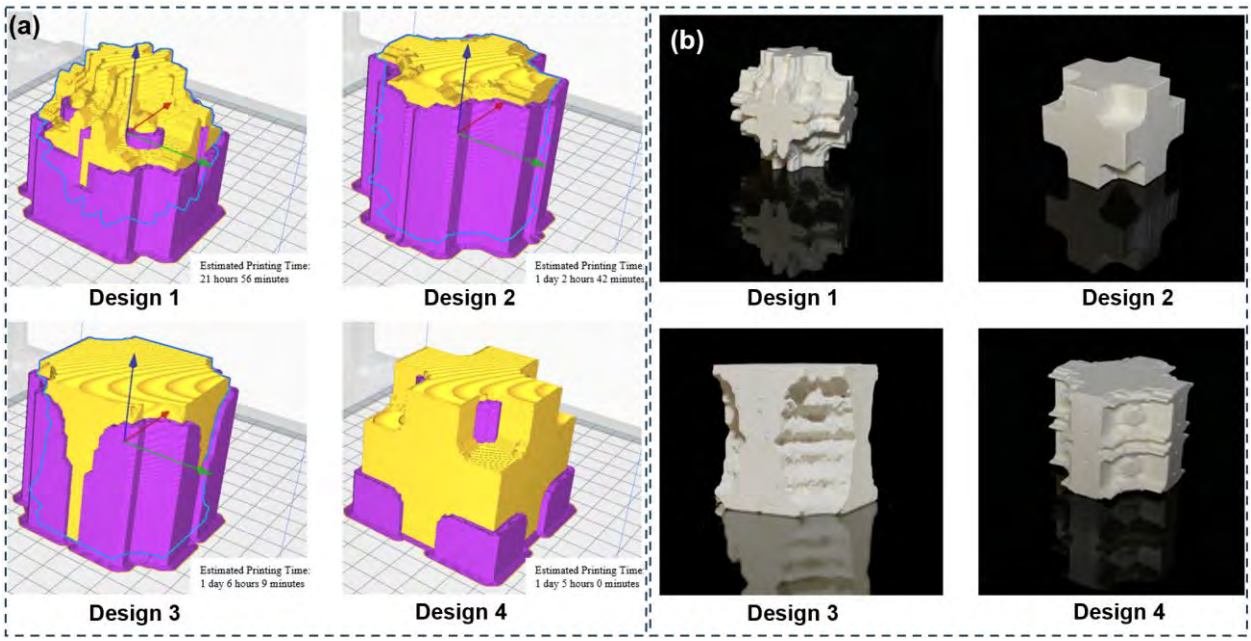


Figure 18. a) Bulk modulus PLA unit cell printing overview. b) Bulk modulus PLA unit cells.

5.3.1.2 Bulk modulus concrete unit cells

Figure 19a illustrates the step-by-step process of transitioning from a 3D-printed PLA unit cell to a silicone mold and finally to a concrete replica. The PLA unit cell acts as the master pattern, capturing the intricate geometric details of the design. This PLA model is used to create a silicone mold, which faithfully preserves the precision and complexity of the original structure. Before casting, the silicone mold was sprayed with a lubricant to ensure easy demolding and to prevent damage to the cast. The silicone mold then serves as a flexible and reusable tool for fabricating the concrete samples, ensuring accurate replication of the intricate features. Using this method, 60 mm

x 60 mm x 60 mm concrete models were successfully fabricated, as shown in Figure 19b. All samples underwent a 28-day curing process under uniform conditions to ensure consistent hydration and development of mechanical properties.

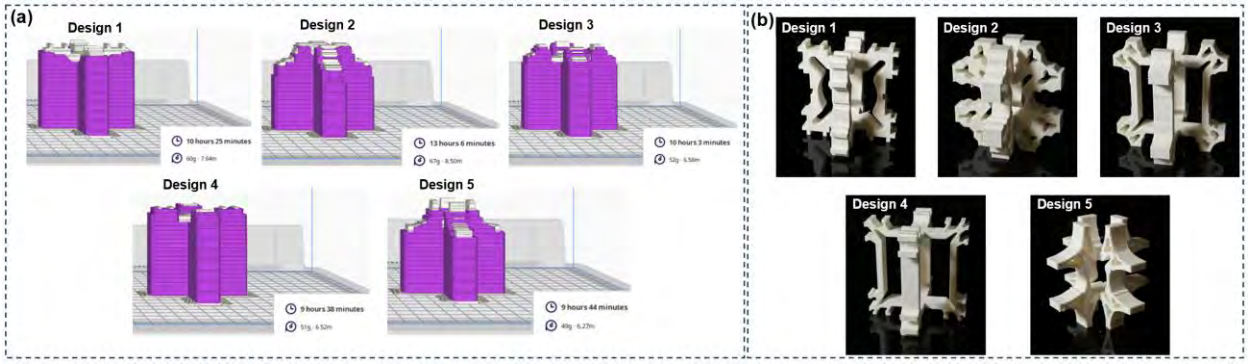


Figure 20. a) Overview of the NPR polymeric unit cell printing process. b) Selected NPR polymeric unit cells.

5.4 Mechanical testing of the unit cells

5.4.1 Bulk modulus and Poisson's ratio tests

A cyclic compression test was performed to determine the bulk modulus and Poisson's ratio of the samples. Each sample was confined within a metal box measuring 60×60×60 mm, restricting deformation to the Y-direction (vertical). This setup ensured that the material's compressive behavior was accurately evaluated, with constraints in the X and Z directions (horizontal) preventing lateral expansion. By confining deformation to a single axis, the test enabled precise measurement of vertical compression under pressure. This configuration, as illustrated in Figure 21, provided a controlled environment for assessing the material's mechanical response and resistance to uniform compression under cyclic loading conditions. This methodology facilitated a reliable evaluation of the samples' bulk modulus and Poisson's ratio. The bulk modulus test was conducted as a cyclic compression test with a displacement of 1 mm at a frequency of 0.5 Hz over 10 cycles (Figure 21a).

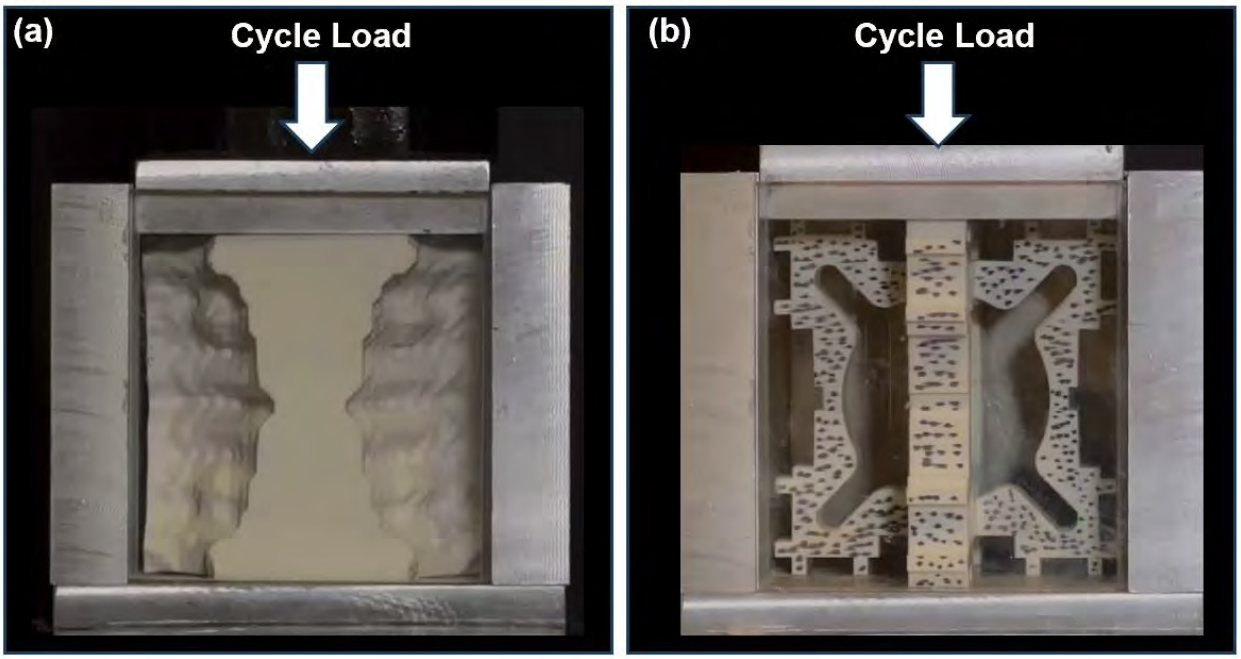


Figure 21. Test setup for a) bulk modulus unit cells. b) Poisson's ratio unit cells.

The NPR test was conducted as a cyclic compression test with a displacement of 0.5 mm, a frequency of 0.5 Hz, and a total of 10 cycles (Figure 21b). Black reference points were marked on the samples to enable accurate strain measurement using video gauge tracking. Tables 4 and 5 provide a comparative summary of the theoretical and experimental values of bulk modulus and Poisson's ratio for the tested MM structures. The discrepancies between the theoretical predictions and experimental measurements are within an acceptable error range. These differences can be attributed to inherent limitations in the precision of the 3D printing process and variability in experimental testing conditions. This comparison underscores the reliability of the theoretical models while highlighting the need to account for practical factors in experimental validations.

Table 4. Calculated theoretical and experimental bulk moduli for the MM concrete unit cells optimized for maximized strength-to-density ratio.

Sample	Material	Theoretical Bulk Modulus (GPa)	Experimental Bulk Modulus (GPa)	Error Rate
 Design 1	PLA	0.91	0.90	1%
	Concrete	0.95	0.89	6%
 Design 2	PLA	1.07	1.02	5%
	Concrete	1.11	1.04	6%
 Design 3	PLA	1.30	1.32	2%
	Concrete	1.30	1.19	8%
 Design 4	PLA	1.71	1.59	7%
	Concrete	2.47	2.10	15%
 Solid Sample	PLA	3.01	2.97	1%
	Concrete	2.7	3	11%

Table 5. Calculated theoretical and experimental Poisson's ratio values for the MM structures designed for maximum flexural strength.

Sample	Theoretical PR (GPa)	Experimental PR (GPa)	Error Rate
 Design 1	-0.241	-0.276	15%
 Design 2	-0.482	-0.463	4%
 Design 3	-0.548	-0.588	7%
 Design 4	-0.614	-0.513	16%
 Design 5	-0.563	-0.564	0%

5.4.2 Compression tests

The concrete specimens were prepared and cured for 28 days to allow sufficient hydration and development of mechanical properties. During the test, the machine applied the load uniformly across the specimen's surface, with the load and deformation recorded continuously. The primary

parameters assessed included the peak compressive stress (σ_c) and the strain at failure (ε_c), which are critical for understanding the material's structural performance under compressive loads using the following equations:

$$\sigma_c = \frac{F}{A} \tag{12}$$

$$\varepsilon_c = \frac{\Delta L}{L_0} \tag{13}$$

where the F is the applied force, A is the cross-section area of the specimen, ΔL is the length of the specimen under load, and L_0 is the original length of the specimen.

Figure 22 illustrates a compression test conducted to evaluate the compressive strength of the material. In this test, the testing machine applies a load at a steady rate of 0.00635 mm/s until the specimen fails. This controlled loading rate ensures precise assessment of the material's capacity to withstand compressive forces. The test is crucial for determining the structural integrity and mechanical properties of materials under compressive stress, offering critical insights for engineering and design purposes. Both PLA and concrete designs underwent this test to compare their compressive performance and analyze their respective mechanical behaviors.

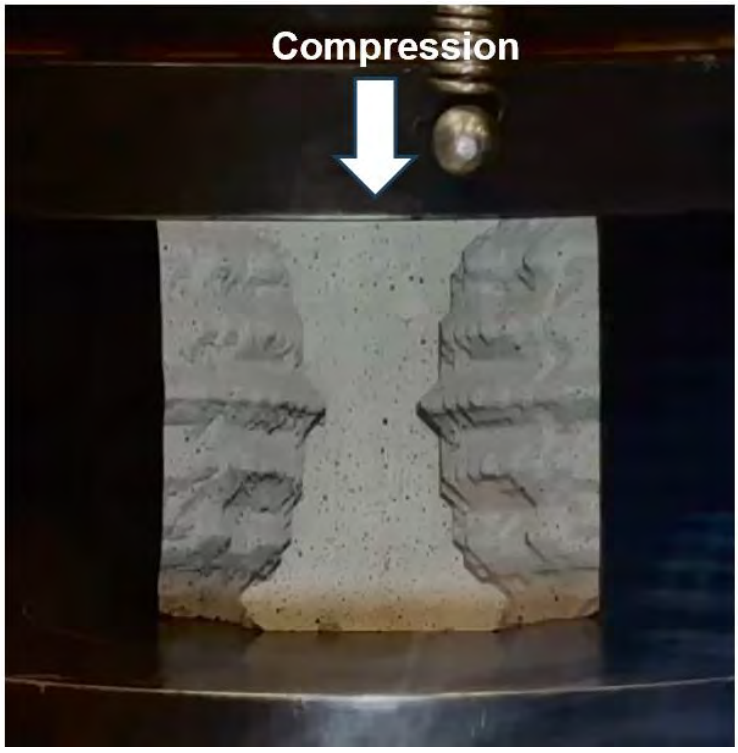


Figure 22. Bulk modulus concrete unit cell compression test.

The PLA unit cells yielded ultimate strength values of 32.71 MPa, 29.34 MPa, 36.00 MPa, 36.77 MPa, 38.82 MPa, 85.57 MPa, 42.10 MPa, 92.20 MPa, and 68.54 MPa for VFs of 0.45, 0.54, 0.63, 0.71, and 1 (solid unit cell), respectively. Table 6 provides a summary of the mechanical properties of MM concrete unit cells optimized for maximum strength by maximizing the bulk modulus and minimizing VF. The VF, which reflects the proportion of solid material to the total sample volume, increases incrementally from 0.45 to 1. As the VF value increases, the weight of the designs also rises, corresponding to the larger amount of material used. One of the most outstanding observations was that the explored metamaterial concrete structures offer a high strength-to-density ratio. The strength-to-density ratio serves as a key metric for material efficiency, indicating how well the material maintains its mechanical performance relative to its weight. The highest strength-to-weight ratios are observed in concrete Design 3 (0.056 MPa·m³/kg) and Design 4 (0.053 MPa·m³/kg), reflecting an optimal balance between structural integrity and material utilization. Design 4 can provide 92.2 MPa ultimate strength at 1726 kg/m³ density, only 2.6% less strength than a solid concrete cube with 94.69 MPa at 2208 kg/m³ density, translating to 22% less weight. This design boasts a strength-to-density ratio of 0.06 MPa·m³/kg, significantly outperforming solid concrete and various construction metals, including mild steel (~0.027 MPa·m³/kg) and structural steel (~0.025-0.035 MPa·m³/kg).

Figure 23 illustrates the results of compression tests for the MM concrete designs. As seen, the strength is increasing with the bulk modulus and VF. Designs 3 and 4 exhibit comparable performance to the solid sample while being significantly lighter. The results suggest a tradeoff between bulk modulus and VF for maximizing strength.

Table 6. Summary of the mechanical properties of MM concrete unit cells optimized for maximized strength-to-density ratio.

Sample	VF (Solid/ Total)	Volume (m³)	Weight (kg)	Density (kg/m3)	Ultimate Strength (MPa)	Strength-to-density Ratio (MPa·m³/kg)
Design 1	0.45	0.00022	0.215	993.8	29.34	0.030
Design 2	0.54	0.00022	0.258	1192.5	36.77	0.031
Design 3	0.63	0.00022	0.301	1391.3	85.57	**0.062**
Design 4	0.71	0.00022	0.339	1567.9	92.2	**0.059**
Solid Sample	1	0.00022	0.477	2208.3	94.69	0.043

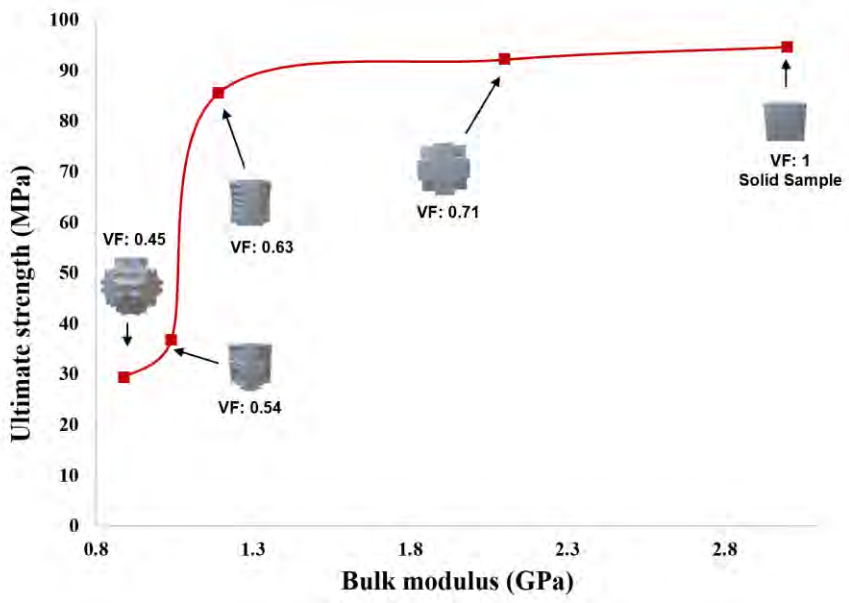


Figure 23. Compression test results of MM concrete designs showing the relationship between strength, bulk modulus, and VF.

5.5 FE simulations

The FE method has seen remarkable advancements in the analysis of reinforced concrete structures since the 1970s [114,115]. In Abaqus, the FE simulation of concrete involves capturing its complex material behavior, including nonlinear phenomena such as cracking, crushing, and plastic deformation. To accurately represent the mechanical properties of concrete, the concrete damage plasticity (CDP) model was utilized [116]. A uniaxial stress-strain relationship for concrete, proposed by Saenz (1964) [117], is given by:

$$\sigma_c = \frac{E_0 \varepsilon_C}{1 + [(E_0 \varepsilon_C / \sigma_p - 2)](\varepsilon_C / \varepsilon_p) + (\varepsilon_C / \varepsilon_p)^2} \tag{14}$$

where σ_c represent the compressive stress, ε_C denotes the compressive strain, σ_p is the peak compressive stress (commonly referred to as compressive strength), ε_p is the strain corresponding to the peak stress, E_0 is the elastic modulus of the concrete, can be estimated by using the ACI equation [118]:

$$E_0 = 4370\sqrt{f_c} \tag{15}$$

where f_c is the compressive strength of the concrete in MPa. This relationship forms the basis for modeling concrete's behavior under uniaxial compression in finite element simulations, enabling detailed analyses of structural performance.

The tensile strength of concrete, f_t, (in MPa), can be estimated using the CEB-FIP code [119], which provides the following relationship:

$$f_t = 1.4(\frac{f_c - 8}{10})^{\frac{2}{3}} \tag{16}$$

To model the tensile behavior of concrete, the tension-softening curve proposed by Hordijk [120] is employed:

$$\frac{\sigma_t}{f_t} = \left[1 + \left(c_1 \frac{w_t}{w_{cr}}\right)^3\right] e^{\left(-c_2 \frac{w_t}{w_{cr}}\right)} - \frac{w_t}{w_{cr}}(1 - c_1^3)e^{-c_2} \tag{17}$$

where σ_t is the tensile stress, f_t is the tensile strength, c_1 and c_2 are constants with values of 3.0 and 6.93, w_t is the crack width, and the w_{cr} is the crack oping displacement (in mm). The crack opening displacement (w_{cr}) can be calculated from the tensile fracture energy (G_F) using the equation:

$$w_{cr} = \frac{5.14 G_F}{f_t} \tag{18}$$

The tensile fracture energy (G_F) was determined using the formulation provided by the CEB-FIP Model Code [121]:

$$G_F = (0.0469 d_a^2 - 0.5 d_a + 26)\left(\frac{f_c}{10}\right)^{0.7} \tag{19}$$

where d_a represents the maximum aggregate size, which is assumed to be 20 mm if no specific data is available.

Damage variables d_c and d_t were utilized to simulate the compressive and tensile damage of concrete. As suggested by Yu et al. [121], the compressive damage variable d_c is set to zero before the maximum stress is reached, as the concrete remains undamaged in this range. However, after the peak stress, d_c is calculated using the equation:

$$d_c = 1 - \frac{\sigma_c}{f_c} \tag{20}$$

For tensile damage, the formula proposed by Chen et al. [122] was adopted, where the rate of shear degradation is governed by the parameter n.The degradation is expressed as:

$$\gamma = (1 - \frac{\varepsilon_{cr}}{\varepsilon_{cr,\mu}})^n \tag{21}$$

and

$$d_t = 1 - \gamma \tag{22}$$

where, ε_{cr} represents the current strain and $\varepsilon_{cr,\mu}$ is the maximum strain.

The simulation process begins with defining the geometry and material properties, including density, elastic parameters, and CDP parameters. The experimental measurements of the stress-strain curves were consistent with the material properties employed in the simulations conducted in this study. The simulation involved creating a mesh using linear eight-node continuum solid elements (C3D8R) for 3D modeling, with refinement in regions where high stress gradients or cracking were anticipated. Dynamic explicit analysis was selected for this study due to its effectiveness in handling high-speed, impact, or transient loading scenarios. This method is particularly suitable for simulations involving complex material behavior, large deformations, and severe nonlinearity, such as crack propagation and failure in concrete [123].

Figure 24 illustrates the displacement magnitude contours for four concrete designs and a solid block reference, as obtained from the FE simulations under compressive loading. For the designs, significant variations in displacement magnitudes are evident, with regions of higher displacement indicating zones of localized cracking or failure. These non-uniform deformation patterns reflect the inherent material heterogeneity and geometric characteristics of each sample. The lower displacement regions correspond to areas with minimal deformation, often near the support or boundary conditions. In contrast, the solid sample exhibits a more uniform deformation pattern, indicative of its homogeneous structure and greater resistance to localized failure. The uniform displacement distribution emphasizes the differences in mechanical behavior between the solid and the designs, further validating the impact of structural properties on performance under loading. Figure 24b illustrates the distribution of minimum principal stress for four concrete designs and a solid block reference under compressive loading. The contour plots reveal significant differences in stress distribution across the designs, with localized high-stress regions indicating areas prone to failure or cracking. These stress concentrations likely result from geometric irregularities, which affect the mechanical response under load. In contrast, the solid reference exhibits a more uniform stress distribution, with fewer localized high-stress regions and a broader presence of lower stress areas, highlighting its homogeneity and superior ability to distribute compressive forces evenly.

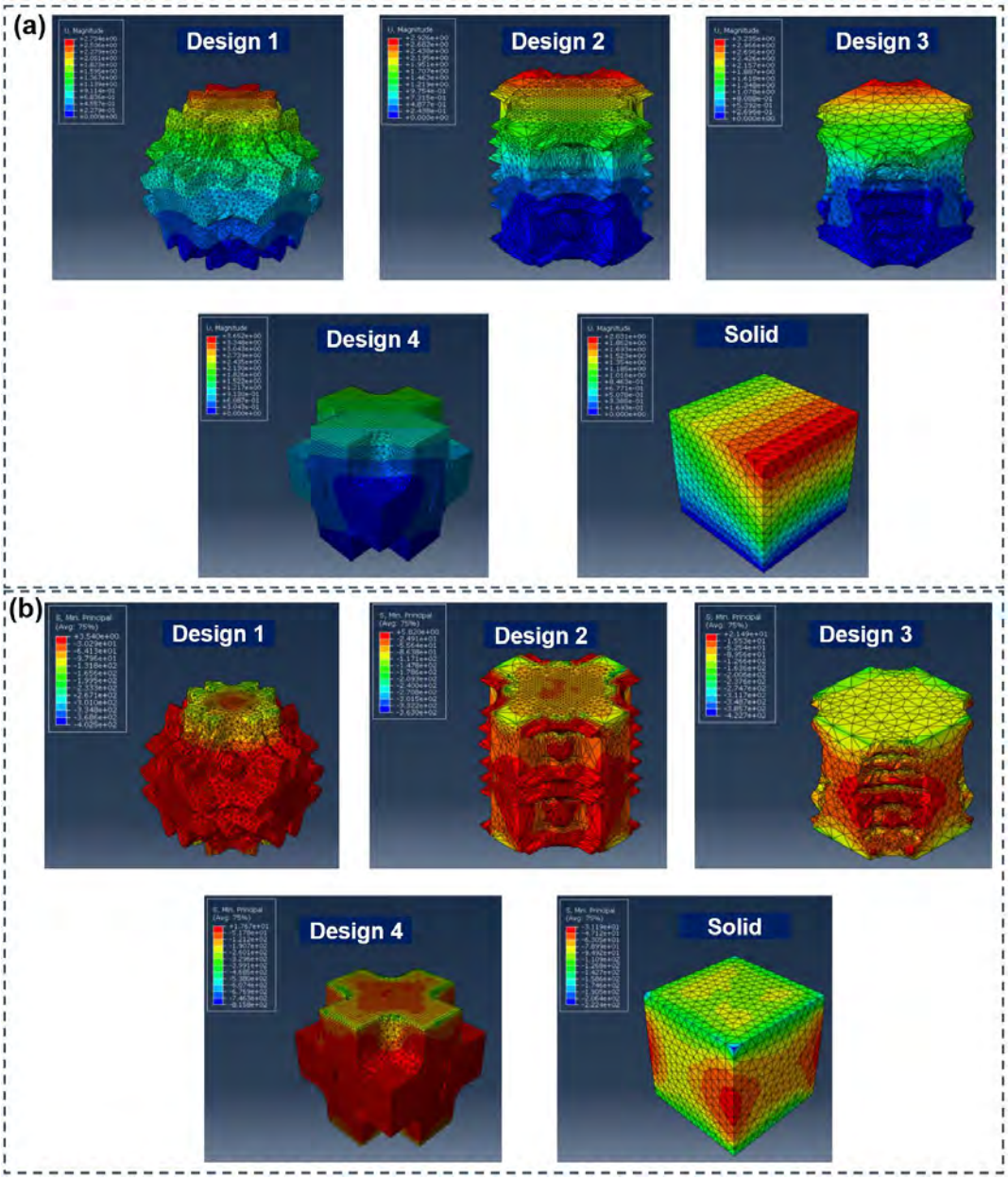


Figure 24. FE simulation results for MM concrete unit cells optimized for maximized strength-to-density ratio: a) Displacements, b) Principal stresses.

5.6 Experiment vs. simulation results

Table 7 provides a quantitative comparison between experimental and simulation results for different concrete designs and a solid control sample. The table shows strains at ultimate strength, ultimate strength values, and the error rate for each sample. The error rates for ultimate strength range from 6% to 9% for the individual designs, while the solid reference shows a minimal error of 0.3%. These error rates are within an acceptable range, indicating that the simulation model

performs reasonably well in predicting the ultimate strength of concrete. The discrepancies observed in the designs compared to the simulation results may be attributed to variations introduced during the fabrication process, such as inconsistencies in mixing, curing conditions, or the influence of air humidity during preparation. These factors can affect the homogeneity and mechanical properties of the designs, leading to minor differences between experimental and simulated results. Despite these limitations, the model demonstrates sufficient reliability for practical engineering applications.

Figure 25 presents the stress-strain curves for MM concrete unit cells optimized for maximum strength-to-density ratio. The experimental data exhibit typical concrete behavior, with an initial linear elastic region followed by nonlinear deformation leading to peak stress. Among the designed designs, Design 4, with the highest volume fraction, demonstrates the greatest ultimate strength and stiffness. The predicted results closely match the experimental curves, particularly in the elastic and peak regions. Some variations arise due to limitations in the simulation model's ability to fully capture real fracture and damage evolution in concrete. However, the differences between experimental and predicted results remain within an acceptable range, indicating the model's reliability for practical applications while accounting for minor deviations from environmental and process-related factors.

Table 6. Comparison of the experimental and FE simulation results for MM concrete unit cells optimized for maximized strength-to-density ratio.

	Experiment		**Simulation**		**Error Rate**
Sample	Strain (mm/mm)	Ultimate Strength (MPa)	Strain (mm/mm)	Ultimate Strength (MPa)	
Design 1	0.0178	29.34	0.027	31.42	7%
Design 2	0.214	36.77	0.035	40.23	9%
Design 3	0.0185	85.57	0.0347	79.11	8%
Design 4	0.018	92.2	0.0385	86.61	6%
Solid Sample	0.0227	94.69	0.026	94.96	0.30%

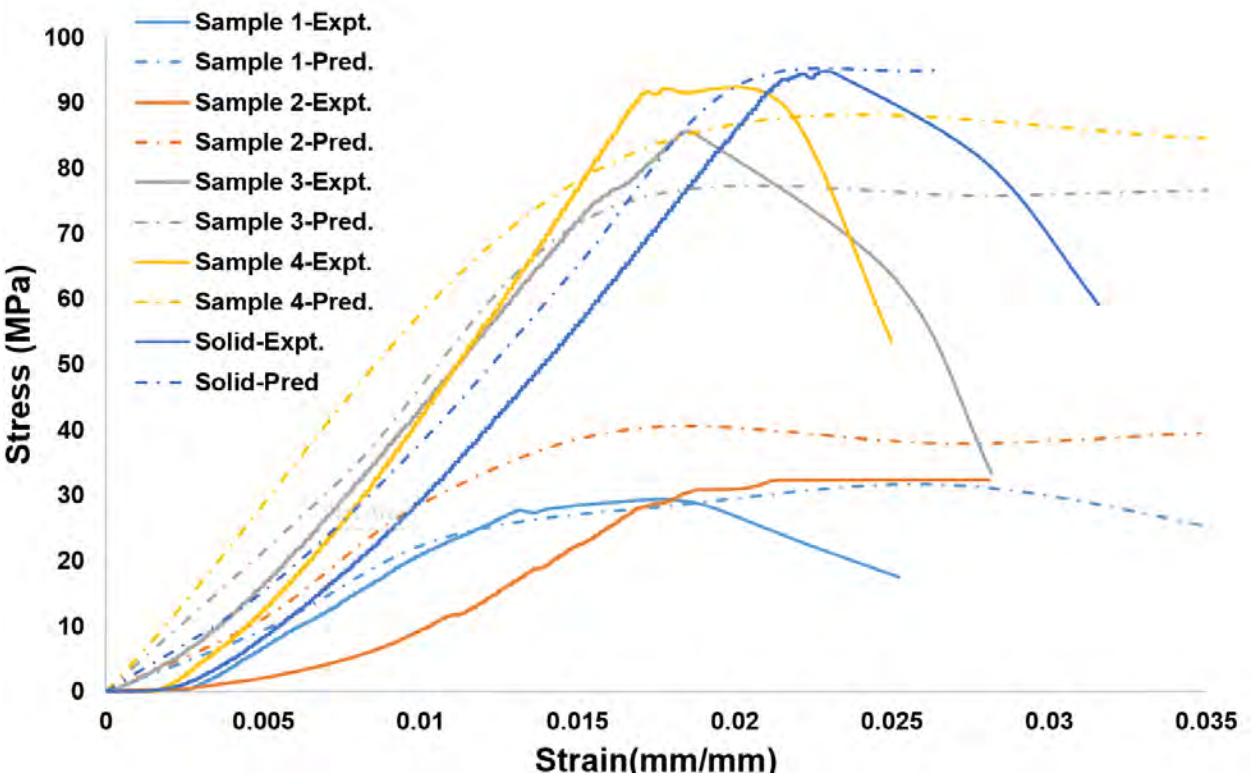


Figure 25. Stress-strain curves of MM concrete unit cells showing experimental and FE results.

6. Design and fabrication of MM-LWC structures

Various MM-LWC structures can be fabricated using the unit cells explored and tested in the previous sections. To assess performance, we selected Design 4, which demonstrated moderate performance, and compared it to a solid cube made entirely of concrete. Two design strategies were considered:

1. A composite MM-LWC structure incorporating 3D polymeric MM reinforcement embedded within the concrete mix.
2. A fully cementitious MM-LWC structure with no embedded reinforcement.

6.1 Composite MM-LWC structure with embedded 3D polymeric MM reinforcement

6.1.1 Design

Figure 26a illustrates the design of the composite MM-LWC structure, featuring an embedded 3D polymeric MM reinforcement. This reinforcement consists of a 3×3×3 unit cell configuration, forming a three-dimensional geometric framework that enhances the mechanical properties of the concrete. Specifically, the MM structure is designed to optimize the strength-to-density ratio,

ensuring efficient load distribution while reducing weight without compromising strength and durability.

Figure 26b presents the schematic of the composite MM-LWC structure, where the 3D-printed polymeric MM reinforcement is integrated within a concrete matrix. Each polymeric unit cell measures 25×25×25 mm, while the reinforced core spans 75×75×75 mm. Encasing this core is a 7.5 mm-thick concrete cover, resulting in an overall structure dimension of 90×90×90 mm. Fabricated using PLA, the polymeric MM core provides localized reinforcement, enhancing the structural integrity of the MM-LWC. By incorporating 3D-printed MM elements, the design capitalizes on advanced metamaterial benefits, including improved load distribution, energy absorption, and controlled failure mechanisms.

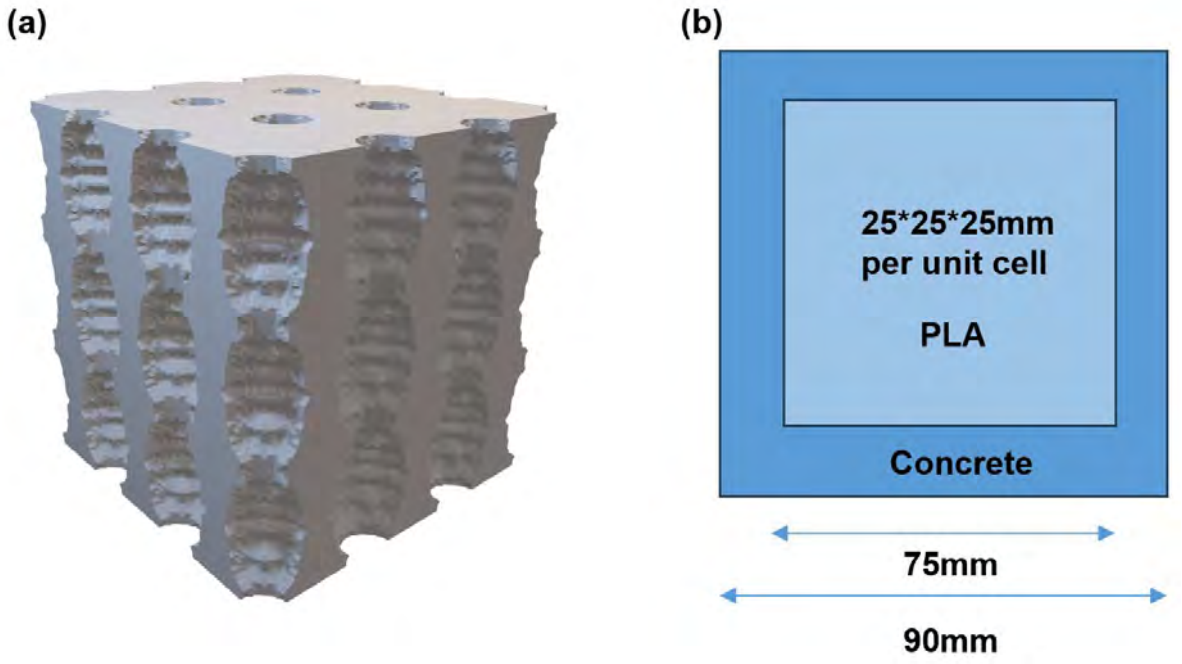


Figure 26. a) 3D model of the designed MM-LWC structure. b) Dimensions of the embedded 3D polymeric MM reinforcement and the entire sample.

6.1.2 Fabrication of the composite MM-LWC structure

The composite metamaterial-reinforced lattice was fabricated using an Ultimaker 3D printer (Figure 27a), utilizing PLA as the primary material and PVA as the support material. After printing, the PVA support was dissolved in water, leaving the PLA lattice intact for use as reinforcement in concrete. The process of creating the LWC system follows a step-by-step procedure. Initially, a 7.5 mm layer of concrete is poured into a cubic silicone mold and left to cure for one day. Once the initial layer has hardened, the PLA lattice is placed on top (Figure 27b). The remaining concrete is then poured around and inside the lattice, completing the casting process. The concrete designs were cured for 28 days to ensure optimal mechanical properties, including compressive and tensile

strength. This curing period allows the cement hydration process to progress sufficiently, resulting in a durable and structurally stable concrete matrix. Throughout this time, the PLA lattice embedded within the concrete serves as reinforcement, enhancing load-bearing capacity and mitigating potential failure mechanisms.

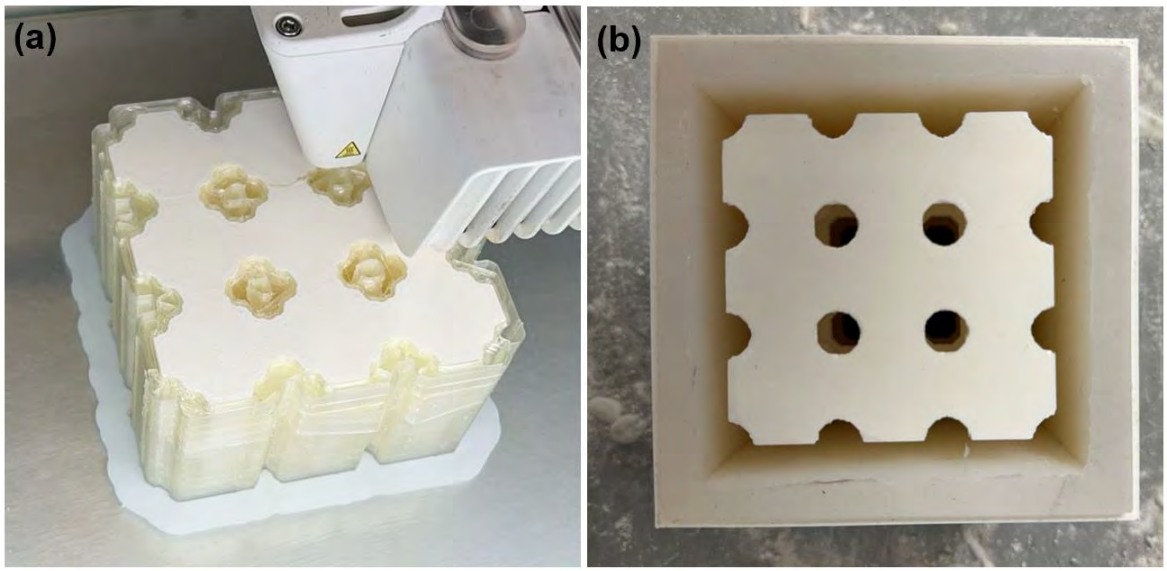


Figure 27. Fabrication of the composite MM-LWC structure. a) MM reinforced structure Printing process of the embedded 3D polymeric MM reinforcement. b) The created mold for pouring concrete mix into the 3D polymeric MM reinforcement structure.

6. Fully cementitious MM-LWC structure

The fabrication of the cementitious MM-LWC sample follows a process similar to unit cell manufacturing, using a PLA unit cell as the master pattern. Unlike reinforced designs, this version consists solely of the cement mix, with no embedded reinforcement. The PLA model precisely captures the intricate geometric details of the lattice design, ensuring high accuracy and complexity. This master pattern is then used to create a silicone mold, which faithfully replicates the design while preserving its fine features. Before casting, the silicone mold is prepared with a release agent, such as a lubricant spray, to facilitate easy demolding and prevent damage to the concrete. As a flexible, reusable tool, the mold enables the production of multiple identical concrete designs with high geometric fidelity. Using this method, 90 mm × 90 mm × 90 mm concrete models were successfully fabricated (Figure 28). After casting, the concrete designs were cured for 28 days under controlled conditions to ensure uniform hydration and full development of mechanical properties, including compressive and tensile strength. This curing period allows the concrete to reach its designed strength and durability, making it suitable for structural and performance testing.



Figure 28. The fabricated composite MM-LWC structure with embedded 3D polymeric MM reinforcement.

Table 7. Summary of the mechanical properties of the MM-LWC structures.

Sample	Volume (m^3)	Weight (kg)	Density (kg/m^3)	Ultimate Strength (MPa)	Strength-to-density Ratio ($MPa \cdot m^3/kg$)
Composite MM-LWC structure	0.000729	1.293	1773.6626	44.27	0.025
Cementitious MM-LWC structure	0.000729	1.096	1503.4294	64.21	0.043
Solid Block	0.000729	1.546	2120.7133	94.69	0.045

6.3 Compression tests

A compression test was conducted to evaluate the compressive strength and mechanical behavior of the materials. During testing, a load was applied at a controlled rate of 0.00635 mm/s until specimen failure. This precise loading rate ensured accurate measurement of the material's compressive strength while minimizing dynamic effects that could alter the results. The test provided critical insights into the structural integrity and mechanical properties of the materials, aiding in engineering and design applications. Concrete specimens were tested to compare their

compressive strength and mechanical behavior, particularly assessing the influence of embedded PLA reinforcement. This comparative analysis helped determine the interaction between PLA and concrete, highlighting their respective contributions to the composite system's mechanical properties and structural behavior. The results presented in Table 7 highlight the performance of the composite MM-LWC structure and the cementitious MM-LWC structure in comparison to the solid block. While the solid block exhibits the highest ultimate strength of 94.69 MPa, it also has the highest density of 2120.71 kg/m³, leading to a strength-to-density ratio of 0.045 MPa·m³/kg. On the other hand, the composite MM-LWC structure, with a density of 1773.66 kg/m³, offers a lower ultimate strength of 44.27 MPa and a strength-to-density ratio of 0.025 MPa·m³/kg, indicating a trade-off between strength and weight efficiency. The cementitious MM-LWC structure, with no embedded reinforcement, demonstrates an ultimate strength of 64.21 MPa and a density of 1503.43 kg/m³, resulting in a strength-to-density ratio of 0.043 MPa·m³/kg, outperforming the composite version. Overall, the cementitious MM-LWC structure offers the best balance between strength and weight efficiency among the two MM-LWC designs, though the solid block remains superior in ultimate strength, albeit at the cost of higher weight. However, it should be noted that for both the composite MM-LWC and cementitious MM-LWC structures, we used a unit cell with moderate performance (Design 3), which has an ultimate strength of 85.57 MPa compared to unit cell Design 4, with an ultimate strength of 92.2 MPa. Despite the lower strength of unit cell Design 3 forming the cementitious MM-LWC structure, the strength-to-density ratio for this structure remains very comparable to the solid block, showing its potential for lightweight, high-performance applications. However, the composite MM-LWC structure seems to underperform, possibly due to the use of PLA material for the 3D MM reinforcement, which may not provide sufficient strength. Incorporating higher-strength materials, such as Nylon or Carbon fiber, could potentially enhance the performance of the composite structure.

7. MM-LWC beam with embedded 3D polymeric reinforcement

Creating a beam using only cementitious unit cells is not an effective solution because cementitious materials are prone to brittleness and cannot effectively resist bending forces. Without reinforcement, the beam would lack the necessary flexibility and strength to withstand bending stresses, leading to potential failure under load. This is why we use polymeric MM structures made of NPR unit cells as reinforcement, as they offer the required flexibility and strength to effectively resist bending forces. By integrating these structures, we hypothesize that the resulting composite could achieve a higher flexural strength-to-weight ratio, improving performance while maintaining or reducing the overall weight of the beam.

7.1 Composite MM-LWC beam fabrication

The detailed design considerations of the samples are discussed in Section 5.1.2. These two specific designs were carefully selected based on key factors, including the VF, unit cell thickness, and overall structural efficiency of the lattices. Figure 29a illustrates the 3D models of the

polymeric MM reinforcement beams formed through the periodic assembly of NPR unit cells for the two distinct designs. Figures 29b,c show the polymeric MM fabricated using PLA as the primary material and PVA as the support material. The use of PVA is essential for achieving intricate geometries, as it provides structural stability during printing and can be easily dissolved in water afterward, leaving behind a precise PLA MM structure that ensures high geometric accuracy and design integrity.

Each NPR unit cell measures 15×15×15 mm, and each polymeric MM beam was fabricated using six unit cells, resulting in a total length of 180 mm. The polymeric MM beams were embedded within the concrete matrix. The MM-LWC beams have a length of 200 mm, a height of 50 mm, and a width of 50 mm (Figure 29d). According to the design specifications, the MM beams must be precisely positioned at the center of the concrete beam. To achieve this, a 0.3 mm wire was used to lift and position the sample during the beam fabrication process. Once the wire was secured to hold the lattice in place, concrete was carefully poured into the rectangular beam mold, ensuring no displacement of the embedded lattice. After casting, the composite MM-LWC beams underwent a 28-day curing process.

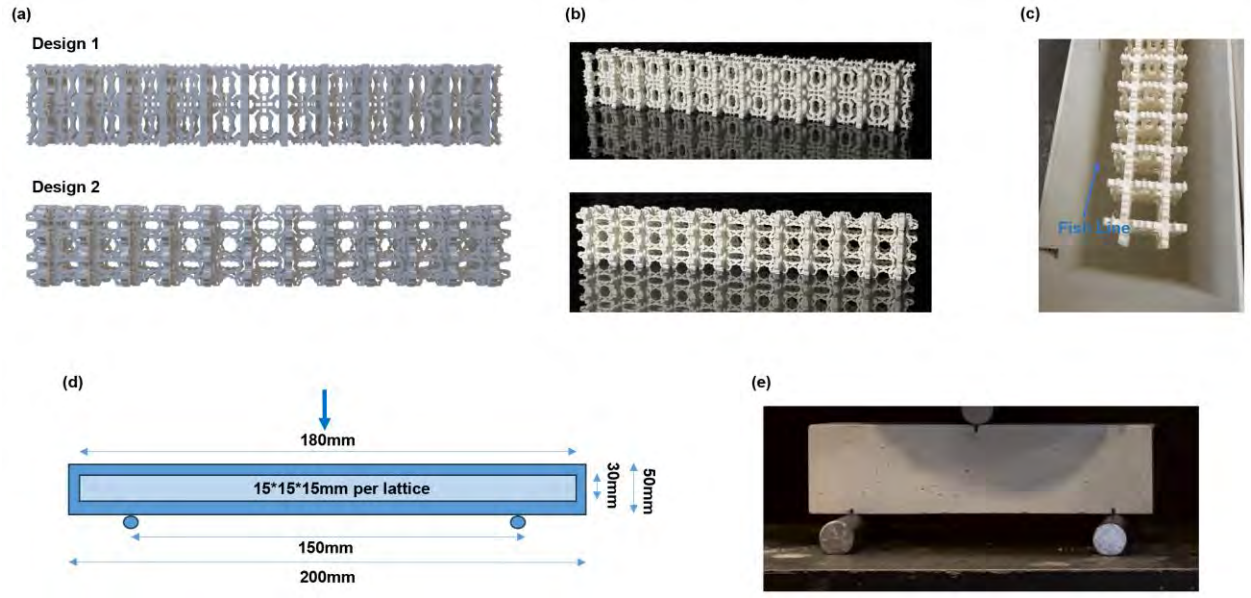


Figure 29. a) 3D model of the polymeric MM reinforcement beams formed through the periodic assembly of two different NPR unit cells. b) MM beams printed using PLA. c) Placing the MM beam inside the mold. d) Beam design and test setup overview. e) 3-point bending test setup for the composite MM-LWC beams.

Table 8. Summary of the mechanical properties of the composite MM-LWC beams.

Sample	Volume (m^3)	Weight (kg)	Density (kg/m3)	Flexural Strength (MPa)	Strength-to-density Ratio (MPa·m^3/kg)
 MM-LWC beam 1	0.0005	1.038	2076	13.45	0.006
 MM-LWC beam 2	0.0005	1.038	2076	9.45	0.005
 Solid Beam	0.0005	1.077	2154	13.07	0.006

7.2 Three-point bending testing of the composite MM-LWC beams

After a 28-day curing period, 3-point bending tests were conducted on three MM-LWC beams, each fabricated using two different types of NPR unit cells, along with a solid beam as a control. Figures 29d and e show the test setup. The test involved applying force to the center of each specimen at a controlled rate of 0.00215 mm/s until failure occurred. The samples were continuously loaded, and observations were recorded until structural failure was evident. During the testing, measurements were taken of the applied force at specific moments and the deflection at the point of load application. These measurements were crucial for determining the flexural stress (σ_f) and flexural strain (ε_f) of the concrete beams. The calculations were based on the following equations:

$$\sigma_f = \frac{3FL}{2bd^2} \tag{23}$$

$$\varepsilon_f = \frac{6Dd}{L^2} \tag{24}$$

where F is the applied force at a given moment, L is the span length, b is the beam width, d is the beam thickness and D is the deflection at the applied force point.

Table 8 presents the mechanical properties of the fabricated beams. The results indicate that MM-LWC beam 1 exhibits the highest flexural strength at 13.45 MPa, slightly outperforming the solid beam, which has a flexural strength of 13.07 MPa. Meanwhile, MM-LWC beam 2 demonstrates a lower flexural strength of 9.45 MPa, suggesting variability in performance between the two MM-LWC beams. In terms of density, both MM-LWC beams have a slightly lower density (2076 kg/m^3) compared to the solid beam (2154 kg/m^3), indicating a minor weight reduction. The strength-to-density ratio for MM-LWC beam 1 and the solid beam is identical at 0.006 MPa·m^3/kg, whereas MM-LWC beam 2 has a slightly lower ratio of 0.005 MPa·m^3/kg. These results suggest that the integration of NPR-based MM reinforcement can potentially match or even exceed the performance of traditional solid beams in flexural applications while maintaining a reduced weight,

although performance variations highlight the need for further optimization in design and fabrication.

It is worth mentioning that PLA used to fabricate the polymeric MM reinforcement beams is a brittle material, making it less than ideal for structural reinforcement in flexural applications. Its limited ductility and tendency to fracture under stress suggest that alternative materials such as nylon or carbon-fiber-reinforced composites could significantly enhance the performance of MM-reinforced beams. These high-strength polymers offer superior flexibility, toughness, and durability, which could easily allow MM-LWC beams to outperform traditional solid concrete beams. However, investigating these materials was beyond the scope of this study. In addition, the use of polymer-based reinforcement is particularly important given the rise of recycled filament technology. By utilizing recycled plastics to fabricate MM reinforcements, it becomes possible to create sustainable, high-performance composite beams while reducing plastic waste. This approach not only enhances structural efficiency but also promotes circular economy principles, allowing for the recycling and repurposing of materials to outperform fully cementitious beams in both strength and environmental impact.

8. Large-scale implementation of the MM-LWC structures

The transition from laboratory-scale research to large-scale implementation is a crucial step in validating the feasibility of innovative materials for civil infrastructure. While small-scale testing provides critical insights into material performance, demonstrating large-scale applications ensures that the material can withstand real-world loads and environmental conditions. Lightweight, high-strength MM-LWC structures hold significant promise for applications in bridges, buildings, and other infrastructure systems. To illustrate the feasibility of large-scale implementation, we fabricated larger MM-LWC designs based on the most efficient unit cell design identified in this study. For this study, we selected Design 3 from the bulk modulus-optimized unit cells, as it exhibited the highest strength-to-density ratio (0.056 MPa·m³/kg) (Table 6). To scale up our experimental framework, we fabricated large cubic MM-LWC specimens with dimensions of 152.4×152.4×152.4 mm (6-inch cubic samples), following the same manufacturing process detailed in Section 5.1. The fabrication method included the use of 3D-printed PLA master patterns, silicone molds, and subsequent casting with a concrete mix.

The fabricated cubic MM-LWC specimens are shown in Figure 30. A total of eight cubic samples were fabricated and assembled into a structural beam measuring 1219.2 mm (4 feet) in length. The MM-LWC designs demonstrate excellent performance under compression, making them well-suited for applications where compressive loads dominate, such as columns, walls, and foundation components. However, for bending-dominated structures like beams, additional reinforcement strategies are necessary to mitigate flexural weaknesses. While the unit cells explored in this study exhibit high strength and low density, their flexural performance remains a challenge when scaled up to beam applications. To address this issue, we investigated post-tensioning as a viable solution.

The post-tensioning technique enhances flexural strength by introducing compressive stresses into the material, counteracting tensile forces that develop under loading. To facilitate post-tensioning, a hole was drilled through each of the MM-LWC cubic specimens, allowing post-tensioning cables and their hoses to pass through the concrete mass. This integration ensures that the beam maintains its lightweight advantages while improving its ability to withstand bending forces. The detailed design and fabrication process of the post-tensioned MM-LWC beam is presented in the Appendix.

The successful fabrication and assembly of large-scale MM-LWC specimens into a functional beam demonstrate the feasibility of scaling up these novel materials for real-world civil infrastructure applications. By selecting the most efficient unit cell and employing post-tensioning for enhanced flexural performance, MM-LWC can potentially replace traditional concrete in structural elements that require both high strength and reduced weight. Future work will further refine these techniques to optimize performance and durability, paving the way for widespread adoption in large-scale engineering projects.

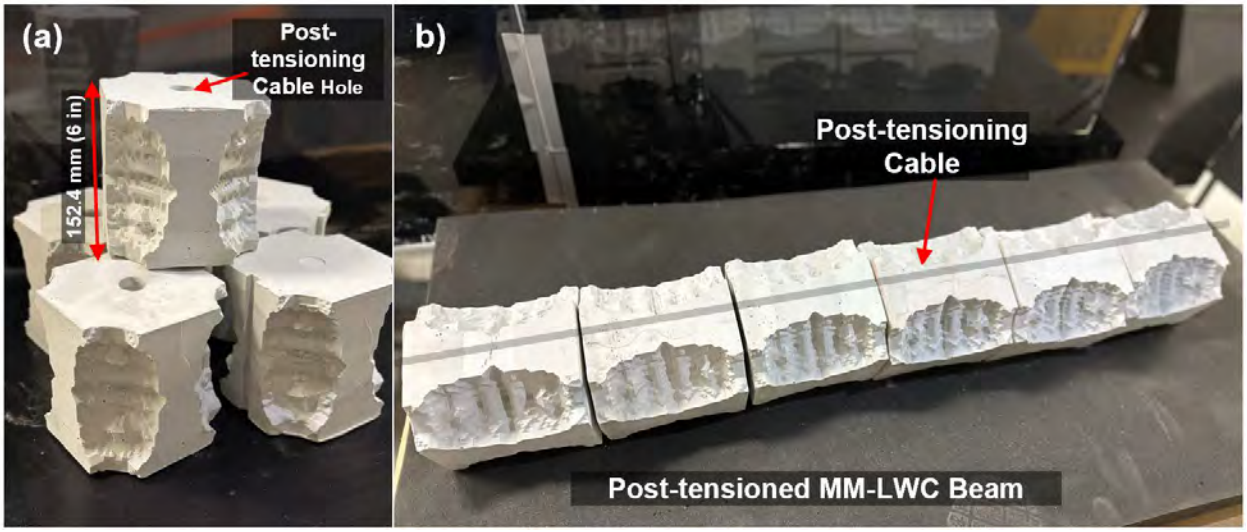


Figure 30. Large-scale implementation of the MM-LWC structures. a) 6-inch cubic samples optimized for highest strength-to-density ratio. b) Construction of a post-tensioned MM-LWC beam through the assembly of unit cells and integration of post-tensioning cables within the concrete mass.

9. Implementation guideline

Translating MM-LWC technology into practical applications requires a structured approach to ensure seamless integration into construction workflows. This section provides guidelines for contractors, engineers, and regulatory agencies to facilitate the large-scale adoption of MM-LWC structures.

1. Material Selection and Procurement: The success of MM-LWC implementation begins with the careful selection of materials. The polymeric MM unit cells for bending-dominated applications should be fabricated from high-strength polymers such as carbon-fiber-reinforced nylon to enhance durability and flexural resistance. The concrete mix must be optimized for lightweight performance while maintaining sufficient workability to ensure uniform integration with the embedded MM structures. Standardized procurement guidelines should be established to facilitate material sourcing and quality assurance.

2. Fabrication and Assembly Procedures: The manufacturing of MM-LWC components follows a multi-step process:

- 3D Printing of Unit Cells: The polymeric MM reinforcement should be produced using high-resolution additive manufacturing techniques, ensuring dimensional accuracy and consistency. Support materials should be water-soluble for efficient post-processing.
- Casting and Curing: The MM-reinforced concrete specimens should be cast using precision molds, with controlled pouring techniques to prevent air entrapment. A 28-day curing process under controlled humidity and temperature conditions is necessary to achieve optimal mechanical properties.

For large-scale implementations, modular prefabrication is recommended, allowing MM-LWC units to be manufactured off-site and assembled on-site, reducing construction time and labor costs.

3. Structural Integration and Reinforcement Strategies: While MM-LWC structures offer superior compressive performance, additional reinforcement is needed for bending-dominated applications. Post-tensioning is a viable approach to enhance flexural strength by introducing compressive stresses within the beam. In practice, this involves:

- Drilling alignment holes in MM-LWC specimens to accommodate post-tensioning cables.
- Pre-stressing the system using hydraulic tensioners before finalizing the assembly.
- Encapsulating the structure in a high-performance grout to improve bond strength and load transfer.
- For cases where embedding post-tensioning cables within the metamaterial voids is complex, alternative external reinforcement strategies can be explored. One promising approach is external post-tensioning, where cables are placed outside the lattice structure, running parallel to the beam and anchored to external plates or brackets. Another option is surface-grooved channels, where shallow grooves are carved along the external surfaces of the blocks to house the cables. Additionally, external trusses or tie beams can be integrated as a hybrid approach, maintaining lattice integrity while enhancing structural performance through controlled tensioning.

4. Design Considerations for Infrastructure Applications: The implementation of MM-LWC should be tailored to specific structural applications, including:

- Bridge Decks and Pavement Systems: MM-LWC can significantly reduce dead loads, leading to lighter bridge structures and improved seismic resilience.
- Prefabricated Structural Components: Wall panels, columns, and modular housing units can benefit from the lightweight and high-strength properties of MM-LWC.
- High-Performance Beams and Slabs: The integration of MM unit cells within flexural members should be complemented by reinforcement techniques to ensure long-term stability.

5. Quality Control and Field Testing: Before full-scale implementation, rigorous testing must be conducted to validate mechanical performance under real-world loading conditions. Standardized compression, bending, and cyclic loading tests should be carried out to assess:

- Load-bearing capacity and deformation characteristics.
- Fatigue resistance and long-term durability.
- Structural behavior under extreme conditions, such as seismic and impact loads.

Additionally, real-time structural health monitoring systems can be incorporated to track in-service performance and identify potential failure modes.

6. Regulatory Compliance and Industry Adoption: For MM-LWC to gain widespread acceptance, collaboration with regulatory bodies is essential. This includes:

- Developing standardized construction codes for MM-LWC applications.
- Conducting pilot projects in collaboration with public agencies to demonstrate feasibility.
- Engaging with industry stakeholders to promote awareness and investment in MM-LWC technologies.

By following these guidelines, MM-LWC can be effectively integrated into civil infrastructure projects, offering a sustainable and high-performance alternative to traditional construction materials

10. Conclusion and future works

10.1 Conclusion

The study successfully demonstrated the feasibility of implementing MM-LWC structures as an innovative alternative to traditional lightweight concrete for infrastructure applications. By leveraging advanced metamaterial design principles, we developed and evaluated structural elements with significantly improved strength-to-weight ratios. The feasibility of the proposed MM-LWC was thoroughly investigated through a multi-faceted approach that included cyclic tests, compression tests, and three-point bending tests. These experimental methods provided critical insights into the material's mechanical behavior, durability, and failure mechanisms. The experimental results confirmed that MM-LWC specimens exhibit superior mechanical properties compared to conventional concrete, particularly in terms of compressive strength. The experimental results were complemented by FEM simulations. FEM modeling enabled detailed

analysis of stress distribution, deformation patterns, and failure progression, ensuring the reliability and accuracy of the proposed system.

The project paves the way for further refinement and optimization of the MM-LWC system through iterative design improvements, enhanced fabrication methods, and targeted performance evaluations. This foundation supports its potential for large-scale implementation in advanced engineering systems, addressing the growing demand for sustainable, cost-effective, and high-performance materials. By setting a new benchmark for efficient infrastructure design, the MM-LWC concept establishes itself as a transformative solution, enabling the construction of resilient structures that meet modern challenges while promoting sustainability and resource conservation.

10.2 Future works

The following recommendations are proposed for future work:

1. Investigation of 3D printing materials:
   Advanced polymers, bioplastics, and metal-polymer composites can be investigated for their potential to improve mechanical properties, durability, and environmental resistance. Incorporating sustainable and recyclable materials should be a priority, aiming to reduce the ecological footprint of production while preserving the structural integrity of the systems. Additionally, hybrid materials can be developed by combining the benefits of multiple material classes, such as embedding high-strength fibers into PLA or other thermoplastics. These hybrids are expected to provide superior load-bearing capacity, enhanced energy absorption, and increased longevity, paving the way for more robust and eco-friendlier MM-LWC solutions.
2. Optimization and automation of fabrication processes:
   Advanced techniques can be developed to ensure consistent quality across complex designs, enabling reliable performance in structural applications. Automation technologies, such as robotic-assisted printing and assembly, can be integrated to streamline the embedding of metamaterial structures within concrete matrices, reducing human error and increasing production speed. Efforts can also target scalability by investigating cost-effective methods to optimize production. Modular construction techniques can be explored to simplify assembly processes and enable the prefabrication of components for large-scale applications. Multi-material printing capabilities can be leveraged to expand the versatility of fabrication, allowing the incorporation of diverse materials within a single structure for improved functionality. Challenges in post-processing, such as the dissolution of PVA supports, will be addressed to enhance overall process efficiency. Solutions may include optimizing support structures to minimize material waste and reduce processing time while maintaining the geometric accuracy of the lattice.
3. Full-scale implementation and field testing:
   MM-LWC systems can be scaled up to full-size prototypes, including structural elements like bridge decks, retaining walls, and pavement panels, to assess their performance in real-world applications. Long-term field testing can be conducted under a variety of

environmental conditions, including temperature fluctuations, moisture exposure, and sustained mechanical loading, to assess the system's durability and adaptability over time. The performance of MM-LWC systems under dynamic and impact loads can also be a key area of focus, particularly for critical infrastructure in earthquake-prone regions and high-traffic areas. These tests verify the system's ability to withstand extreme conditions while maintaining structural integrity and safety. To further enhance the reliability of MM-LWC systems, methods for in situ performance monitoring can be developed. This includes the integration of advanced sensor technologies to enable real-time structural health monitoring, providing continuous feedback on stress, strain, and potential damage.

By focusing on these critical areas, future research could ensure that MM-LWC systems are refined to deliver exceptional performance not only in controlled laboratory and theoretical conditions but also in practical, real-world applications. These advancements will address the challenges of scalability, durability, and sustainability, paving the way for widespread adoption of MM-LWC systems in modern infrastructure. Through innovative design, material optimization, and advanced fabrication and testing methods, MM-LWC systems will establish themselves as a benchmark for high-performance, eco-friendly construction materials. This will enable their application across a diverse range of fields, including transportation, urban development, and disaster-resistant structures, setting a new standard for sustainable and efficient engineering solutions.

References

[1] S. Mindess, "Acoustic emission methods," Handbook on Nondestructive Testing of Concrete Second Edition, Dec. 2003. doi:10.1201/9781420040050.ch16

[2] ACI Committee 213, Guide for Structural Lightweight Aggregate Concrete, Farmington Hills, MI: American Concrete Institute, 2001.

[3] A. Chaipanich and P. Chindaprasirt, "The properties and durability of autoclaved aerated concrete masonry blocks," Eco-Efficient Masonry Bricks and Blocks, pp. 215–230, 2015. doi:10.1016/b978-1-78242-305-8.00009-7

[4] A. Haddadian, U. Johnson Alengaram, P. Ayough, K. H. Mo, and A. Mahmoud Alnahhal, "Inherent characteristics of agro and industrial by-products based Lightweight Concrete – a comprehensive review," Construction and Building Materials, vol. 397, p. 132298, Sep. 2023. doi:10.1016/j.conbuildmat.2023.132298

[5] Li, J., Wu, Z., Shi, C., Yuan, Q., & Zhang, Z. (2020). Durability of ultra-high performance concrete–A review. Construction and Building Materials, 255, 119296.

[6] B. Graybeal, Ultra-High Performance Concrete, No. FHWA-HRT-11-038, 2011.

[7] X. Wang et al., "The unification of light weight and ultra-high strength in LWC: A new homogeneity enhancement approach," Construction and Building Materials, vol. 315, p. 125647, Jan. 2022. doi:10.1016/j.conbuildmat.2021.125647

[8] Zhang, J.; Zhao, Y.; Li, H. Experimental Investigation and Prediction of Compressive Strength of Ultra-High Performance Concrete Containing Supplementary Cementitious Materials. Adv. Mater. Sci. Eng. 2017, 2017, 4563164.
[9] Wang, L., Jiang, H., Li, Z., & Ma, G. (2020). Mechanical behaviors of 3D printed lightweight concrete structure with hollow section. Archives of Civil and Mechanical Engineering, 20(1), 1-17.
[10] Aghdasi, P., Williams, I. D., Salazar, B., Panditi, N., Taylor, H. K., & Ostertag, C. P. (2019). An octet-truss engineered concrete (OTEC) for lightweight structures. Composite Structures, 207, 373-384.
[11] J. E. Bolander, S. Choi, and S. R. Duddukuri, "Fracture of fiber-reinforced cement composites: Effects of fiber dispersion," International Journal of Fracture, vol. 154, no. 1–2, pp. 73–86, Nov. 2008. doi:10.1007/s10704-008-9269-4
[12] Salazar, B., Aghdasi, P., Williams, I. D., Ostertag, C. P., & Taylor, H. K. (2020). Polymer lattice-reinforcement for enhancing ductility of concrete. Materials & Design, 196, 109184.
[13] O. Švec, G. Žirgulis, J. E. Bolander, and H. Stang, "Influence of formwork surface on the orientation of steel fibres within self-compacting concrete and on the mechanical properties of cast structural elements," Cement and Concrete Composites, vol. 50, pp. 60–72, Jul. 2014. doi:10.1016/j.cemconcomp.2013.12.002
[14]A.H. Alavi, K.J. Barri, Q. Zhang, L. Khazanovich, "Super-compressible metamaterial concrete and method for making same," U.S. Provisional Pat. Ser. No. 63/245,300, June 2021.
[15] Q. Zhang et al., "Bio-inspired morphological evolution of Metastructures with new operation modalities," Advanced Intelligent Systems, vol. 5, no. 5, May 2023. doi:10.1002/aisy.202370016
[16] H.-O. Lamprecht, Opus Caementitium: Bautechnik der Römer, 5th ed. Düsseldorf, Germany: Beton-Verlag GmbH, 1996, p. 264, ISBN 3-7640-0350-2.
[17] "ESCSI: Expanded shale, clay and slate institute," For Construction Pros, https://www.forconstructionpros.com/home/company/22379339/escsi-expanded-shale-clay-and-slate-institute (accessed Nov. 25, 2024).
[18] S. Chandra and L. Berntsson, "Lightweight aggregate concrete microstructure," Lightweight Aggregate Concrete, pp. 131–166, 2002. doi:10.1016/b978-081551486-2.50009-2
[19] S. Mindess, J. F. Young, and D. Darwin, Concrete. Upper Saddle River, NJ: Prentice Hall, 2003.
[20] S. H. Kosmatka, B. Kerkhoff, and W. C. Panarese, Design and Control of Concrete Mixtures. Skokie, IL: Portland Cement Association, 2011.
[21] A. Short and W. Kinniburgh, Lightweight Concrete. London, UK: Applied Science Publishers, 1978.
[22] M. Schlaich and M. E. Zareef, "Infraleichtbeton," Beton- und Stahlbetonbau, vol. 103, no. 3, pp. 175–182, Feb. 2008. doi:10.1002/best.200700605
[23] DIN EN 1520:2011-06, Vorgefertigte Bauteile aus Haufwerksporigem Leichtbeton und mit statisch anrechenbarer oder nicht anrechenbarer bewehrung; Deutsche Fassung EN_1520:2011. doi:10.31030/1720849

[24] Eurocode 2: Design of concrete structures. doi:10.3403/03178016
[25] P. G. Bergan, K. Bakken, and K.-C. Thienel, “Analysis and design of sandwich structures made of steel and lightweight concrete,” III European Conference on Computational Mechanics, pp. 9–9. doi:10.1007/1-4020-5370-3_9
[26] European Committee for Standardization, EN 1520: Precast Concrete Products – Lightweight Aggregate Concrete with Open Structure, 2011.
[27] B. H. Spratt, An Introduction to Lightweight Concrete. London, UK: Cement and Concrete Association, 1980.
[28] A. J. Hamad, “Materials, production, properties and application of Aerated Lightweight Concrete: Review,” International Journal of Materials Science and Engineering, 2014. doi:10.12720/ijmse.2.2.152-157
[29] ASTM C 33-97, Standard Specification for Concrete Aggregates, in Annual Book of ASTM Standards, vol. 4.02, pp. 10–6, 1997.
[30] DIN EN 13055, Leichte Gesteinskörnungen (Lightweight Aggregates). Berlin, Germany: Beuth-Verlag, 2016, p. 58.
[31] ASTM C330M-17a, Standard Specification for Lightweight Aggregates for Structural Concrete. West Conshohocken, PA, USA: ASTM International, 2017.
[32] S. Chandra and L. Berntsson, Lightweight Aggregate Concrete. Oxford, UK: Noyes Publications, 2002.
[33] J. L. Clarke, Structural Lightweight Aggregate Concrete. London, UK: Taylor & Francis, 1993.
[34] S. Chandra and L. Berntsson, “Lightweight aggregate concrete microstructure,” Lightweight Aggregate Concrete, pp. 131–166, 2002. doi:10.1016/b978-081551486-2.50009-2 M Hassanpour, P Shafigh, HB Mahmud - Construction and Building …, 2012 – Elsevier
[35] Y. Ke, A. L. Beaucour, S. Ortola, H. Dumontet, and R. Cabrillac, “Influence of volume fraction and characteristics of lightweight aggregates on the mechanical properties of concrete,” Construction and Building Materials, vol. 23, no. 8, pp. 2821–2828, Aug. 2009. doi:10.1016/j.conbuildmat.2009.02.038
[36] M. J. Shannag, “Characteristics of lightweight concrete containing mineral admixtures,” Construction and Building Materials, vol. 25, no. 2, pp. 658–662, Feb. 2011. doi:10.1016/j.conbuildmat.2010.07.025
[37] Author links open overlay panelTommy Y. Lo et al., “The effects of aggregate properties on lightweight concrete,” Building and Environment, https://www.sciencedirect.com/science/article/abs/pii/S036013230600179X (accessed Nov. 25, 2024).
[38] DIN 1045-2. Tragwerke aus Beton, Stahlbeton und Spannbeton–Teil 2: Beton–Festlegung, Eigenschaften, Herstellung und Konformität–Anwendungsregeln zu DIN EN 206-1 (Concrete, reinforced and prestressed concrete structures–Part 2: Concrete–Specification, Properties, Production and Conformity–Application Rules for DIN EN 206-1); Beuth-Verlag: Berlin, Germany, 2008; p. 62.

[39] J. Newman, B. S. Choo, and P. Owens, Advanced Concrete Technology: Processes. Oxford, UK: Elsevier Ltd, 2003. [40] M. A. El Zareef, Conceptual and Structural Design of Buildings Made of Lightweight and Infra Lightweight Concrete. [Online]. Available: [Include relevant URL or publisher details if available]. [Accessed: Nov. 25, 2024].concrete", PhD thesis, Berlin University of Technology, 2010.
[41] Deutscher Beton- und Bautechnik-Verein e.V., Merkblatt "Sichtbeton" (Leaflet-Exposed Concrete). Berlin, Germany: Deutscher Beton- und Bautechnik-Verein e.V., 2015, p. 53.
[42] Z. Li, Advanced Concrete Technology. Hoboken, NJ: John Wiley & Sons, 2011.
[43] K.-C. Thienel, T. Haller, and N. Beuntner, "Lightweight Concrete—From Basics to Innovations," Materials, vol. 13, no. 5, p. 1120, 2020. [Online]. Available: https://www.mdpi.com/1996-1944/13/5/1120. [Accessed: Nov. 25, 2024].
by Karl-Christian Thienel *ORCID,Timo HallerORCID andNancy Beuntner
[44] "Light Weight Concrete Market Size, Share, Growth, and Industry Analysis, By Type (Light weight aggregate concrete, Aerated concrete, No fines concrete), By Application (Civil construction, Industrial construction, Infrastructure Construction & others), Regional Insights and Forecast to 2032," Business Research Insights, Aug. 19, 2024. [Online]. Available: https://www.businessresearchinsights.com/market-reports/light-weight-concrete-market-109426. [Accessed: Nov. 25, 2024].
[45] M. F. Ashby, Materials Selection in Mechanical Design, 2nd ed. Oxford, UK: Butterworth-Heinemann, 1992.
[46] A. A. Zadpoor, “Mechanical meta-materials,” Materials Horizons, vol. 3, no. 5, pp. 371–381, 2016. doi:10.1039/c6mh00065g
[47] J. U. Surjadi et al., “Mechanical metamaterials and their engineering applications,” Advanced Engineering Materials, vol. 21, no. 3, Jan. 2019. doi:10.1002/adem.201800864
[48] H. Chen, C. T. Chan, and P. Sheng, “Transformation optics and Metamaterials,” Nature Materials, vol. 9, no. 5, pp. 387–396, Apr. 2010. doi:10.1038/nmat2743
[49] G. Singh, R. ni, and A. Marwaha, “A review of metamaterials and its applications,” International Journal of Engineering Trends and Technology, vol. 19, no. 6, pp. 305–310, Jan. 2015. doi:10.14445/22315381/ijett-v19p254
[50] R. Grimberg, “Electromagnetic metamaterials,” Materials Science and Engineering: B, vol. 178, no. 19, pp. 1285–1295, Nov. 2013. doi:10.1016/j.mseb.2013.03.022
[51] M. Kadic, T. Bückmann, R. Schittny, and M. Wegener, “Metamaterials beyond electromagnetism,” Reports on Progress in Physics, vol. 76, no. 12, p. 126501, Nov. 2013. doi:10.1088/0034-4885/76/12/126501
[52] K. Fan and W. J. Padilla, “Dynamic electromagnetic metamaterials,” Materials Today, vol. 18, no. 1, pp. 39–50, Jan. 2015. doi:10.1016/j.mattod.2014.07.010
[53] R. Grimberg, “Electromagnetic metamaterials,” Materials Science and Engineering: B, vol. 178, no. 19, pp. 1285–1295, Nov. 2013. doi:10.1016/j.mseb.2013.03.022
[54] G. Singh, G. Singh, A. Marwaha, "A review of metamaterials and its applications," Int. J. Eng. Trends Technol. 19 (2015) 305–310.

[55] C. M. Soukoulis and M. Wegener, “Past achievements and future challenges in the development of three-dimensional photonic metamaterials,” Nature Photonics, vol. 5, no. 9, pp. 523–530, Jul. 2011. doi:10.1038/nphoton.2011.154
[56] G. W. Milton and A. V. Cherkaev, “Which elasticity tensors are realizable?,” Journal of Engineering Materials and Technology, vol. 117, no. 4, pp. 483–493, Oct. 1995. doi:10.1115/1.2804743
[57] R. Gatt and J. N. Grima, “Negative compressibility,” physica status solidi (RRL) - Rapid Research Letters, vol. 2, no. 5, pp. 236–238, Oct. 2008. doi:10.1002/pssr.200802101
[58] Z. G. Nicolaou and A. E. Motter, “Mechanical metamaterials with negative compressibility transitions,” Nature Materials, vol. 11, no. 7, pp. 608–613, May 2012. doi:10.1038/nmat3331
[59] T.-C. Lim, “Mechanics of metamaterials with negative parameters,” Engineering Materials, 2020. doi:10.1007/978-981-15-6446-8
[60] Formlabs, Stereolithography (SLA) 3D Printing Guide, 2022. [Online]. Available: https://formlabs.com/blog/ultimate-guide-to-stereolithography-sla-3d-printing/. [Accessed: May 22, 2022].
[61] M. Leary, “Surface roughness optimisation for selective laser melting (SLM),” Laser Additive Manufacturing, pp. 99–118, 2017. doi:10.1016/b978-0-08-100433-3.00004-x
[62] C. Xu, B. Quinn, L. L. Lebel, D. Therriault, and G. L’espérance, "Multi-Material Direct Ink Writing (DIW) for Complex 3D Metallic Structures with Removable Supports," ACS Applied Materials & Interfaces, vol. 11, pp. 8499–8506, 2019. [Online]. Available: https://doi.org/10.1021/ACSAMI.8B19986/SUPPL_FILE/AM8B19986_SI_004.AVI. [Accessed: Nov. 25, 2024].
[63] Introducing chatgpt enterprise, https://openai.com/index/introducing-chatgpt-enterprise (accessed Nov. 25, 2024).
[64] Y. LeCun, Y. Bengio, and G. Hinton, “Deep learning,” Nature, vol. 521, no. 7553, pp. 436–444, May 2015. doi:10.1038/nature14539
[65] A. Krizhevsky, I. Sutskever, and G. E. Hinton, “ImageNet classification with deep convolutional Neural Networks,” Communications of the ACM, vol. 60, no. 6, pp. 84–90, May 2017. doi:10.1145/3065386
[66] I. J. Goodfellow et al., "Generative adversarial networks," arXiv preprint, arXiv:1406.2661, 2014. [Online]. Available: https://arxiv.org/abs/1406.2661. [Accessed: Nov. 25, 2024].
[67] G. Zhou, S. Xie, G. Hao, S. Chen, B. Huang, X. Xu, et al., "Emerging synergies in causality and deep generative models: A survey," arXiv preprint, arXiv:2301.12351, 2023. [Online]. Available: https://arxiv.org/abs/2301.12351. [Accessed: Nov. 25, 2024].
[68] N. R. Mannuru, S. Shahriar, Z. A. Teel, T. Wang, B. D. Lund, S. Tijani, et al., "Artificial intelligence in developing countries: The impact of generative artificial intelligence (AI) technologies for development," Information Development, Sep. 2023.
[69] E. Ziambaras and E. Schröder, “Theory for structure and bulk modulus determination,” Physical Review B, vol. 68, no. 6, Aug. 2003. doi:10.1103/physrevb.68.064112

[70] W. Akl and A. Baz, “Multi-cell active acoustic metamaterial with programmable bulk modulus,” Journal of Intelligent Material Systems and Structures, vol. 21, no. 5, pp. 541–556, Jan. 2010. doi:10.1177/1045389x09359434
[71] G. N. Greaves, A. L. Greer, R. S. Lakes, and T. Rouxel, “Poisson’s ratio and modern materials,” Nature Materials, vol. 10, no. 11, pp. 823–837, Oct. 2011. doi:10.1038/nmat3134
[72] C. Huang and L. Chen, “Negative poisson’s ratio in modern functional materials,” Advanced Materials, vol. 28, no. 37, pp. 8079–8096, Jul. 2016. doi:10.1002/adma.201601363
[73] M. J. Khoshgoftar et al., “Bending analysis of sandwich panel composite with a re-entrant lattice core using zig-zag theory,” Scientific Reports, vol. 12, no. 1, Sep. 2022. doi:10.1038/s41598-022-19930-x
[74] Z. Xia, C. Zhou, Q. Yong, and X. Wang, “On selection of repeated unit cell model and application of unified periodic boundary conditions in micro-mechanical analysis of Composites,” International Journal of Solids and Structures, vol. 43, no. 2, pp. 266–278, Jan. 2006. doi:10.1016/j.ijsolstr.2005.03.055
[75] O. Sigmund, “Morphology-based black and white filters for topology optimization,” Structural and Multidisciplinary Optimization, vol. 33, no. 4–5, pp. 401–424, Jan. 2007. doi:10.1007/s00158-006-0087-x
[76] G. Allaire, F. Jouve, and A.-M. Toader, “Structural optimization using sensitivity analysis and a level-set method,” Journal of Computational Physics, vol. 194, no. 1, pp. 363–393, Feb. 2004. doi:10.1016/j.jcp.2003.09.032
[77] M. P. Bendsøe and O. Sigmund, “Extensions and applications,” Topology Optimization, pp. 71–158, 2004. doi:10.1007/978-3-662-05086-6_2
[78] J. Li, Z. Wu, C. Shi, Q. Yuan, and Z. Zhang, “Durability of ultra-high performance concrete – a review,” Construction and Building Materials, vol. 255, p. 119296, Sep. 2020. doi:10.1016/j.conbuildmat.2020.119296
[79] "Ultra-high performance concrete (UHPC) technology from material to structure: A review," Proceedings of the International Building & Infrastructure Technology Conference, 2014, p. 355.
[80] S. Ahmad, I. Hakeem, and A. K. Azad, “Effect of curing, fibre content and exposures on compressive strength and elasticity of UHPC,” Advances in Cement Research, vol. 27, no. 4, pp. 233–239, Apr. 2015. doi:10.1680/adcr.13.00090
[81] S. Abbas, A. M. Soliman, and M. L. Nehdi, “Exploring mechanical and durability properties of ultra-high performance concrete incorporating various steel fiber lengths and dosages,” Construction and Building Materials, vol. 75, pp. 429–441, Jan. 2015. doi:10.1016/j.conbuildmat.2014.11.017
[82] F. de Larrard and T. Sedran, “Optimization of ultra-high-performance concrete by the use of a packing model,” Cement and Concrete Research, vol. 24, no. 6, pp. 997–1009, 1994. doi:10.1016/0008-8846(94)90022-1
[83] M. A. Bajaber and I. Y. Hakeem, “UHPC evolution, development, and utilization in construction: A Review,” Journal of Materials Research and Technology, vol. 10, pp. 1058–1074, Jan. 2021. doi:10.1016/j.jmrt.2020.12.051

[84] B. A. Graybeal, Material Property Characterization of Ultra-High Performance Concrete. McLean, Va, Springfield, VA: Federal Highway Administration, Office of Research, Development and Technology, Turner-Fairbank Highway Research Center ; Available through the National Technical Information Service, 2006.
[85] K. Wille, A. Naaman, and S. El-Tawil, "Optimizing ultra-high-performance fiber-reinforced concrete," ACI Concrete International, vol. 33, no. 9, pp. 35–41, Jan. 2011.
[86] N. J. Delatte, “Lessons from roman cement and concrete,” Journal of Professional Issues in Engineering Education and Practice, vol. 127, no. 3, pp. 109–115, Jul. 2001. doi:10.1061/(asce)1052-3928(2001)127:3(109)
[87] M. G. Sohail et al., “Advancements in concrete mix designs: High-performance and ultrahigh-performance concretes from 1970 to 2016,” Journal of Materials in Civil Engineering, vol. 30, no. 3, Mar. 2018. doi:10.1061/(asce)mt.1943-5533.0002144
[88] A. Rajasekar, K. Arunachalam, and M. Kottaisamy, “Assessment of strength and durability characteristics of copper slag incorporated Ultra High Strength Concrete,” Journal of Cleaner Production, vol. 208, pp. 402–414, Jan. 2019. doi:10.1016/j.jclepro.2018.10.118 J. Clean. Prod., 208 (2019), pp. 402-414, 10.1016/j.jclepro.2018.10.118
[89] S. D. Pham, V. T. Nguyen, T. T. Le, and C. T. Nguyen, “Possibility of using high volume fly ash to produce low cement Ultra High Performance Concrete,” Lecture Notes in Civil Engineering, pp. 589–597, 2020. doi:10.1007/978-981-15-5144-4_56
[90] "High-performance high-volume fly ash concrete," Indian Concrete Journal, vol. 78, pp. 13–21, 2004.
[91] D. Wang et al., “A review on Ultra High Performance Concrete: Part II. hydration, microstructure and properties,” Construction and Building Materials, vol. 96, pp. 368–377, Oct. 2015. doi:10.1016/j.conbuildmat.2015.08.095
[92] C. Shi et al., “A review on Ultra High Performance Concrete: Part I. Raw Materials and mixture design,” Construction and Building Materials, vol. 101, pp. 741–751, Dec. 2015. doi:10.1016/j.conbuildmat.2015.10.088
[93] “Global Rare Earth Metals Recycling Market Report 2022: Increasing demand for clean energy fuelling growth,” Focus on Catalysts, vol. 2023, no. 1, p. 2, Jan. 2023. doi:10.1016/j.focat.2022.12.004
[94] Trinic LLC, "UHPC Premix," Trinic, [Online]. Available: https://trinic.us/products/uhpc-premix. [Accessed: Nov. 25, 2024].
[95] J. B. Berger, H. N. Wadley, and R. M. McMeeking, “Mechanical metamaterials at the theoretical limit of isotropic elastic stiffness,” Nature, vol. 543, no. 7646, pp. 533–537, Feb. 2017. doi:10.1038/nature21075
[96] T. Li, X. Hu, Y. Chen, and L. Wang, “Harnessing out-of-plane deformation to design 3D architected lattice metamaterials with tunable Poisson’s ratio,” Scientific Reports, vol. 7, no. 1, Aug. 2017. doi:10.1038/s41598-017-09218-w

[97] Z. Lu, Q. Wang, X. Li, and Z. Yang, “Elastic properties of two novel auxetic 3D cellular structures,” International Journal of Solids and Structures, vol. 124, pp. 46–56, Oct. 2017. doi:10.1016/j.ijsolstr.2017.05.031
[98] M.-H. Fu, B.-B. Zheng, and W.-H. Li, “A novel chiral three-dimensional material with negative Poisson’s ratio and the equivalent elastic parameters,” Composite Structures, vol. 176, pp. 442–448, Sep. 2017. doi:10.1016/j.compstruct.2017.05.027
[99] H. Wang, Z. Lu, Z. Yang, and X. Li, "A novel re-entrant auxetic honeycomb with enhanced in-plane impact resistance," Composite Structures, vol. 208, pp. 758–770, 2019. [Online]. Available: https://doi.org/10.1016/j.compstruct.2018.10.024. [Accessed: Nov. 25, 2024].
[100] X. Ren, R. Das, P. Tran, T. D. Ngo, and Y. M. Xie, “Auxetic metamaterials and structures: A Review,” Smart Materials and Structures, vol. 27, no. 2, p. 023001, Jan. 2018. doi:10.1088/1361-665x/aaa61c
[101] T. Wang, J. An, H. He, X. Wen, and X. Xi, “A novel 3D impact energy absorption structure with negative Poisson’s ratio and its application in aircraft crashworthiness,” Composite Structures, vol. 262, p. 113663, Apr. 2021. doi:10.1016/j.compstruct.2021.113663
[102] D. Li, R. Gao, L. Dong, W.-K. Lam, and F. Zhang, “A novel 3D re-entrant unit cell structure with negative Poisson’s ratio and tunable stiffness,” Smart Materials and Structures, vol. 29, no. 4, p. 045015, Mar. 2020. doi:10.1088/1361-665x/ab6696
[103] E. J. Hunt, C. Zhang, N. Anzalone, and J. M. Pearce, “Polymer recycling codes for distributed manufacturing with 3-D printers,” Resources, Conservation and Recycling, vol. 97, pp. 24–30, Apr. 2015. doi:10.1016/j.resconrec.2015.02.004
[104] M. Groenendyk and R. Gallant, “3D printing and scanning at the Dalhousie University Libraries: A pilot project,” Library Hi Tech, vol. 31, no. 1, pp. 34–41, Mar. 2013. doi:10.1108/07378831311303912
[105] S. Valvez, A. P. Silva, and P. N. Reis, “Optimization of printing parameters to maximize the mechanical properties of 3D-printed PETG-based parts,” Polymers, vol. 14, no. 13, p. 2564, Jun. 2022. doi:10.3390/polym14132564
[106] I. M. Alarifi, “A performance evaluation study of 3D printed nylon/glass fiber and nylon/carbon fiber composite materials,” Journal of Materials Research and Technology, vol. 21, pp. 884–892, Nov. 2022. doi:10.1016/j.jmrt.2022.09.085
[107] X. Yan and P. Gu, “A review of Rapid Prototyping Technologies and Systems,” Computer-Aided Design, vol. 28, no. 4, pp. 307–318, Apr. 1996. doi:10.1016/0010-4485(95)00035-6
[108] B. Wittbrodt and J. M. Pearce, “The effects of PLA color on material properties of 3-D printed components,” Additive Manufacturing, vol. 8, pp. 110–116, Oct. 2015. doi:10.1016/j.addma.2015.09.006
[109] E. H. Tümer and H. Y. Erbil, “Extrusion-based 3D printing applications of PLA Composites: A Review,” Coatings, vol. 11, no. 4, p. 390, Mar. 2021. doi:10.3390/coatings11040390
[110] B. G. Compton and J. A. Lewis, "3D-printing of Lightweight Cellular Composites," Advanced Materials, vol. 26, no. 34, pp. 5930–5935, Jun. 2014. doi:10.1002/adma.201401804

[111] Ultimaker, Ultimaker PLA Technical Data Sheet, [Online]. Available: https://ultimaker.com. [Accessed: Nov. 25, 2024].
[112] P. Kumar et al., “Pineapple Peel extract incorporated poly(vinyl alcohol)-corn starch film for active food packaging: Preparation, characterization and antioxidant activity,” International Journal of Biological Macromolecules, vol. 187, pp. 223–231, Sep. 2021. doi:10.1016/j.ijbiomac.2021.07.136
[113] A. Rajkumar, D. Prithiviraj, P. Chithambaranathan, and M. Chenthil, “Manufacturing of bromelain based PVA support structure for 3D printing,” Materials Today: Proceedings, vol. 62, pp. 1102–1106, 2022. doi:10.1016/j.matpr.2022.04.319
[114] Kwak, H. G., & Filippou, F. (1990). Finite element analysis of reinforced concrete structures under monotonic loads.
[115] S. V.Chaudhari and M. A. Chakrabarti, “Modeling of concrete for nonlinear analysis using Finite Element Code Abaqus,” International Journal of Computer Applications, vol. 44, no. 7, pp. 14–18, Apr. 2012. doi:10.5120/6274-8437
[116] J. Xiao, H. Liu, and T. Ding, "Finite element analysis on the anisotropic behavior of 3D printed concrete under compression and flexure," Additive Manufacturing, vol. 39, 2021. [Online]. Available: https://doi.org/10.1016/j.addma.2020.101712. [Accessed: Nov. 25, 2024].
[117] L. P. Saenz, "Discussion of 'Equation for the stress-strain curve of concrete' by Desayi and Krishnan," ACI Journal, vol. 61, no. 9, pp. 1229–1235, 1964.
[118] American Concrete Institute (ACI), Building Code Requirements for Structural Concrete and Commentary (ACI 318). Farmington Hills,
[119] Fib Model Code for Concrete Structures 2010. Lausanne, Switzerland: International Federation for Structural Concrete (fib), 2010.
[120] D. A. Hordijk, Local Approach to Fatigue of Concrete. Ph.D. dissertation, Delft University of Technology, Delft, Netherlands, 1991.
[121] T. Yu, J. G. Teng, Y. L. Wong, and S. L. Dong, "Finite element modeling of confined concrete-II: Plastic-damage model," Engineering Structures, vol. 32, pp. 680–691, 2010. [Online]. Available: https://doi.org/10.1016/j.engstruct.2009.11.013. [Accessed: Nov. 25, 2024].
[122] G. M. Chen, J. F. Chen, and J. G. Teng, “On the finite element modelling of RC beams shear-strengthened with FRP,” Construction and Building Materials, vol. 32, pp. 13–26, Jul. 2012. doi:10.1016/j.conbuildmat.2010.11.101
[123] J. Xiao, H. Liu, and T. Ding, “Finite element analysis on the anisotropic behavior of 3D printed concrete under compression and flexure,” Additive Manufacturing, vol. 39, p. 101712, Mar. 2021. doi:10.1016/j.addma.2020.101712



University of Pittsburgh

Swanson School of Engineering

Department of Civil and Environmental Engineering

IRISE Consortium

742 Benedum Hall

3700 O'Hara Street

Pittsburgh, PA 15261

The information printed in this document was accurate to the best of our knowledge at the time of printing and is subject to change at any time at the University's sole discretion.

The University of Pittsburgh is an affirmative action, equal opportunity institution.